JAERI-M
89-074

DEVELOPMENT AND APPLICATION OF AN ON-LINE TRITIUM PRODUCTION RATE MEASURING METHOD

June 1989

Seiya YAMAGUCHI

日本原子力研究所
Japan Atomic Energy Research Institute

JAERI-Mレポートは，日本原子力研究所が不定期に公刊している研究報告書です。
入手の問合わせは，日本原子力研究所技術情報部情報資料課（〒319－11茨城県那珂郡東海村）あて，お申しこしください。なお，このほかに財団法人原子力弘済会資料センター（〒319-11茨城県那珂郡東海村日本原子力研究所内）で複写による実費頒布をおこなっております。

JAERI-M reports are issued irregularly.
Inquiries about availability of the reports should be addressed to Information Division, Department of Technical Information, Japan Atomic Energy Research Institute, Tokai-mura, Naka-gun, Ibaraki-ken 319-11, Japan.

編集兼発行　日本原子力研究所
印　　刷　日立高速印刷株式会社

JAERI-M 89-074

Development and Application of an On-Line Tritium Production Rate Measuring Method

Seiya YAMAGUCHI

Department of Reactor Engineering
Tokai Research Establishment
Japan Atomic Energy Research Institute
Tokai-mura, Naka-gun, Ibarakiken

(Received May 19, 1989)

A highly sensitive on-line method for measuring the tritium production rate (TPR) of ^{6}Li was developed using the response difference of ^{6}Li and ^{7}Li-glass scintillators in a mixed neutron-gamma radiation field. A fitting method for subtracting the pulse height spectrum of ^{7}Li-glass from that of ^{6}Li-glass was introduced. The contribution of competing reactions such as $^{6}Li(n,n'd)^{4}He$ was estimated by kinematical analyses. An absolute value of the ^{6}Li content was determined by a chemical analysis.

The thermal flux perturbation due to ^{6}Li-glass of various thickness and ^{6}Li contents was evaluated by measurment in a thermal neutron field and calculation by the modified Skyrme theory. A Monte Carlo calculation of the self-shielding effect was also made. The dependence of the self-shielding on neutron energy was examined by this Monte Carlo code.

The edge effect, i.e., distortion of the pulse height spectrum due to partial energy deposition of the alpha and/or the triton, was investigated by measurment in a thermal neutron field and by a Monte Carlo simulation that was based on the scintillation mechanism and considered Bragg absorption and the ratio of contributions to luminescence by the alpha and the triton. The dependence of the edge effect on neutron energy was examined by this Monte Carlo code.

This method was applied to the measurement of TPR distributions

in simulated fusion blanket assemblies bombarded by D-T neutrons. Absolute values of the TPR were obtained with an experimental error of 3~6 %. The measured results were compared with those of conventional β-counting methods and good agreement was obtained.

An optical fiber system, using miniature lithium-glass scintillators, was fabricated for purpose of microminiaturization of detector size and adaption to strong electromagnetic field. Applicability of this system to a D-T neutron field was demonstrated.

Keywords: Fusion Reactor Blanket, D-T Neutrons, Tritium Production Rate, Lithium-Glass Scintillator, Neutron Flux Depression, Self-Shielding Effect, Edge-Effect, Stopping Power, Range, Optical Fiber

オンライントリチウム生成率測定法の開発と応用

日本原子力研究所東海研究所原子炉工学部
山口　誠哉

（1989年5月19日受理）

中性子・ガンマ線混在場における，^{6}Li，^{7}Liガラス・シンチレータの応答の差を利用して，^{6}Liによるトリチウム生成率（ＴＰＲ）を高感度かつオンラインで測定する方法を開発した。

^{6}Liガラスの波高分布から^{7}Liガラスの波高分布を差引くための手法を開発した。^{6}Li（n，n'd）^{4}He反応等の競合反応の寄与は，運動学的解析により評価した。^{6}Li含有率の絶対値は化学分析により決定した。

^{6}Li ガラスの熱中性子束に対するバータベーションを，いろいろな厚さと^{6}Li 含有率について，熱中性子場における測定および修正されたスキルム理論に基づく計算により評価した。また自己遮蔽効果のモンテカルロ計算も行なった。自己遮蔽効果の中性子エネルギー依存性を本モンテカルロ・コードにより調べた。

端効果，既ち，アルファ粒子およびトリトンの部分的エネルギー付与による波高分布の歪みについて，熱中性子場における測定および発光機構に基づくモンテカルロ・シミュレーションにより調べた。本シミュレーションにおいては，ブラッグ吸収およびアルファ粒子とトリトンの発光への寄与の比が考慮されている。本モンテカルロ・コードにより，端効果の中性子エネルギー依存性を調べた。

本方法を，Ｄ－Ｔ中性子で照射された核融合炉ブランケット模擬体系中のＴＰＲ分布測定に適用し，ＴＰＲの絶対値を３～６％の実験誤差で得た。測定結果を，よく用いられているβ線計数法による結果と比較し，よい一致を得た。

検出器の超小型化と強電磁場への適用を目的に，小型リチウム・ガラス・シンチレータを用いた光ファイバー・システムを製作し，本システムのＤ－Ｔ中性子場への適用性を実証した。

東海研究所：〒319-11 茨城県那珂郡東海村白方字白根２－４

Contents

目　　次

List of Tables

List of Figures

1. Introduction

1.1 Background of the Present Study

Of all the proposed thermonuclear fusion reactors, the DT reactor, fueled with deuterium (D) and tritium (T), now seems closest to realization. As the tritium fuel component does not occur naturally, it must be reproduced in a lithium-containing blanket that surrounds the plasma. In the present stage of DT fusion reactor R & D, efforts are focused on the conceptual design of the next fusion devices, that is, fusion experimental reactors (FER[1], TIBER[2], NET[3], ITER[4]) as well as the investigation of plasma behavior using Tokamak type critical plasma testing facilities such as JT-60 and JET. The design of the blanket is one of the most important parts of reactor design, because it deals directly with the issues of energy extraction and fuel breeding. Numerous design studies carried out worldwide have proposed a large number of design concepts. Two comprehensive design studies have been made in the United States in order to clarify the issues and to optimize the R & D strategy : 1) BCSS (Blanket Comparison and Selection Study)[5,6] and 2) FINESSE (Fusion Integral Nuclear Experiments Strategy Study Efforts)[7~9].

One of the key issues in blanket design is tritium self-sufficiency, that is, achievement of the tritium fuel cycle.[10] Therefore, careful evaluation of the conditions for attaining self-sufficiency is necessary in order to define blanket design conceptual selection criteria. In the case of the solid breeder blanket, the uncertainty of the tritium breeding ratio (TBR) is larger than that for liquid breeder blanket because the tritium breeding capability is reduced by the presence of non-breeder materials such as coolant and pipes. The required accuracy for the predicted value of TBR is 3~5 %, however, the present level of the prediction error is about 10 %.[10] The error is caused mainly by the uncertainty of the neutronics calculation, that is, the uncertainty of nuclear data and calculational methods. In order to examine the validity of data and methods, investigation through integral experiments is necessary, as well as differential experiments such as cross section measurements. From this point of view, measurements of the tritium production rate (TPR) in DT neutron fields have been made since the 1960's. Typical examples of such

tritium production measurements are listed chronologically in Table 1.1.1.

Techniques for TPR measurement are roughly clasified into two categories :

A : Irradiation of samples containing lithium and subsequent extraction and measurement of tritium β activity,

B : Detection of the charged particles produced in $^{6}Li(n,\alpha)T$ reactions.

Category A requires a heavy irradiation because the half life of tritium is long (12.35 years) and detection efficiency is low. It also requires special tritium extraction equipment and procedures as well as tritium counting facilities that provide low background through shielding and/or coincidence counting. Considerable efforts are needed for sample preparation, processing and counting. Three methods have been used for tritium counting.

A-1 : Proportional counter[11~18]

Lithium metal samples are encapsulated in copper or aluminum and irradiated. After extracting the tritium by heating in a hydrogen atmosphere, the gas is translated into the proportional counter, whereupon the β activity is measured. This method is very cumbersome and require careful adjustment of the gas quantity as well as highly accurate measurement of the pressure, mixing ratio etc. for each sample.

A-2 : Liquid scintillation counter[19~25]

Lithium metal foils enclosed in aluminum capsules or sintered pellets of lithium salts (Li_2O, Li_2CO_3, LiOH) are used as irradiation samples. After irradiation, tritium is extracted as HTO by extraction and oxidation or by appropriate chemical processing. The β activity is measured by mixing the recovered HTO with liquid scintillator. Corrections for collection yield and detection efficiency are needed. Very low background is necessary to obtain acceptable statistics.

A-3 : Self-irradiation[26~28]

In this method, the tritium β activity produced in the lithium-containing sample is measured by the sample itself. So far, this technique has been applied to LiF thermo-

luminescence dosimeters (TLD) and lithium-glass scintillators. This method is simple, but is not suitable for absolute measurement with high accuracy because of the difficulty of the determination of the Li atom number in the sample as well as low inherent signal-to-noise ratio.

Category B has relatively high detection efficiency and thus needs no heavy irradiation. Three methods can be distinguished in this category.

B-1 : Sandwiched Counter Method[29,30]

Tritium-producing events due to neutron interaction with a thin ^{6}LiF film result in α particle and triton emission in opposite directions. The particles are detected by surface barrier detectors or ionization chambers. A coincidence scheme is provided to sort out real events from single events. This method has the disadvantages that the detection efficiency depends on the incident angle of the neutrons and that the size of the detector is rather large.

B-2 : Nuclear Emulsion method[31,32]

α and triton tracks produced in nuclear emulsions by neutron interactions with ^{6}Li or ^{7}Li are counted. This scheme demands skill in discrimination of the particle. The acuuracy limit of this method is about 10 %.

B-3 : Solid State Track Detector method[33,34]

Lithium compounds are used as the radiator. Corrections are necessary for the recoil of C, N, O atoms, competing reactions producing charged particles, loss of tracks at etching. Thus, this method is not suitable for the absolute measurement with high accuracy.

Methods in category A demand a heavy irradiation, consequently, a long machine time and activation of the apparatus surrounding the target. However, the accuracy of measurement may still not be high enough, especially for deep locations in the assembly, where the neutron intensity is not sufficient even with the strongest neutron sources presently available. Methods in category B also demand medium-heavy irradiation except for method B-1. All methods in both categorie except B-1 are off-line measurements, and take much time for preparation and processing of samples. As for the B-1 method, the sensitive region is relatively large (2.6 cm^3),consequently, spatial

resolution is poor. Flux perturbation also is rather large as a results of overall detector size.

For purposes of blanket design, it is necessary to investigate experimentally the effects of various configurations of the first wall, neutron multiplier, coolant channels etc. on TPR distributions.[35,36] Examination of the the effect of each component thus calls for numerous measurements. Such an extensive program is jeopardized by the problems inherent in heavy irradiation, 1) long machine time (>10 h/run), 2) consumption of ^{3}T target, 3) activation of the apparatus around the target. Consequently, development of a highly sensitive on-line method for TPR measurement that does not require heavy irradiation is desirable.

1.2 Objectives and Outline of the Present Study

Since, in the blanket configurations examined so far, the TPR of ^{6}Li (T_6) is dominant,[35] that measurement is important. In this thesis, I describe a method of measuring the ^{6}Li tritium production rate that satisfies the above requirements and yields absolute measurements with high accuracy. This method makes use of a pair of small Li-glass scintillators (Li-glass method), of which one is enriched in ^{6}Li and the other, in ^{7}Li. The TPR's are obtained from the response difference of these scintillators in a mixed neutron-gamma field. T_7 can be measured by using detectors sensitive to high-energy neutrons, such as a NE213 liquid scintillation counter.

In the next Chapter, the γ-ray background subtraction scheme, based on adjusting the difference of the γ-ray detection efficiencies and gains of both scintillators, is presented.[37,38] The evaluation of the competing reactions and determination of the ^{6}Li atom number in the ^{6}Li-glass scintillator are described. In Chap. 3, the perturbation of the neutron flux by the lithium-glass scintillator is investigated by measurement, supported by theoretical calculations and a Monte Carlo calculations.[39] It is shown that the flux depression is small compared with the self-shielding effect and that the perturbation can be neglected by using a very thin and low ^{6}Li content scintillator. In Chap. 4, the edge effect — distortion of the pulse height spectrum at the low energy side of the thermal peak due to partial energy deposition of the alpha particle and/or the triton — is examined

experimentally and by a calculation.[40] Measurements of the pulse height spectrum in a thermal neutron field were made for five values of scintillator thickness. A Monte Carlo calculation based on the scintillation mechanism was also made. The correction factor for edge effect was shown quantitatively. In Chap. 5, the measurment of the TPR distribution in simulated fusion blanket assemblies and comparison with conventional β counting are described.[41~43] In Chap. 6, the application of optical fiber light guides to the Li-glass method, for purposes of detector size microminiaturization and adaptation to strong electromagnetic fields, is described. Chap. 7 presents some general concluding remarks on the results obtained in this thesis.

References

1) Tomabechi K., et al. : 9th Conf. on Plasma Physics and Controlled Fusion Research, Baltimore, (1982), IAEA-CN-41/E-4.
2) Henning C. D., et al. : "A Tokamak Ignition/Burn Experimental Research Device", Proc. 6th Topical Meeting on Technol. Fusion Energy, San Francisco (1985); Fusion Technol., 8, 1351 (1985).
3) Toschi R. : "Objectives and Main Features of the Next Europian Torus Project," Proc. 6th Topical Meeting on Technol. of Fusion Energy, San Francisco, (1985); Fusion Technol., 8, 291 (1985).
4) Tomabechi K. : "International Thermonuclear Experimental Reactor, ITER," Proc. Int. Sympo. Fusion Nucl. Technol., Tokyo (1988).
5) Abdou M. A., et al. : "Blanket comparison and selection study — Interm. report," ANL/FPP-83-1, (1983).
6) Smith D. L., et al. : *ibid.* Final report, ANL/FPP-84-1, (1984).
7) Abdou M. A., et al. : FINESSE; A study of the issues, experiments, and facilities for fusion nuclear technology research & development — Interim report, UCLA-PPG-821, UCLA-ENG-84-30, (1984).
8) Abdou M. A. : Fusion Technol. 8[1], 1081 (1985).
9) Tillack, M. et al. : *ibid.* 8[1], 1091 (1985).
10) Abdou M. A. : *ibid.* 9, 250 (1986).
11) Wyman M. E. : "An integral experiment to measure the tritium production from ^{7}Li by 14-MeV neutrons in a lithium deuteride sphere," LA-2234 (1972).
12) Benjamin P. W., et al. : "A technique for measuring the tritium content of small samples of irradiated lithium metal," AWRE NR/A-2/62 (1962).
13) Spangler P. S. : "Fusion reactor blanket experiment," Technical report 437 (1965) MIT, AD 619671
14) Cloth P., et al. : "Studies of the space dependent tritium production and the fast flux distribution in a lithium blanket experiment," Proc. 8th symp. on Fusion Technol., Noordwijkerhout, Netherlands, (1974).
15) Qaim S. M., et al. : J. Radioanal. Chem., 30, 35 (1976).
16) Hemmendinger A., et al. : "Tritium production in a sphere of ^{6}LiD irradiated by 14-MeV neutrons," LA-7310 (1978).
17) Hemmendinger A., et al. : Nucl. Sci. Eng. 70, 274 (1979).
18) Liskien H. : Proc. Int'l Conf. Nucl. data for Sci. Technol., p349

Antwerp, (1982).

19) Dierckx R. : Nucl. Instr. Meth. 107, 397 (1973).

20) Herzing R. : "Erprobung neutronenphsikalischer Rechenverfarren an Lithiummblanketmodellen fur einen Fusionsreactor," PhD Thesis, Aachen, Federal Republic of Germany (1976) ; Jül-1357 (1976).

21) Herzing R., et al. : Nucl. Sci. Eng. 60, 169 (1976).

22) Herzing R., et al. : *ibid.* 63, 341 (1977).

23) Fritscher U., et al. : Nucl. Instr. Meth. 153, 563 (1978).

24) Bretscher M. S. : 10th Symp. on Fusion Eng., Philadelphia (1983).

25) Tsuda K., et al. : "A Method for Tritium Production-Rate Measurement with Sintered Li_2O Pellets and its Application to a 60 cm-Thick Li_2O Slab Assembly," JAERI-M 84-138, 88 (1984).

26) Maekawa H. : "A method for Obtaining the Tritium Production Rate Distribution with a LiF Thermoluminescence Dosimeters," JAERI-M 6055 [in Japanese](1975) ; UCRL-TRANS-11196 (1977).

27) Sharabati H., et al. : Nucl. Instr. Meth. 201, 445 (1982).

28) Gmuer K., et al. : Int'l Conf. on Nucl. Data for Basic and Appl. Sci., JC12 ,Santa Fe (1985).

29) Herold T. R. : Nucl. Instr. Meth. 71, 40 (1969).

30) Joneja O. P., et al. : *ibid.* 193, 563 (1982).

31) Rosen L., et al. : Phys. Rev. 126, 1150 (1962).

32) Lisowski P. W., et al. : "Cross sections of Neutron-Induced, Neutron Producing Reactions in ^6Li and ^7Li at 5.96 and 9.83 MeV," LA-8342 (1980).

33) Herzing R., et al. : Nucl. Sci. Eng., 60, 169 (1976).

34) Kuijpers L. J. M. : "Experimental model studies for a fusion reactor blanket," PhD thesis, Eindhoven, The Netherlands (1976) ; Jül-1356 (1976).

35) Nakamura T., et al. : Proc. 7th Topical Meeting on Technol. of Fusion Energy, Reno, (1986) ; Fusion Technol. 10, 541 (1986); Trans. Am. Nucl. Soc. 52, 106, (1986).

36) Nakamura T., et al. : Int'l Symp. on Fusion Nucl. Technol., Tokyo, (1988).

37) Yamaguchi S., et al. : "A method for measuring tritium production rate by lithium-glass scintillators," JAERI-M 85-086 (1985) [in Japanese].

38) Yamaguchi S., et al. : Nucl. Instr. Meth. A254, 413 (1987).

39) Yamaguchi S. : Nucl. Instr. Meth. A274, 568 (1989).

40) Yamaguchi S. : Nucl. Instr. Meth. A274, 573 (1989).

41) Yamaguchi S., et al. : Proc. 7th Topical Meeting on the Technol. of Fusion Energy; Fusion Technol.,10, 573 (1986); Trans. Am. Nucl. Soc. , 52, 110 (1986).

42) Oyama Y., et al. : Proc. Int'l Symp. on Fusion Nucl. Technol., Tokyo, (1988); To be published in J. Fusion Eng. Design. (1988).

43) Oyama Y., et al. : submitted to 8th Topical Meeting on the Technol. Fusion Energy. (1988).

Table 1.1.1 Typical examples of tritium production measurements

date	affiliation	person	technique	detection	error[%][d]	ref.
1958[a]	LASL	M.Wyman	Li metal, prop. counter	β-ray	∿4	11)
1962	AWRE	P.Benjamin	Li metal, prop. counter	β-ray	∿4	12)
1965	MIT	P.Splangler	Flibe, prop. counter	β-ray	—	13)
1973	Euratom CCR	R.Dierckx	Li_2CO_3 pellet, liq. scint.	β-ray	—	19)
1974	Jülich	P.Cloth	Li metal, prop. counter	β-ray	—	14)
1975	JAERI	H.Maekawa	TLD, self irad.	β-ray	—	26)
1976	Jülich	R.Herzing	Li_2CO_3 pellet, liq. scint.	β-ray	3∿6	20∿22)
1976[b]	Jülich	R.Herzing	SSTD	α,t	—	23)
1976	Jülich	S.Qaim	Li pellet, prop. counter	β-ray	—	15)
1978	KfK	U.Fritscher	Li_2CO_3 pellet, liq. scint.	β-ray	∿4	33)
1979	LASL	A.Hemmen-dinger	LiH, prop. counter	β-ray	∿9	16,17)
1980	LASL	P.Lisowski	nucl. emulsion	α,t	10<	32)
1982[c]	Jülich	O.Joneja	sandwich count.	α,t	∿5	30)
1982	Jülich	H.Sharabati	TLD, self irad.	β-ray	—	27)
1983	ANL	M.Bretscher	Li metal, liq. scint.	β-ray	—	24)
1984	JAERI	K.Tsuda	Li_2O pellet, liq. scint.	β-ray	∿5	25)
1985	Swiss Fed.Inst.	K.Gmuer	Li-glass, self. irad.	β-ray	—	28)

a) for military purpose

b) tritium production rate of ^6Li only

c) tritium ptoduction rate of ^6Li only, on-line measurement

d) excluding error of source intensity

2. Paired Li-Glass Scintillator Subtraction Scheme[1)]

2.1 Introduction

In the present method, the TPR of ^{6}Li is measured by using the difference between the response of ^{6}Li-glass and that of ^{7}Li-glass in a mixed neutron-gamma radiation field. Typical examples of the pulse height spectra (PHS) of ^{6}Li- and ^{7}Li-glass scintillators in a simulated fusion blanket assembly are shown in Fig. 2.1.1. A sharp peak caused by the $^{6}Li(n,\alpha)^{3}T$ reaction appeares on a Compton electron background produced by γ-rays in the PHS of ^{6}Li-glass, for ^{7}Li-glass, only the γ-ray background is observed. As is shown later, it can be assumed that the γ-ray responses of both scintillators are almost identical. Consequently, the γ-ray background can be rejected by subtracting the PHS of ^{7}Li-glass from that of ^{6}Li-glass. Figure 2.1.2 shows a typical subtracted spectrum. The total number of counts in the subtracted spectrum, is equal to the total number of $^{6}Li(n,\alpha)^{3}T$ events in the scintillator, is proportional to the tritium production rate of ^{6}Li.

Although it is basic to this scheme that both scintillators have the same gains and the same γ-ray detection efficiencies, there are usually some differences between scintillators. A method of adjusting these differences will be described in the following.

In the fast neutron fields as encountered in the fusion blanket, competing reactions such as elastic scattering of ^{6}Li and ^{7}Li, as well as $^{6}Li(n,n'd)^{4}He$, also occur. The contribution of such competing reactions was examined by kinematical analyses using a typical calculated neutron spectrum in a simulated fusion blanket assembly. Contributions of Si, O, Ce and Al are also examined.

An accurate knowledge of the ^{6}Li content in the ^{6}Li-glass scintillator is required to obtain absolute TPR values. Manufacture's data of the ^{6}Li content are generally unreliable, hence, the ^{6}Li content was determined by isotopic dillution analysis.

If pulse shape discrimination of neutrons and gamma-rays were feasible for lithium-glas scintillator, then one could measure the TPR using only ^{6}Li-glass scintillator. Neutron-gamma discrimination was thus investigated, as described in section 2.3.

2.2 Scintillator and Electronic Circuit

Cerium-activated lithium loaded silicate glass scintillators have been widely used for neutron detection since their development [2~13] in the late 1950's because of their large neutron cross section and a high Q-value (4.78 MeV). At present, several kinds of scintillators of various lithium content and ^{6}Li enrichment (^{6}Li enriched, depleted and natural) are commercialy available from Nuclear Enterprise Ltd. and Koch-Light Laboratories Ltd. The characteristics of these scintillators were examined systematically by Spowart.[14~17] The first such scintillator made in Japan is NS15[18] for ^{6}Li enriched (in 1980) and BS15 for ^{7}Li enriched (in 1985) manufactured by the Nikon Corp. (Nippon Kogaku Corp.).

From the point view of measurement of the reaction rate in a certain assembly, it is desirable that the flux perturbation be as small as possible, implying low ^{6}Li content and small depth. As is shown in the next chapter, the reaction rate is strongly reduced by a large ^{6}Li content and large glass depth, especially in a soft neutron spectrum field. On the other hand, it takes much time to adequate statistics with a thin glass scintillator of low ^{6}Li content. In the present study, NS15 (6.3 % ^{6}Li) ^{6}Li enriched glass and the corresponding ^{7}Li enriched glass, BS15, were used with a diameter and thickness of 10 mm and 0.3 mm, respectively.

The chemical composition, nuclide densities and physical properties of these glasses are shown in Tables 2.2.1 ~ 2.2.3, respectively. Excitation and emission spectra of NS15 are shown in Fig. 2.2.1. The wavelength of maximum emission is 390 nm.

The scintillators were coupled to 13 mm-diameter photomultiplier tubes (PMT, Hamamatsu Photonics Corp. R647-01) using quartz light guides of 10 mm-diameter by 4 mm-thick with silicon gel. On the PMT face, the scintillators were optically polished, the other face and on the lateral surface, they were roughened. NE560 reflector was applied to the surfaces of the scintillators and light guides. The scintillator, light guide and photomultiplier tube were put into a magnetic-shield case (see Fig. 2.2.2). A sectional view of the Li-glass scintillation detector assembly is shown in Fig. 2.2.3. The outer diameter and total length of the detector assembly are 19 mm and 175 mm, respectively.

A schematic diagram of the electric circuit and the data acquisition system are shown in Fig. 2.2.4. The signal from the anode of the photomultiplier tube is fed to the pre-amplifier (ORTEC 113), hence to the amplifier (ORTEC 571). Amplified and shaped signal pulses were accumulated in a 1024 channel multichannel pulse height analyzer, MCA (CANBERRA, series 80) through an analog-to-digital converter, (CANBERRA, 8080). The data stored in the MCA were transfered to a computrt (VAX 11/780) through a mini-computer (PDP 11/34) and processed.

2.3 Neutron-Gamma Discrimination Characteristics of NS15 ^{6}Li-glass scintillator

The neutron and gamma-ray (n-γ) discrimination characteristics were examined for NS15 ^{6}Li-glass scintillator.

(I) Discrimination by pulse height difference

The larger the α/β ratio, i.e., the ratio of the light output per unit energy of the α and the triton, and that of the electron, the better the signal-to-noise (S/N) ratio, i.e., the ratio of signal neutron count rate to gamma-ray background count rate at certain pulse height. The α/β ratio of the NS15 was determined by measuring the pulse height for thermal neutrons from an Am-Be source moderated in a graphite pile ($E_{\alpha+t}$ = 4.78 MeV) and for the Compton edges of ^{137}Cs, ^{57}Mn and ^{22}Na γ-ray sources (E_e = 0.477, 0.640, 0.341 and 1.062 MeV, respectively). The relation between the pulse height (channel number of MCA) and energy is shown in Fig. 2.3.1. Assuming a linear relation between pulse height and energy for both electrons and heavy particles, two lines can be drawn through the measured points. The ratio of slopes corresponding to the α/β ratio, comes to 0.27. This value agrees approximately with that in Ref.[7]. The α/β ratio of lithium glass is smaller than that of NaI(Tl), ZnS(As) and LiI(Tl), 0.6, 2.0 and 0.95, respectively. Thus the n-γ discrimination performance by pulse height difference is rather poor for Li-glass scintillator.

(II) Discrimination by pulse shape difference

Coceva[19] and Winyard[20] have examined the pulse shape discrimi-

nation capability of ^{6}Li glass scintillator, employing anode-dynode correlation and zero-crossing, respectively. Both methods are based on the difference of integrated pulse rise times resulting from different decay times of photomultiplier current pulses. Their results showed that pulse shape-based techniques yielded inadequate neutron-gamma discrimination for Li-glass. Yamada et al.[21,22] examined a neutron-gamma discrimination scheme based on the pulse width difference for neutrons and gamma-rays. Their results also indicated poor discrimination.

In the schemes mentioned so far, n-γ discrimation was based on one parameter analysis, i.e., rise time or pulse width. We tested the pulse shape discrimination performance of a two parameter scheme using a RHC (rise time to height converter) module. The electronics circuit is shown in Fig. 2.3.2. The rise time distribution, and a two dimensional map of rise time vs. pulse height are shown in Figs. 2.3.3 and 2.3.4, respectively. The figures suggest that discrimination, while somewhat better than for one-parameter schemes, still cannot effect a clean separation of neutron and gamma-related events.

2.4 Pulse Height Spectrum Fitting

Since it is impractical to achieve a perfect match of the gains of both detector channels and there is some difference in γ-ray detection efficiencies, it is necessary to adjust gains (horizontal axis in PHS) and efficiencies (vertical axis in PHS) of ^{6}Li- and ^{7}Li-glass scintillator pulse height spectra by suitable data processing. The adjustment is performed by fitting the spectra within the region below the $^{6}Li(n,\alpha)^{3}T$ peak which includes only the γ-ray background ——— fitting region. The fitting is carried out by a linear transformation of the ^{7}Li-glass spectrum, as follows :

$$X' = aX+b, \tag{2.4.1}$$

$$Y' = \frac{Y}{a\gamma_{\varepsilon}}, \tag{2.4.2}$$

where

X : Pulse height of ^{7}Li-glass (before transformation),

X' : Pulse height of ^{7}Li-glass (after transformation),

Y : Counts of ^{7}Li-glass (before transformation),

Y' : Counts of ^{7}Li-glass (after transformation),

γ_{ε} : ratio of γ-ray detection efficiencies between two scintillators (γ-ray detection efficiency of ^{6}Li-glass / γ-ray detection efficiency of ^{7}Li-glass).

The adjustable parameters a and b are determined by least square fitting. The ratio of γ-ray detection efficiencies was experimentally detemined using a 5 mCi ^{137}Cs source (described in detail in next section).

Figure 2.4.1 illustrates typical ^{6}Li- and ^{7}Li-glass pulse height spectra in the fitting region. A chain line, a dashed line and a solid line represent ^{7}Li-glass spectra before and after the transformation and ^{6}Li-glass spectra, respectively. We assume that the linear transformation moves the point A(i,C(i)) to B. The X-coordinate of the point B is $ai+b$. Usually $ai+b$ does not exactly correspond to a channel number. Then, fitting is performed as follows: Let the channel numbers located at both sides of $ai+b$ be $[ai+b]$ and $[ai+b]+1$ ([ ] is Gauss's symbol); let points C, D and E be defined as shown in Fig. 2.4.1 (point E is the intersection of line CD and a line perpendicular to the base through the point B). Let the counts at points B, C, D and E be Y_i, A_i, B_i and X_i, then

$$A_i = C6([ai+b]), \tag{2.4.3}$$

$$B_i = C6([ai+b]+1), \tag{2.4.4}$$

$$X_i = \{A_i-(A_i-B_i)(ai+b-[ai+b])\}/N_6, \tag{2.4.5}$$

$$Y_i = C7(i)/N_7/\gamma_{\varepsilon}/a, \tag{2.4.6}$$

where

C6(i) : counts of ^{6}Li-glass at channel i,

C7(i) : counts of ^{7}Li-glass at channel i,

N_6 : neutron yield during the measurement of ^{6}Li-glass,

N_7 : neutron yield during the measurement of ^{7}Li-glass.

Values of a and b are determined so as to minimize the quadratic sum

of residuals of X_i and Y_i :

$$S = \sum_{i=LC}^{RC} (X_i - Y_i)^2 \cdot W_i, \tag{2.4.7}$$

where

W_i : statistical weight ($= \sqrt{X_i^2 + Y_i^2}$),

LC : minimum channel of the fitting region,

RC : maximum channel of the fitting region.

The values of a and b which yields the minimum value of S can be found by successive approximation, from an initial set (a_0, b_0):

$$a = 1 + \frac{m - n}{n} \cdot a_0 \quad (m = 0,1,2,\cdots,2n),$$

$$b = \frac{m' - n'}{n'} \cdot b_0 \quad (m' = 0,1,2,\cdots,2n'). \tag{2.4.8}$$

Figure 2.4.2 shows the values of S as a function of a and b. Usually, $a_0 = 0.20$, $b_0 = 0.30$, n = 40, n' = 150. Thus the minimum value of S, $S_0 = S(a_{min}, b_{min})$ can be determined. Dividing S_0 by the atom number of ^{6}Li in the ^{6}Li-glass scintillator and the total neutron yield, the tritium production rate per ^{6}Li atom per source neutron can be obtained :

$$TPR = \frac{S_0}{N_6 . Y_n} \ [T/^6Li/source]. \tag{2.4.9}$$

The adjustment of gains and γ-ray detection efficiencies was successfully performed by means of this fitting method.

2.5 Measurement of the γ-ray Detection Efficiency Ratio

A small difference between the γ-ray detection efficiency of

^{6}Li-glass and that of ^{7}Li-glass results from the difference in compositions and volume. The γ-ray detection efficiency ratio of ^{6}Li to ^{7}Li-glass scintillators, γ_{ε}, was determined experimentally. Discrimination levels were set for each ADC and only pulses which exceeded the discrimination levels were accumulated. If amplifier gains of the scintillator channels were exactly equal and ADC discrimination levels also were exactly equal, the ratio of the sum of counts above some arbitrary level would then equal γ_{ε}. However, ordinarily gains and discrimination levels do not agree.

The ratio γ_{ε} was thus determined as follows :

1) roughly adjust the gains of both scintillators,
2) measure the pulse height spectra for a γ-ray source,
3) calibrate each scintillator before and after the measurement using a ^{22}Na γ-ray source,
4) adjust the gains of both scintillator channels by using the fitting method described in the previous section. The parameters a and b were determined on the basis of the differentiated ^{22}Na pulse height spectrum of each scintillator,
5) As the ratio of the sum of counts above the discrimination channel DC will converge when the discrimination channel approaches zero, γ_{ε} is given by :

$$\gamma_{\varepsilon} = \lim_{DC \to 0} \frac{\sum_{I=DC}^{1023} C6(I)}{\sum_{I=DC}^{1023} C7(I)}, \qquad (2.5.1)$$

where

C6(I) : counts of ^{6}Li-glass at channel I,

C7(I) : counts of ^{7}Li-glass at channel I.

The arrangement of the measurement is shown in Fig. 2.5.1. The distance between the γ-ray source and each scintillators was 1 m $\pm$ 1 mm. A 5 mCi ^{137}Cs γ-ray source was used. The measured results of the pulse height spectra are shown in Fig. 2.5.2. In Fig. 2.5.3, the results of γ_{ε} measurement is shown. In this example, the γ_{ε} comes to 0.944.

2.6 Contribution of Competing Reactions

In the ^{6}Li- and ^{7}Li-glass scintillators, neutron reactions other than the $^{6}Li(n,\alpha)^{3}T$ reaction — charged particle production reactions such as $^{6}Li(n,n'd)^{4}He$, $Al(n,\alpha)^{24}Na$ and elastic scattering such as Si(n,n)Si occur. Charged particles and recoil nuclei producd in those reactions contribute scintillation pulses. These contributions were estimated for a typical neutron spectrum in a simulated fusion blanket assembly described in Chapt. 5. The calculation of the neutron spectrum was made by the two dimensional transport code DOT3.5[23] and neutron nuclear data libralies JENDL-3T[24],*, JENDL- 3PR1[25].[26] The calculated neutron spectrum is shown in Fig. 2.6.1.
Here, it is assumed that the scintillation efficiencies for all charged particles are equal.

2.6.1 Charged Particle Production Reactions

The main charged particle production reactions occuring in the ^{6}Li- and ^{7}Li-glass scintillators placed at 14 MeV neutron field are as follows (reactions with Mg and Ce were omitted because amounts of these nuclides presents in the material are small, [see Table 2.2.2] and cross sections are also small).

	Q-value
$^{6}Li(n,n'd)^{4}He$	-1.47 MeV
$^{6}Li(n,p)^{5}He$	-2.73 MeV
$^{6}Li(n,2n)^{5}Li$	-3.70 MeV
$^{7}Li(n,n'\alpha)^{3}T$	-2.47 MeV
$^{16}O(n,\alpha)^{13}C$	-2.22 MeV
$^{28}Si(n,\alpha)^{25}Mg$	-2.65 MeV
$^{28}Si(n,p)^{27}Al$	-3.51 MeV
$^{27}Al(n,\alpha)^{24}Na$	-3.10 MeV

Cross sections for these reactions are shown in Fig. 2.6.2.

Reactions other than $^{6}Li(n,n'd)^{4}He$ and $^{7}Li(n,n'\alpha)^{3}T$

For an incident neutron energy E_n, the energy E of produced

* JENDL-3T is a temporary file for testing the evaluated data for JENDL-3. The data for JENDL-3T will be partly revised in JENDL-3.

charged particles is given by :

$$E = E_n + Q. \tag{2.6.1}$$

The reaction rates are given by :

$$R_{ij}(E_n) = N_i \sigma_{ij}(E_n) \phi(E_n), \tag{2.6.2}$$

where

N_i : number density of nuclei i,
$\sigma_{ij}(E_n)$: cross section for reaction j of nuclei i,
$\phi(E_n)$: neutron flux,
i : kind of nucleus,
j : type of reaction.

Supposing that the energy resolution of the lithium-glass scintillator were close to zero, then the energy distribution would be equal to the pulse height distribution and $R_{ij}(E_n)$ would give the pulse height spectrum at energy $E=E_n+Q$. The resultant pulse height spectra calculated by Eq. 2.6.2 are shown in Fig. 2.6.3. For all reactions, the reaction rates rise strongly at 11 - 13 MeV. The reason is that neutron flux at 14 MeV is very large as is shown in Fig. 2.6.1. However, contributions of these reactions are fairly small in the $^6Li(n,\alpha)^3T$ peak region and the fitting region below the peak. Moreover, contributions by O, Si and Al are cancelled through subtraction of the ^7Li spectrum from the ^6Li spectrum. It is therefore concluded that the effect of charged particle production reactions can be neglected.

<u>$^6Li(n,n'd)^4He$ and $^7Li(n,n'\alpha)^3T$ reactions</u>

These reactions lead to three products, one of which is a neutron that largely escapes from the scintillator; hence, only a low-energy continum should be expected even for monoenergetic incident neutrons. Assuming that the reaction energy products is invested only in the charged particles, and that the sum of energies of the two charged particles (d and α, α and t) has a simple rectanglular distributiion between zero and E_n + E, the reaction rates per unit energy are given by $R_{ij}(E_n)/E$. The overall energy distribution for all incident

neutrons is found by convolution of these rectangular distributions. Pulse height spectra calculated by this procedure for the two reactions are also shown in Fig. 2.6.3. As evident from this plot, the contribution of these reactions can be neglected.

2.6.2 Elastic Scattering

Here, elasctic scattering of ^{6}Li, ^{7}Li, O, Si and Al was considered. Cross sections for these reactions are shown in Fig. 2.6.4. Again assuming that the energy distribution of recoiled nuclei is rectangular between zero and the maximum energy E_{max} determined by the mass number A of the nucleus and the incident neutron energy E_n. The value of E_{max} is given by :

$$E_{max} = \frac{4A}{(A+1)^2} \cdot E_n \ . \qquad (2.6.3)$$

The reaction rates per unit energy come to $R_{ij}(E_n)/E_{max}(E_n)$. Overall energy distribution vs. incident neutron energy is calculated by convolution of these rectanglular distributions. Results are shown in Fig. 2.6.5. Clearly, the elastic scattering contribution can be neglected.

2.7 Chemical Analysis of the ^{6}LI-Content of ^{6}Li-Glass Scintillator

An accurate knowlege of the ^{6}Li content in the ^{6}Li-glass scintillator is required to obtain the TPR in absolute value. For this, manufacturer's data of the ^{6}Li content cannot be reliable because of volatilization loss of ^{6}Li atoms during dissolution.[27,28] Thus, a chemical analysis of the ^{6}Li content of NS15 ^{6}Li-glass scintillator was made by an isotope dilution analysis[29]

In an isotope dilution analysis, the amount of an element in a given sample is quantitatively determined as follows:[30]

1) add a fixed quantity of "spike" — a compound which has a different isotope composition than the sample,
2) mix uniformly,
3) calculate the amount of the element in the sample from the change of isotope composition.

If, X : atom number of Li($=^{6}Li+^{7}Li$) in the sample (Li-glass),

Y : atom number of Li(=^{6}Li+^{7}Li) in the spike (Li_2CO_3),

a_6 : atom fraction of ^{6}Li in the sample,

a_7 : atom fraction of ^{7}Li in the sample,

b_6 : atom fraction of ^{6}Li in the spike,

b_7 : atom fraction of ^{7}Li in the spike,

then, the isotope ratio of ^{6}Li and ^{7}Li in the mixture is given by the following equation:

$$\frac{c_6}{c_7} = \frac{a_6X + b_6Y}{a_7X + b_7Y} . \qquad (2.7.1)$$

Solving this equation for X,

$$X = \frac{c_7b_6 - c_6b_7}{c_6a_7 - c_7a_6} \cdot Y$$

$$= \frac{B-C}{C-A} \cdot \frac{b_7}{a_7} \cdot Y , \qquad (2.7.2)$$

where

$A = \frac{a_6}{a_7}$: isotope ratio of ^{6}Li and ^{7}Li in the sample,

$B = \frac{b_6}{b_7}$: isotope ratio of ^{6}Li and ^{7}Li in the spike,

$C = \frac{c_6}{c_7}$: isotope ratio of ^{6}Li and ^{7}Li in the mixture.

The isotope ratios were determined by mass spectrometry.

The samples were four 5 mm x 5 mm x 1 mm pieces of NS15 ^{6}Li-glass scintillator (5 mm x 5 mm x 1 mm) made from the batch the scintillator used in the TPR measurement was also made from. The spike was a standard sample of Li_2CO_3, NBS SRM 924 [^{6}Li content = 3.70$_6$ atom

percent]. The measured results are shown in Table 2.7.1. The average value of the ^{6}Li content was 6.63_0 weight percent (± 0.5 %). The isotopic fractions by weight w_6 and w_7 of the isotopes are given by :

$$w_6 = \frac{m_6 a_6}{m_6 a_6 + m_7 a_7}, \qquad (2.7.3)$$

$$w_7 = \frac{m_7 a_7}{m_6 a_6 + m_7 a_7}, \qquad (2.7.4)$$

where

m_6 : mass of ^{6}Li,

m_7 : mass of ^{7}Li.

Substituting 0.9549_1, 0.0450_9, 6.01512[31] and 7.01600[31] for a_6, a_7, m_6 and m_7, we obtain $w_6 = 0.9478_6$. Thus the, ^{6}Li content comes to $6.63_0 \times 0.9478_0 = 6.28_4$ wt %. This value agree with the manufacturer's data, 6.3 wt % , indicating that the loss of ^{6}Li atom due to the volatilization is small. The ^{6}Li atom number derived from this value of 6.28_4 wt % was used for the calculation of the TPR's.

2.8 Conclusion

To develop a method of measuring ^{6}Li tritium production rate of based on the difference between the response of ^{6}Li-glass and that of ^{7}Li-glass in a mixed neutron-gamma radiation field, the following measuremnts and determinations were made:

(1) The intrinsic neutron-gamma discrimination of ^{6}Li-glass scintillator was examined. Discrimination by pulse height and that by pulse shape individually as well as in combination both were found inadequate.

(2) A method of fitting pulse height spectra of ^{6}Li and ^{7}Li-glass was developed.

(3) The ratio of γ-ray detection efficiencies was measured.

(4) The contributions of competing reactions — charged particle production reactions and elastic scattering — were evaluated for

a typical neutron spectrum in a simulated fusion blanket assembly. It was shown that these contributions can be neglected.

(5) The atom number of ^{6}Li in the ^{6}Li-glass scintillator was determined by isotope dilution analysis.

By these various steps, a subtraction method of ^{6}Li and ^{7}Li-glass scintillators was established.

References

1) Yamaguchi S., et al. : Nucl. Instr. Meth. A254, 413 (1987).
2) Ginther R. J. and Schuman J. H. : IRE Trans. Nucl. Sci. NS-5, 92 (1958).
3) Bollinger L. M., et al. : Rev. Sci. Instr. 30, 1135 (1959).
4) Ginther R. J. : IRE Trans. Nucl. Sci. NS-7, 28 (1960).
5) Voitovetski V. K., et al. : Atommaya Energya 6, 321 (1959); also 472 (1959).
6) Wargin V. W. W. and Karapetyan G. O. : Glastech. Berlin 32[11], 443 (1959).
7) Anderson D. G. : "Glass Scintillators for the Detection of Nuclear Radiations", Proc. 5th Int'l Instr. Meas. Conf., Stockholm (1960).
8) Anderson D. G., et al. : Proc. 5th IM Conf., Stockholm (1960).
9) Flanagan T. P., et al. : Proc. Symp. on Photographic image devices, Imperial College (Academic Press, New York, 1962).
10) Anderson D. G., et al. : Proc. 6th Int. Congress on Glass, 429 (1962).
11) Firsk F. W. K., et al. : Nucl. Instr. Meth. 13, 313 (1961).
12) Bollinger L. M.,et al. : *ibid*. 17, 97 (1962).
13) Harris D., et al. : "Scintillation Counters for neutron Scattering Experiments" Proc. of Symp. on Inelastic Scattering of Neutrons in Solids and Liquids", Chalk River, (1962).
14) Spowart A. R. : Nucl. Instr. Meth. 75, 35 (1969).
15) Spowart A. R. : *ibid*. 82, 1 (1970).
16) Spowart A. R. : *ibid*. 135, 441 (1976).
17) Spowart A. R. : *ibid*. 140, 19 (1977).
18) Niimura N., et al. : Kakuriken Kenkyu Hokoku 13[1], 102 (1980) [in Japanese].
19) Coceva C. : Nucl. Instr. Meth. 21, 93 (1963).
20) Winyard R. A. : *ibid*. 95, 141 (1971).
21) Yamada K., et al. Kakuriken Kenkyu Hokoku 15[1], 84 (1982) [in Japanese].
22) Yamada K., et al. *ibid*. 16[1], 78 (1983).
23) Rhodes W. A. and Mynatt F. R. : "The DOT-III Two Dimensional Discrete Ordinate Transport Code," ORNL/TM-4280 (1973).
24) JENDL Compilation Group (Nuclear Data Center, JAERI) : JENDL-3T, private communication (1988).

25) Shibata K. : "Evaluation of Neutron Nuclear Data of ^{6}Li for JENDL-3," JAERI-M 84-198 (1984).

26) Kosako K. : private communication.

27) Poenitz W. P. : Z. Physik 268, 359 (1974).

28) Moxon M. C., et al. : "The measurement of the ^{6}Li content of Li loaded glass scintillators," AERE-R 8409 (1976).

29) Tamura S. and Tamura K. : private communication.

30) Komori T. and Tamura S. : Japan Analyst 23[7], 804 (1974).

31) Nuclear Data Tables, 9, 265 (1971).

Table 2.2.1 Chemical composition of lithium-glass scintillators

commercial code	type of lithium	weight percent in melt						
		SiO_2	MgO	Al_2O_3	CeO_2	Li_2O	Li	^6Li
NS15	^6Li enriched	58	4.0	18.5	4.0	15.4	6.6	6.3
BS15	^7Li enriched	57	4.0	18	4.0	17	7.9	—

Table 2.2.2 Nuclide densities of lithium-glass scintillators

commercial code	x 10^{22} atom/cm^3						
	^6Li	^7Li	O	Si	Ce	Mg	Al
NS15	1.59	0.0645	4.77	1.46	0.0366	0.149	0.546
BS15	< 0.002	1.70	4.71	1.40	0.0366	0.149	0.531

Table 2.2.3 Physical properties of lithium-glass scintillator (NS15)

refractive index	1.56	
Abbe's number	57.8	
density	2.5	[g/cm^3]
coefficient of linear expansion*	99	[x10^{-7}/°C]
transition temperature	482	[°C]
softening temperature	521	[°C]

*) 100°C ∿ 300°C

Table 2.7.1 Results on isotopic dilution analysis of ^6Li content

No. of piece	^6Li enrichment [^6Li atom %]	Li content [wt %]	Li_2O content [wt %]
1	95.49_1	———	———
2	95.49_1	6.62_8	15.38
3	95.49_5	6.63_3	15.39
4	95.48_8	6.63_0	15.38
average	95.49_1	6.63_0	15.38

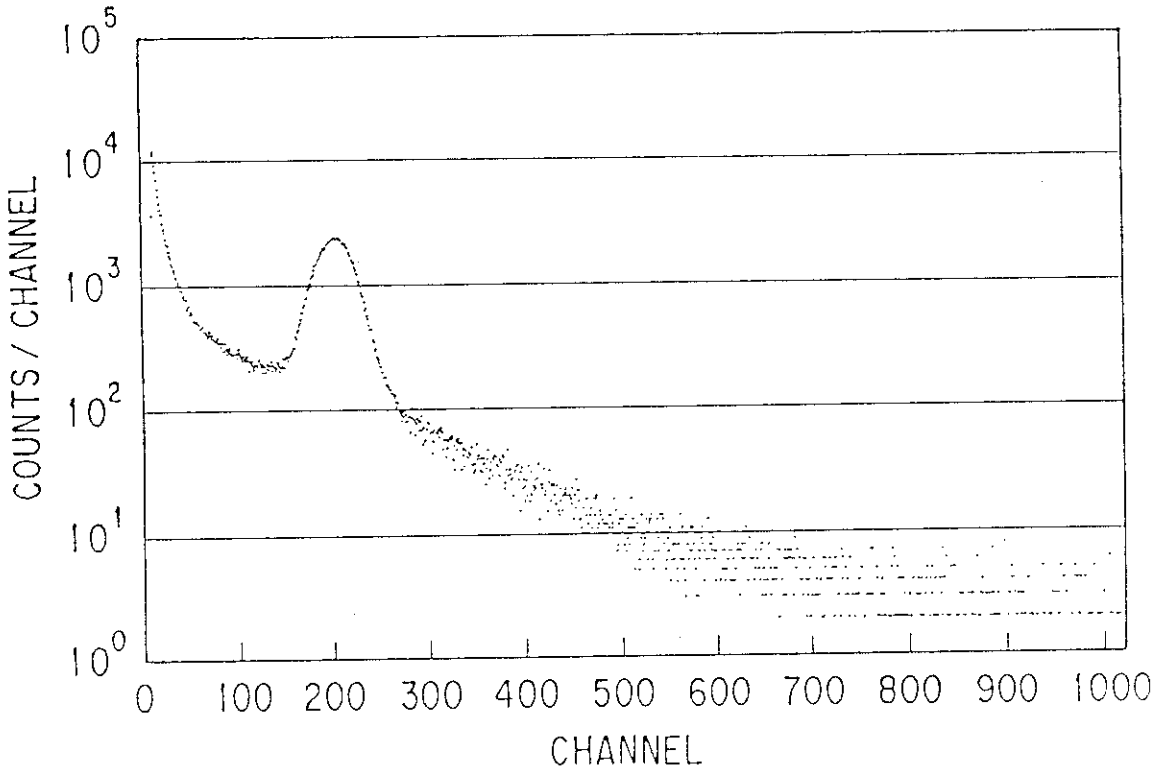

(a)

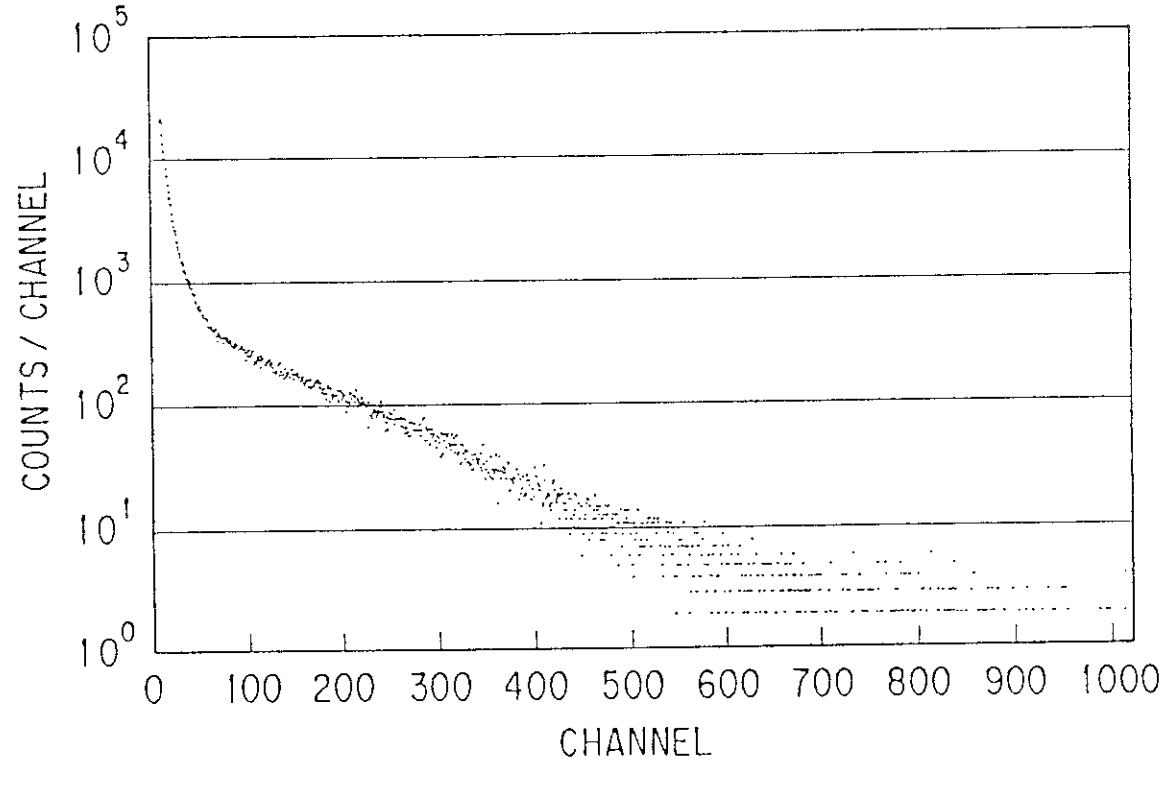

(b)

Fig. 2.1.1 Typical pulse-height spectra measured with (a) ^{6}Li-glass and (b) ^{7}Li-glass scintillators in a simulated fusion blanket assembly

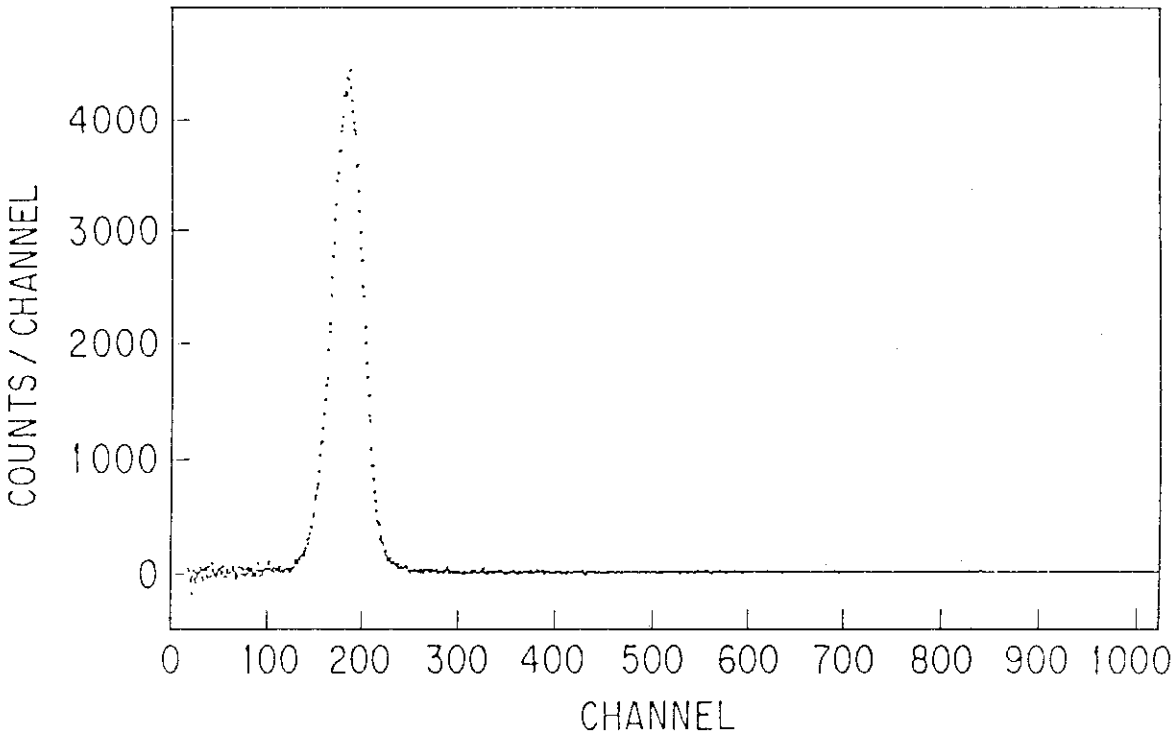

Fig. 2.1.2 Typical subtracted spectrum

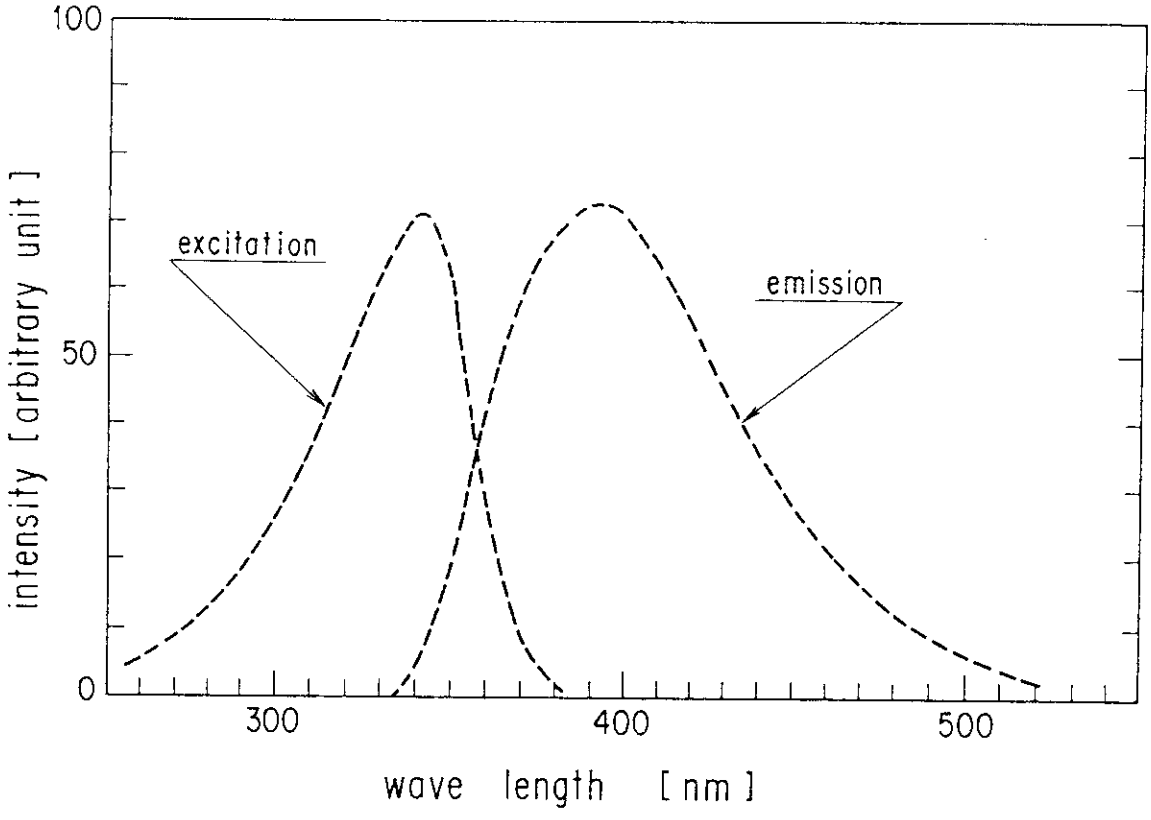

Fig. 2.2.1 Excitation and emission spectra of NS15 ^{6}Li-glass scintillator

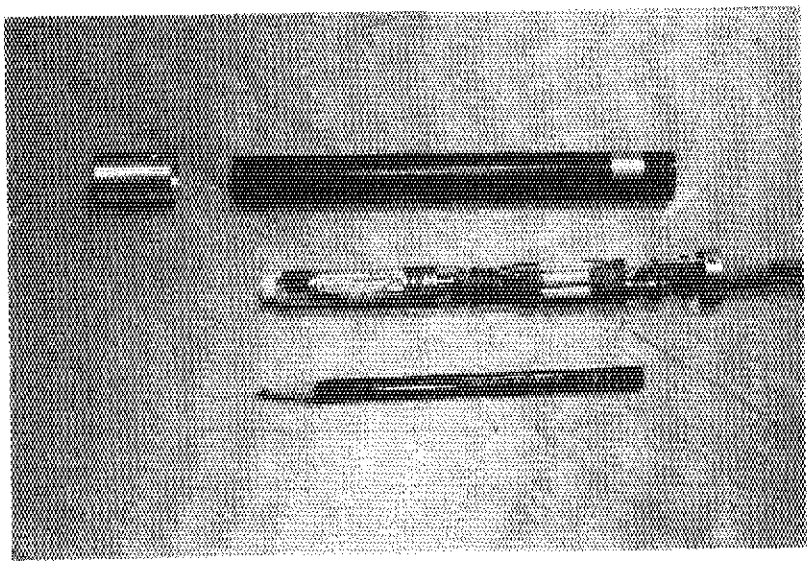

Fig. 2.2.2 Detector Assembly

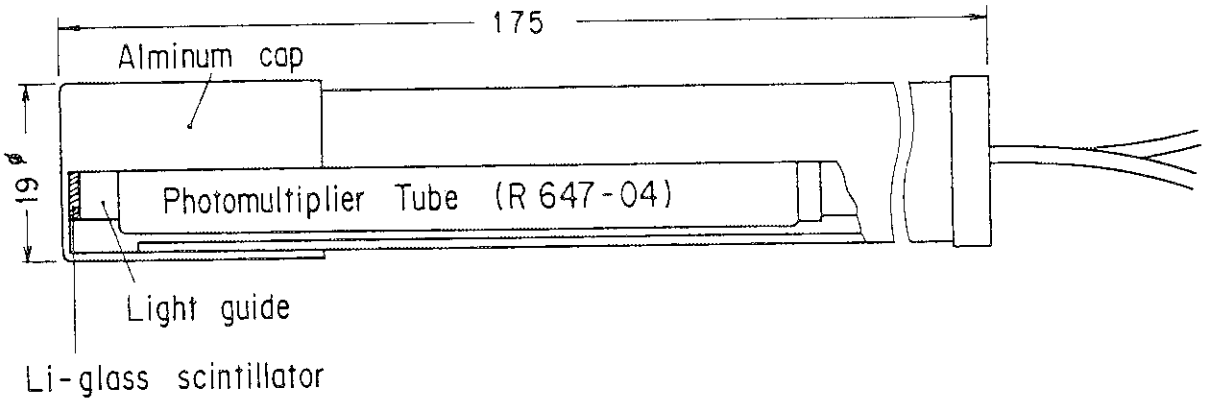

Fig. 2.2.3 Cross sectional view of Li-glass detector

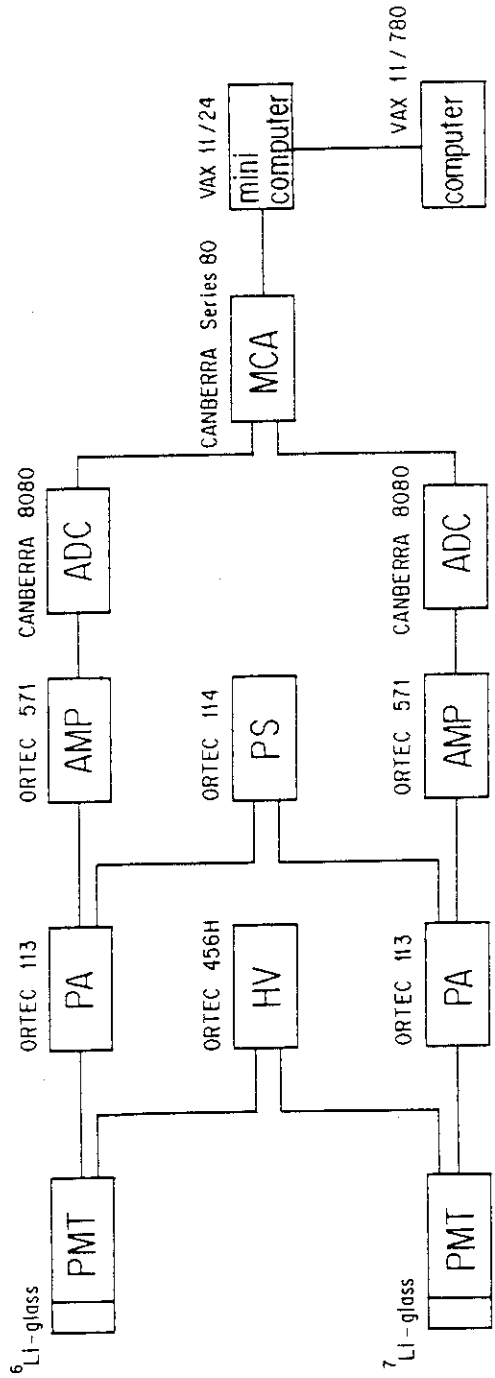

PMT : Photo-Multiplier Tube

PA : Pre-Amprefier

PS : Power Supply

HV : High Voltage Power Supply

AMP : Linear Amplifier

ADC : Analogue to Digital Converter

MCA : Multi Channel Pulse Height Analyzer

Fig. 2.2.4 Schematic diagram of electronic circuit

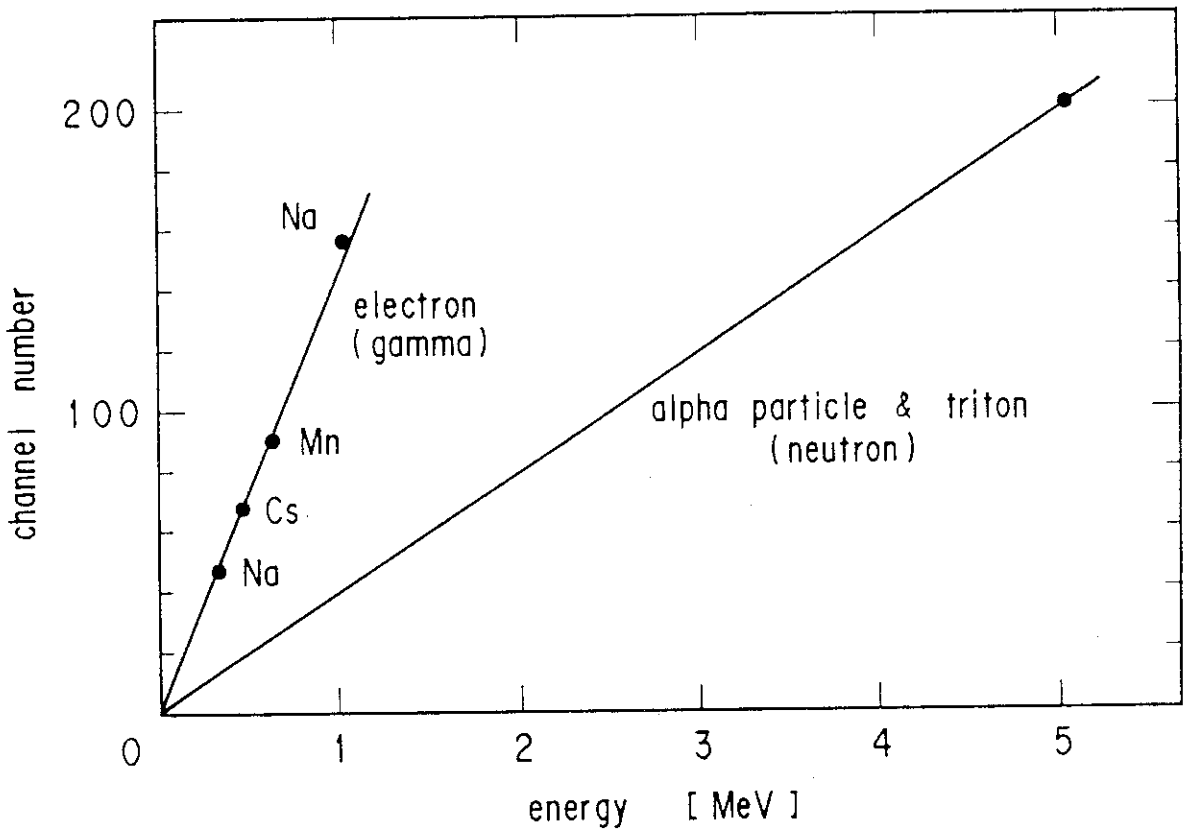

Fig. 2.3.1 Relation between energy and pulse heihght for neutron and gamma-ray

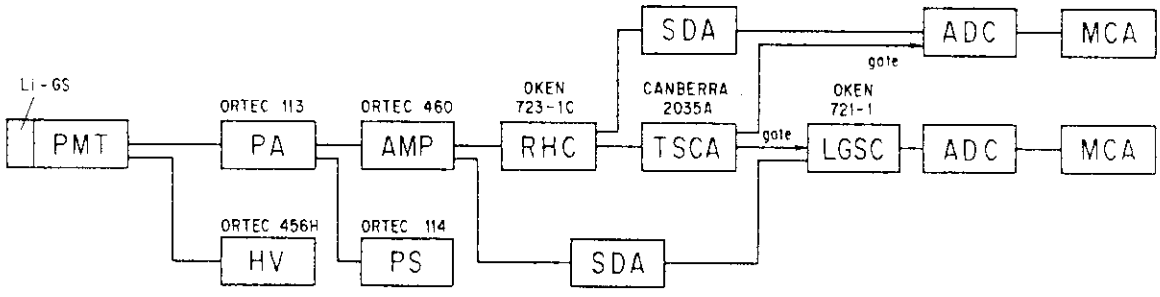

PMT : Photo-Multiplier Tube

PA : Pre Amprefier

PS : Power Supply

HV : High Voltage Power Supply

AMP : Linear Amplifier

RHC : Rise Time to Height Converter

SDA : Sum Delay Amplifier

TSCA : Timing Single Channel Analyzer

LGSC : Linear Gate and Slow Coincidence

ADC : Analogue to Digital Converter

MCA : Multi Channel Pulse HEight Analyzer

Fig. 2.3.2 Schematic diagram of electronic circuit for neutron-gamma discrimination

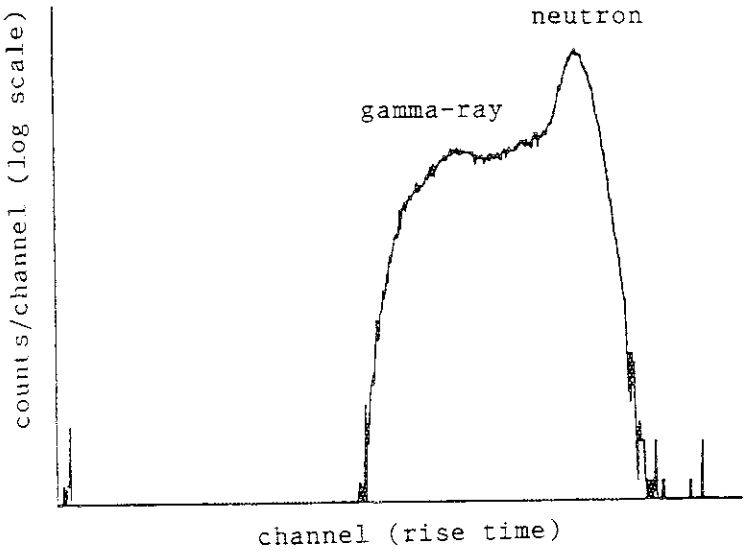

Fig. 2.3.3 Rise time distribution of lithium-glass scintillator

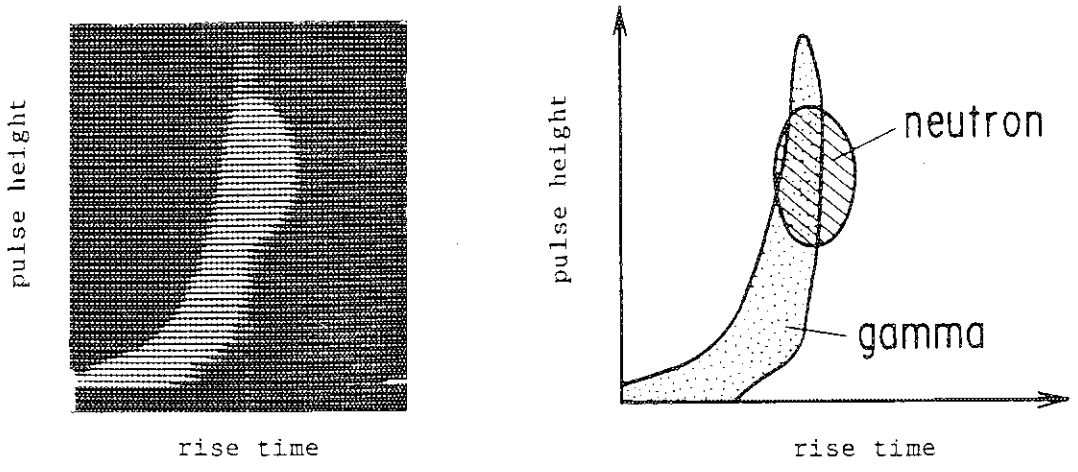

Fig. 2.3.4 Two dimensional map of rise time and pulse height

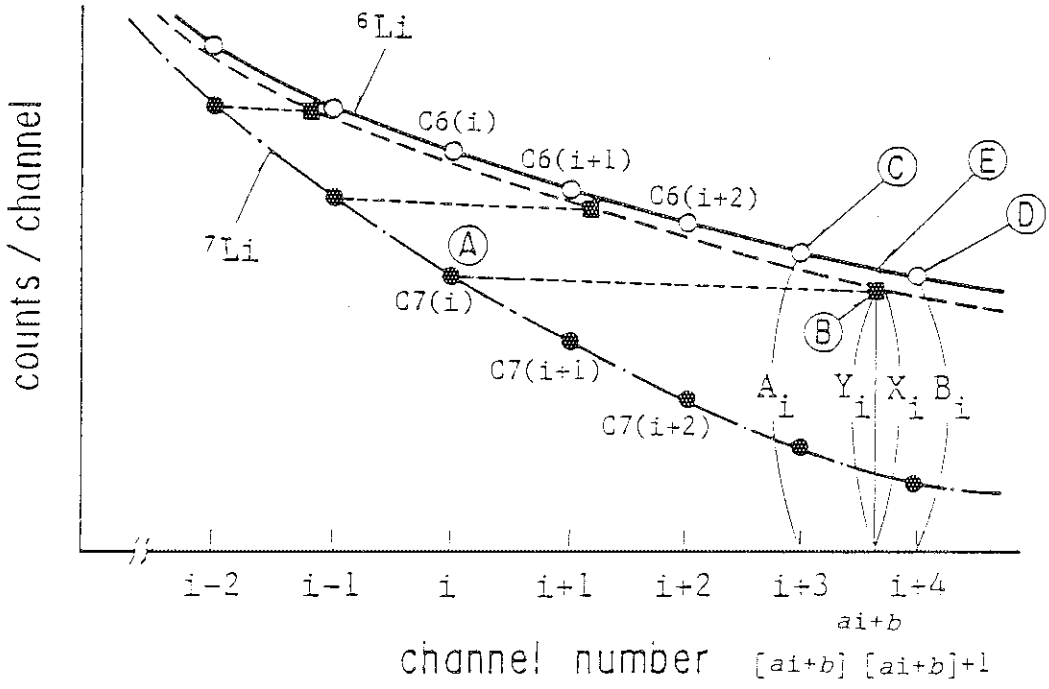

Fig. 2.4.1 Coordiate transformation of pulse height spectrum

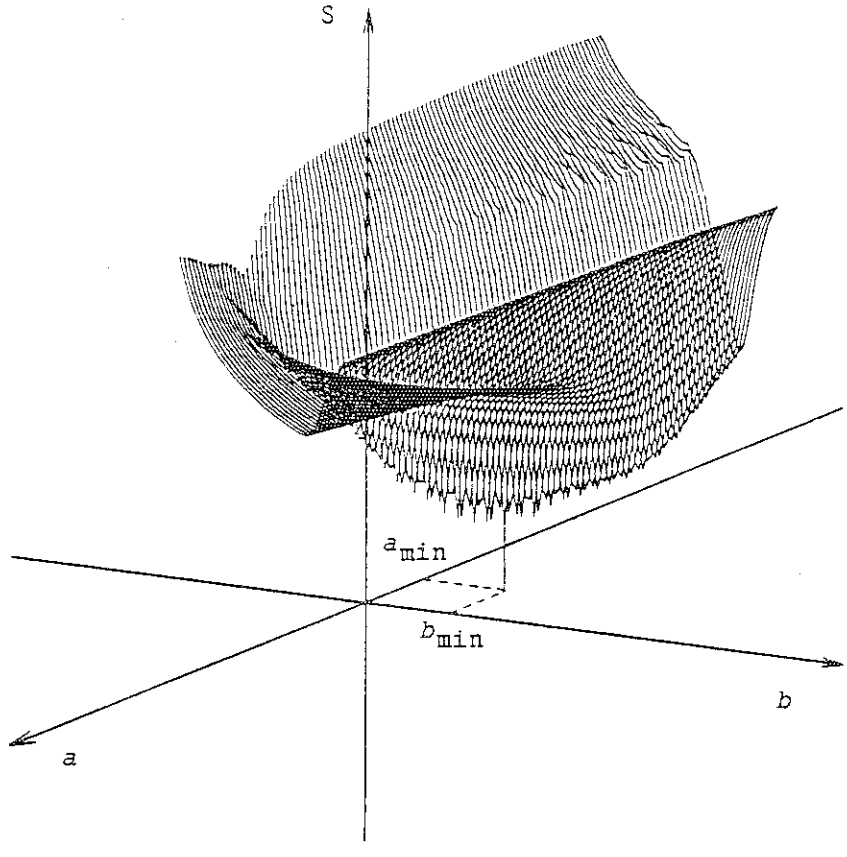

Fig. 2.4.2 Values of S as a function of a and b

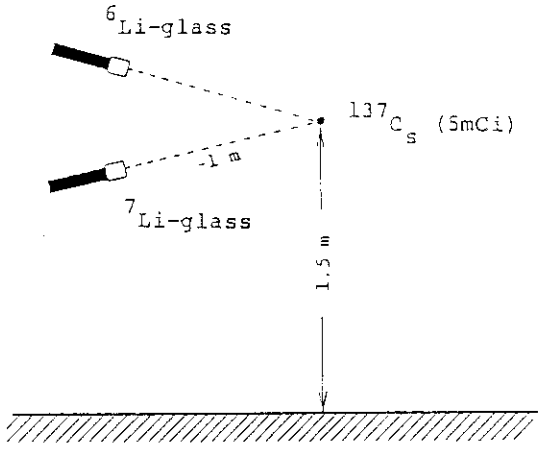

Fig. 2.5.1 Measurement of γ-ray detection efficiency ratio of ^{6}Li and ^{7}Li-glass scintillators

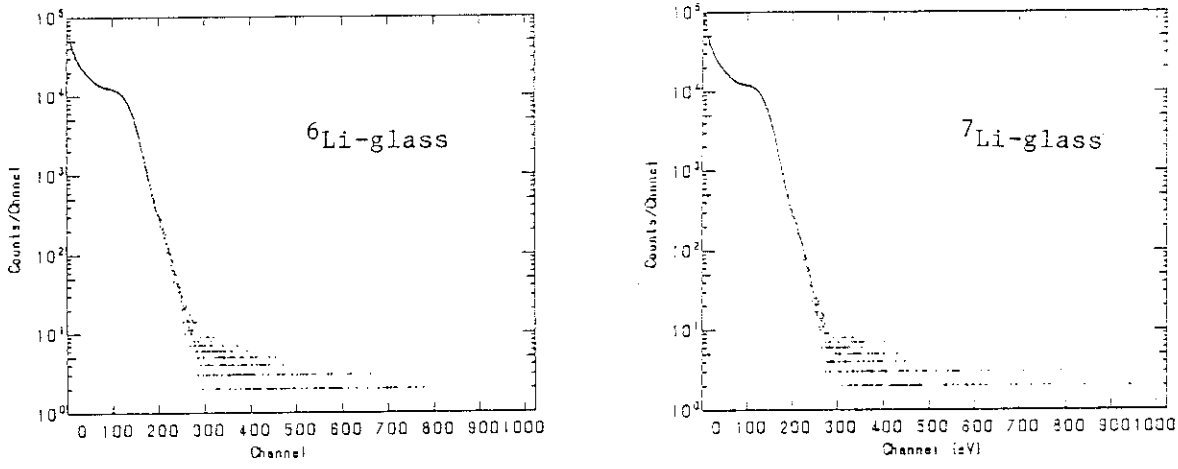

Fig. 2.5.2 Pulse height spectra of ^{6}Li and ^{7}Li-glass scintillators for ^{137}Cs

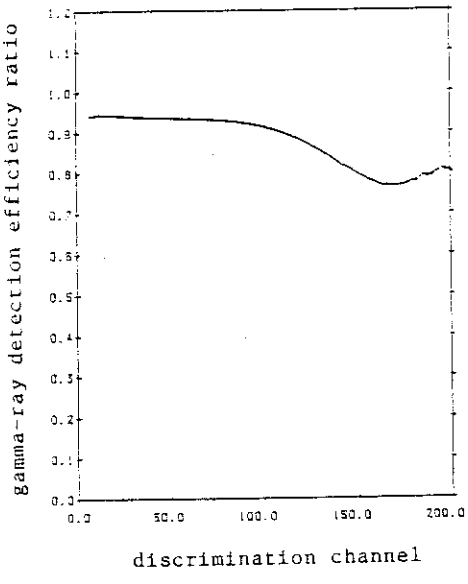

Fig. 2.5.3 Gamma-ray detection efficiency ratio (γ-ray detection efficiency of ^{6}Li-glass / γ-ray detection efficiency of ^{7}Li-glass

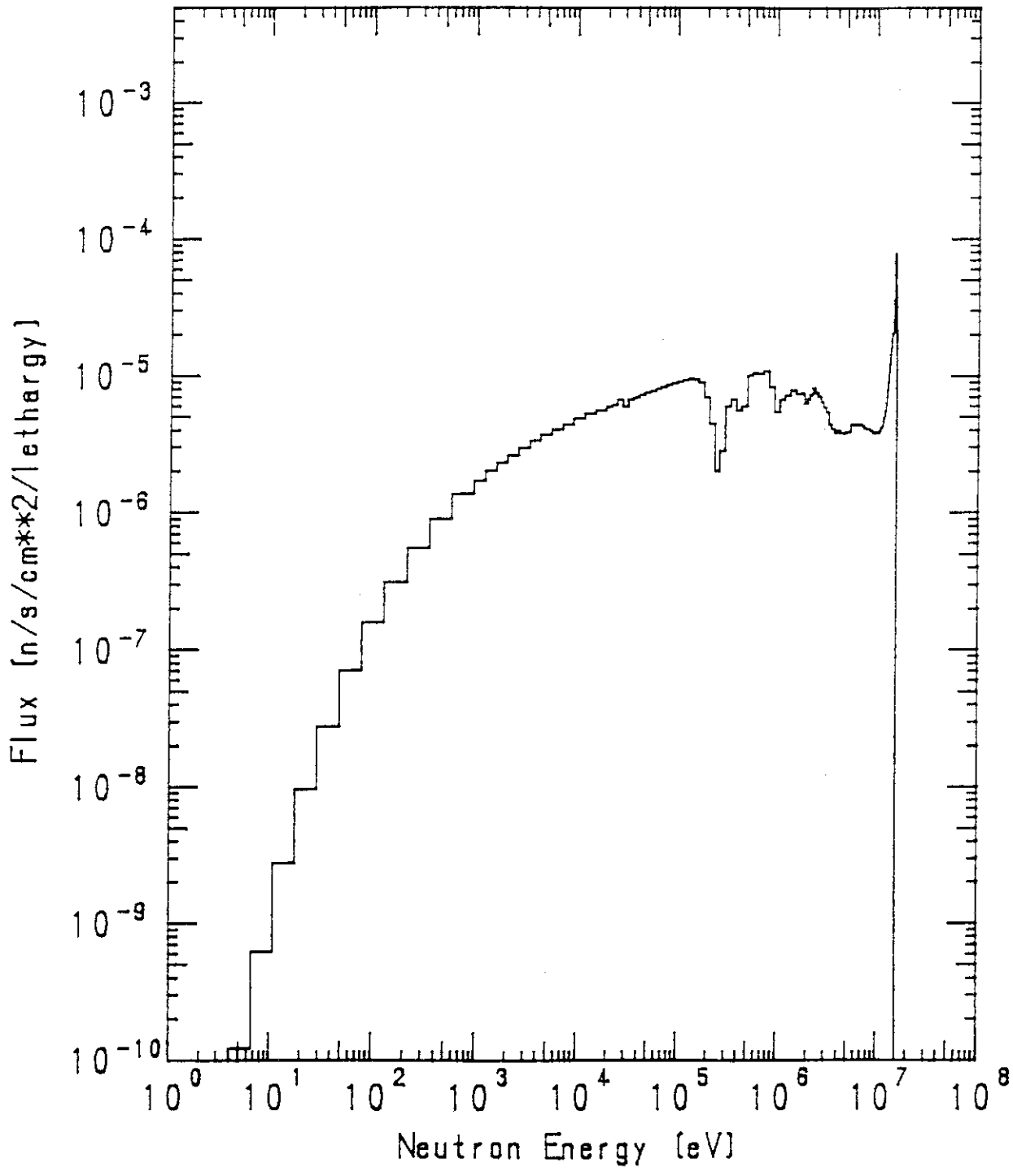

Fig. 2.6.1 Typical calculated neutron spectrum in a simulated fusion blanket assembly

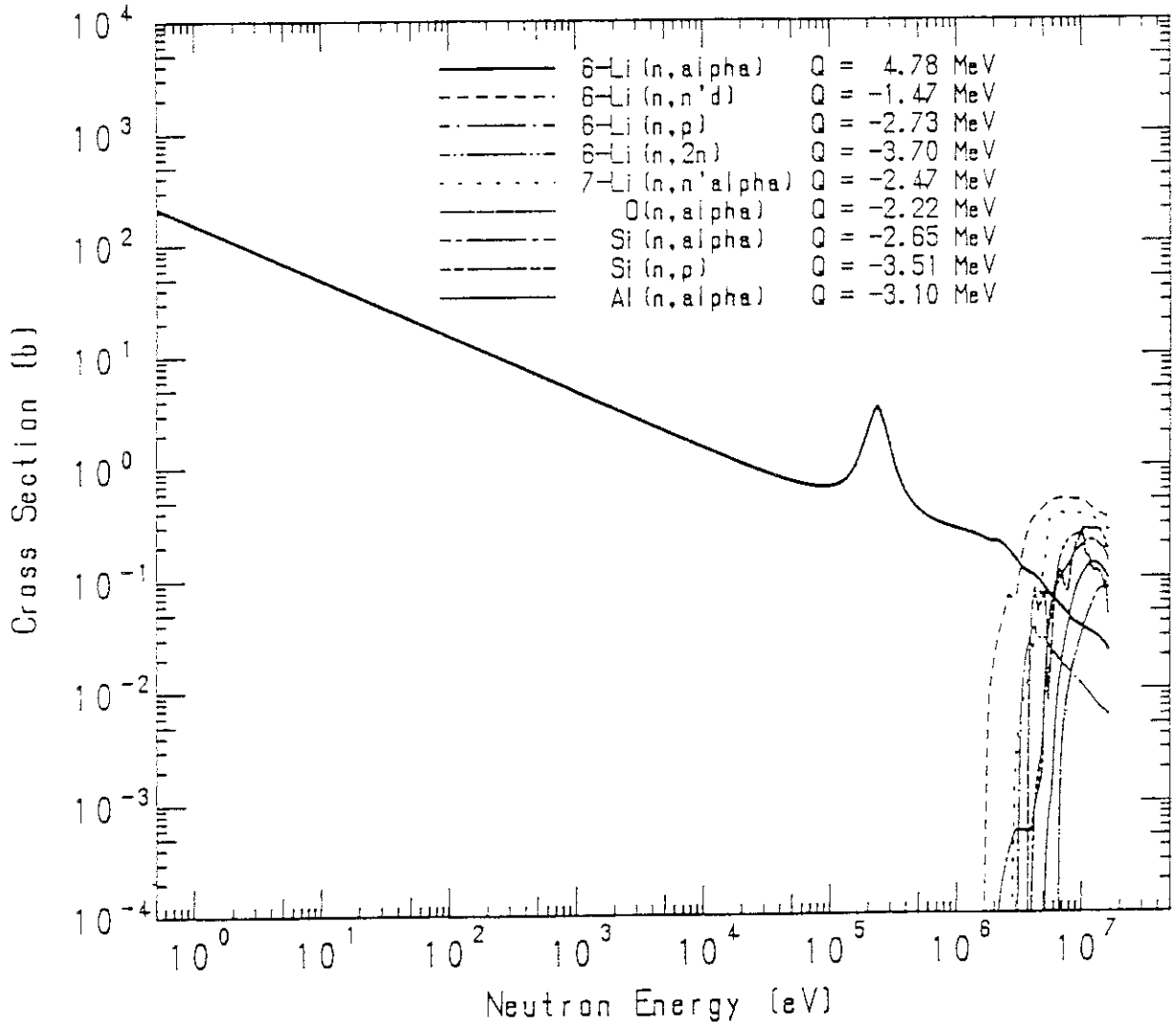

Fig. 2.6.2 Charged particle production cross sections of ^{6}Li, ^{7}Li, O, Si and Al

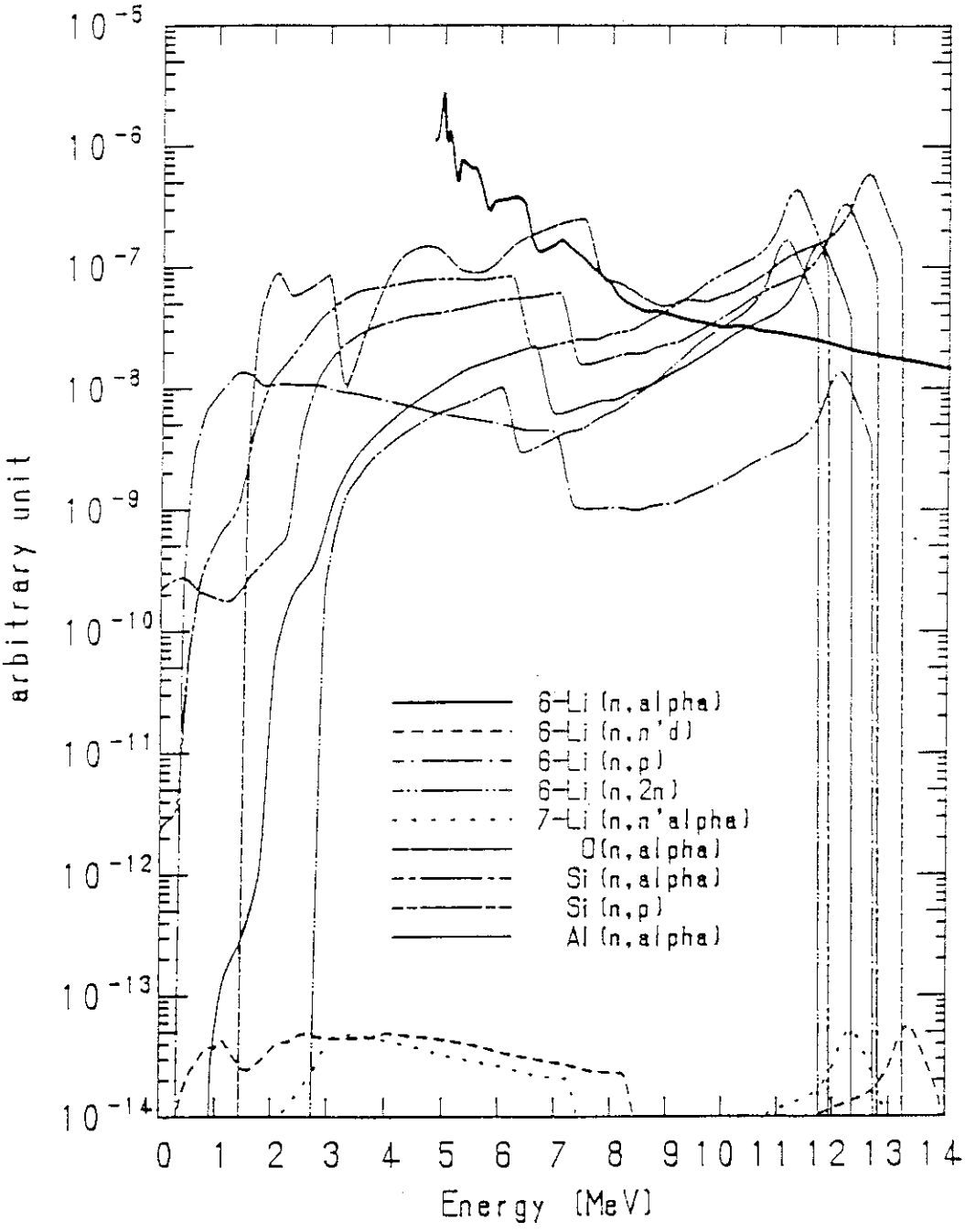

Fig. 2.6.3 Contribution of charged particle production reactions of ^{6}Li, ^{7}Li, O, Si and Al

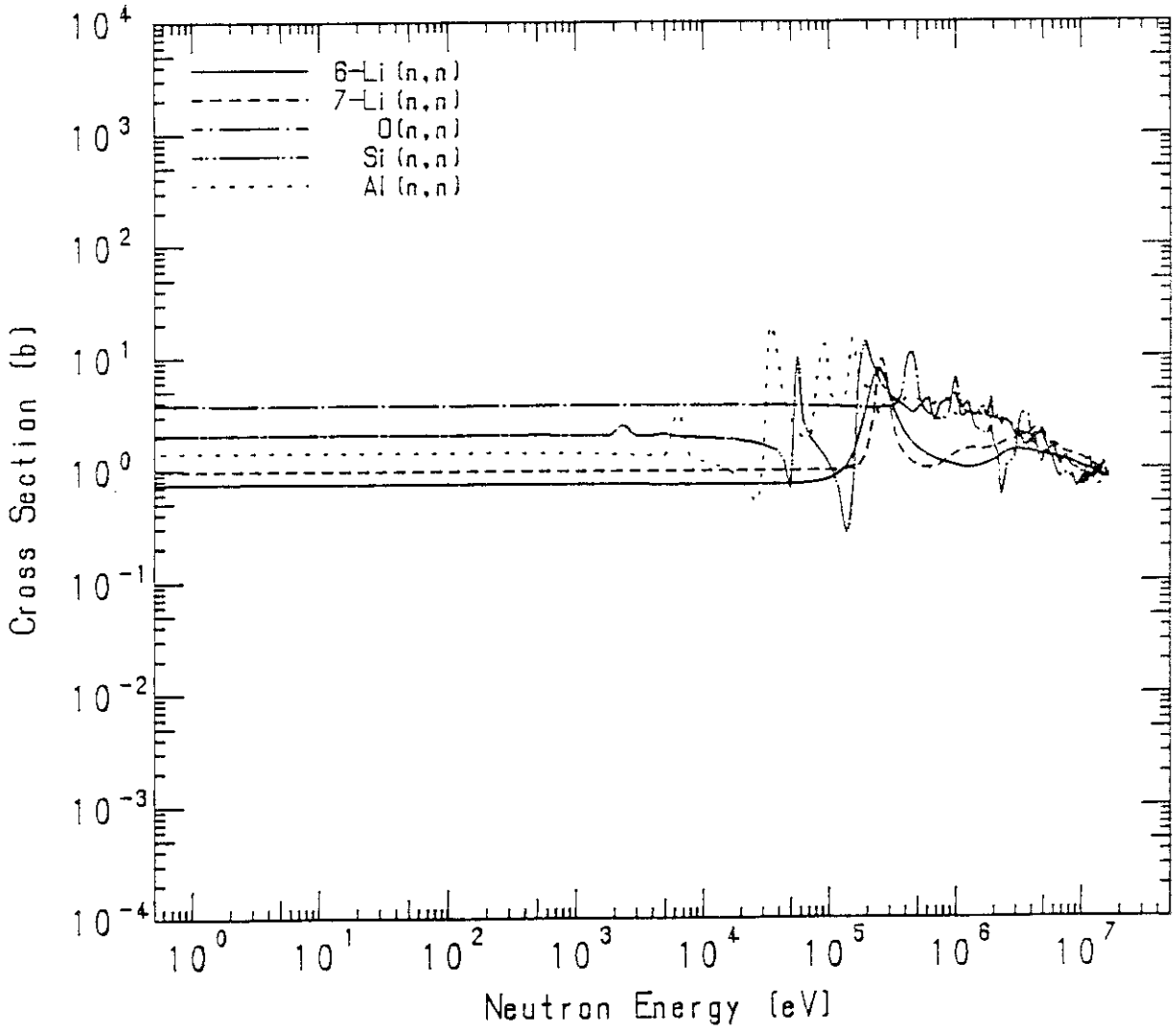

Fig. 2.6.4 Elastic scattering cross section of ^{6}Li, ^{7}Li, O, Si, and Al

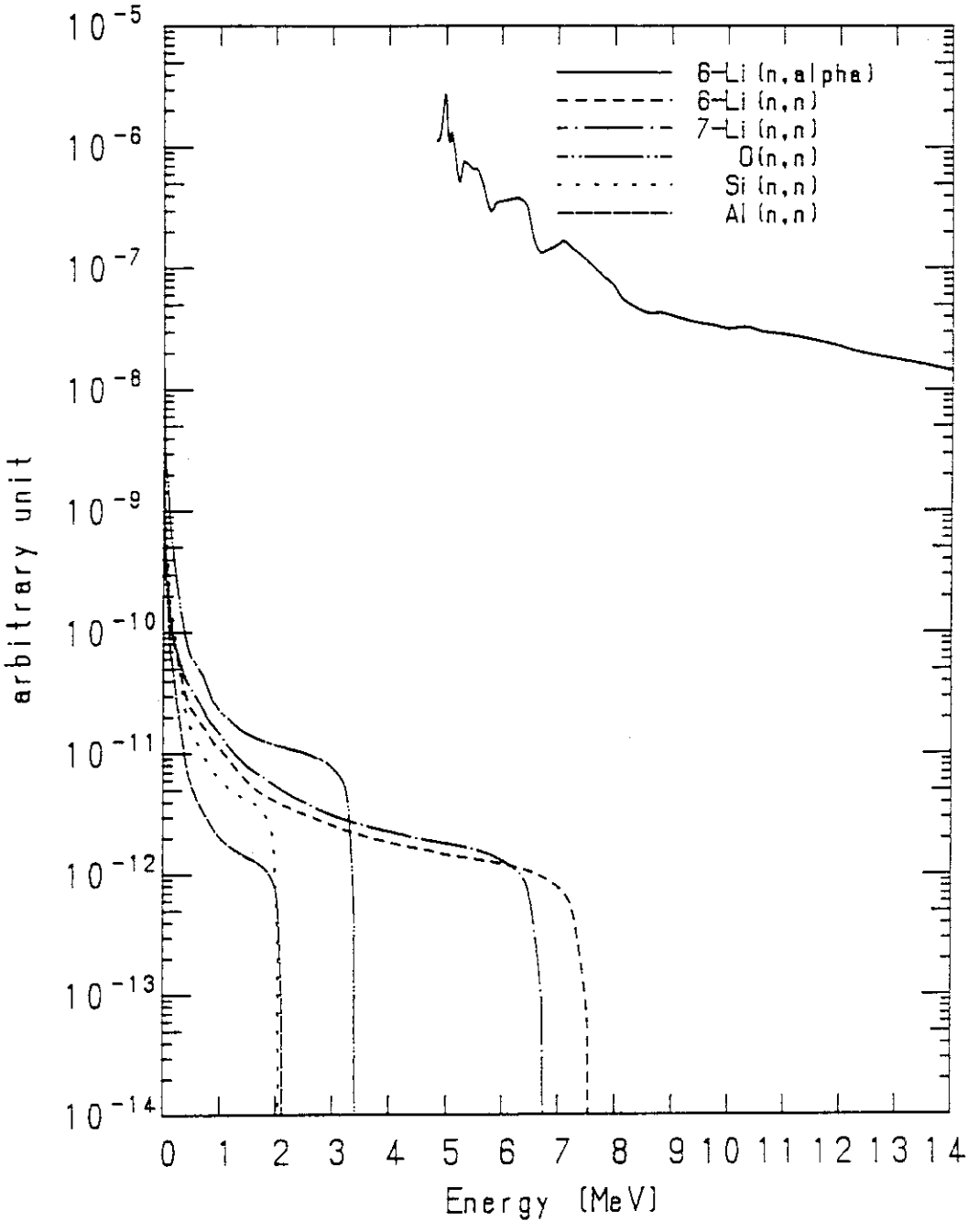

Fig. 2.6.5 Contribution of elastic scattering of ^{6}Li, ^{7}Li, O, Si and Al

3. Flux Perturbation by the Lithium-Glass Scintillator[1)]

3.1 Introduction

In simulated fusion blanket assemblies, lithium compounds such as Li_2O, beryllium and graphite are employed as a breeder, neutron multiplier and reflector, respectively (see Chap 5). A transport calculation indicated that the energy region which contributed mainly to the tritium production in Li_2O was near the 250 keV resonance. For this energy region, the effect of the probe on the local flux —— self-shielding and flux perturbation —— can be neglected for a 0.3 mm thick scintillator.[2)] However, for the soft neutron spectrum near a beryllium or graphite layer, the effect is appreciable for that thickness.[2)] The perturbation of a thermal flux by activation foils such as gold or indium has been extensively examined by experimental and theoretical investigations.[3~7)] On the other hand, very few reports have considered the flux perturbation effect of enriched ^6Li glass scintillators.

The flux perturbation factor G is given by the ratio of the (n,α) reaction rate per ^6Li atom, R, in the scintillator to that of an infinitely thin glass, R_0: $G=R/R_0$. In this chapter, thermal flux measurement of these factors for four thicknesses and three ^6Li contents are described. The flux perturbation factors for these glasses were calculated by a modified Skyrme theory[7)] to confirm its applicability to lithium-glass scintillators and to examine the ratio of flux depression and self-shielding effect. A calculation of the self-shielding was also performed by a Monte Carlo method to determine its energy dependence.

3.2 Measurement

The reaction rates of ^6Li-glasses were obtained by integrating pulse height spectra measured in a thermal neutron field. Values were normalized to the number of ^6Li atom in each scintillator and to the neutron flux. The scintillators used included NS15[8)], NS3 and NS1 manufactured by the Nikon Corp. The ^6Li content in the melt of these scintillators comes to 6.30, 3.14 and 1.03 weight percent, respectively. The chemical compositions of these scintillators are shown in

Table 3.2.1. The enrichment of ^{6}Li is 95.6 % for all scintillators. NS1 has the lowest content of ^{6}Li among of currently available ^{6}Li-glass scintillators currently available. All samples had a diameter of 10 mm. Thicknesses had nominal values of 0.1, 0.3, 0.6 and 1.0 mm for each type. Actual thicknesses were measured by a digital micrometer with a precision of 5∿10 μm. These measurements are shown in Table 3.2.2. In the integration of the pulse height spectra, the "tail" on the lower energy side of the thermal peak due to the edge-effect[10] (see Chap. 4) was taken into account because it makes a considerable contribution for thin scintillators. Each scintillator wax coupled to a 13 mm diameter photomultiplier tube (Hamamatsu Photonics Corp. R647-01) using a quartz light guide with silicon grease. The electronic circuit was the same as that in Chap. 2. The gamma-ray background at the thermal peak was negligible because of the very low level of gamma flux in the graphite pile. The thermal neutron field was produced by an Am-Be neutron source located at the center of a graphite pile of 1 m x 1 m x 0.9 m, scintillators were placed at a depth of 50 mm from the top of the pile (see Fig. 3.2.1).

The measured perturbation factors are shown in Table 3.2.2 and in Fig. 3.2.2 as a function of scintillator thickness, t. In Table 3.2.2, τ is the thickness times detector absorption cross section ; $\tau=N\sigma_a t$, where, N the atom density of ^{6}Li in the scintillator, σ_a the average microscopic cross section of the $^{6}Li(n,\alpha)^{3}T$ reaction for a Maxwell distribution of thermal neutrons (σ_a = 833 b), and t the thickness of the scintillator. Values of "infinitely thin" reaction rates R_0's were determined by extrapolating t to zero. The experimental error due to the uncertainty of the extrapolation is about 2 - 3 %. It is shown that the reaction rate decrease due to the flux perturbation amounts to 66 % and 3 % for 6.3 wt %, 1.0 mm scintillator (τ = 1.37) and 1.0 wt %, 0.1 mm scintillator (τ = 0.0264), respectively.

3.3 Calculation of the Flux Perturbation by the Modified Skyrme Theory

The theoretical treatment of the local perturbation in a thermal neutron field due to absorbing detector was originally developed by Skyrme[3]. His theory was modified by Ritchie and Eldridge[4] for the flux depression, an "edge-correction" ,i.e., correction for finite size of the detector was obtained by Hanna[7]. In this treatment,

labelled MS (modified Skyrme theory), the flux perturbation factor for $1/v$ absorber in a Maxwellian spectrum is given by;

$$G = \frac{R}{R_0} = \frac{\bar{\alpha}}{2\bar{\tau}} \cdot \frac{1+\bar{\varepsilon}}{1+g\bar{\alpha}/2}, \qquad (3.3.1)$$

where

$\bar{\alpha}$: spectrum averaged value of α ($= 1-2\int_1^\infty x^{-3}\exp(-\tau x)dx$),

$\bar{\varepsilon}$: $(2\bar{\tau}/\bar{\alpha})(t/\pi r)(1-\sqrt{\pi}\tau_0/3)$,

r : detector radius,

g : flux depression parameter,

τ : product of thickness and detector absorption cross section.

The subscript zero denotes the value at the most probable velocity (2200 m/s). For graphite, beryllium and other nonhydrogeneous moderators, where $r \ll \lambda_{tr}$ (transport mean free path), $g = 0.84r/\lambda_s$, according to Meister.[11] $g = 0.84r/\lambda_s$. The values of transport and scattering mean free path and flux depression parameter for graphite are $\lambda_{tr} = 2.5$, $\lambda_s = 2.4$ cm and $g = 0.18$ respectively. Values of G calculated by the MS theory are shown in Table 3.2.2 and Fig. 3.2.2. These results agree well with the measurements described in the foregoing. Values of $(\bar{\alpha}/2\bar{\tau})\cdot(1+\bar{\varepsilon})$, which account for self-shielding only, are also shown in Fig. 3.2.2. It is evident that the overall flux perturbation is mainly caused by self-shielding.

The fact that the flux perturbation factor of ^{6}Li-glass in graphite was closely predicted by the MS theory suggests that the flux perturbation factor for arbitrary thickness and ^{6}Li content can be calculated by this theory to sufficient accuracy. Accordingly, calculations of the perturbation factors of beryllium weree also calculated by this theory. The values of the transport and scattering mean free path and flux depression parameter for beryllium are $\lambda_{tr} = 1.5$, $\lambda_s = 1.4$ cm and $g = 0.30$, respectively. The beryllium flux depression comes out slightly larger than that for graphite.

3.4 Calculation of the Self-Shielding Effect by a Monte Carlo Method

The self-shielding effect was calculated by a Monte Carlo method, assuming isotropic incidence of neutrons and dominance of absorption

compared with scattering in the detector. These assumptions are valid for thermal neutrons in a large graphite pile. For a disk-shaped detector whose symmetry axis is oriented at angle θ to a collimated beam of thermal neutrons, the self-shielding factor G is given by

$$G(N,t,\theta,\mathbf{r}) = \frac{1-\exp(-\sum_a(N)\cdot d(\theta,\mathbf{r},t))}{\sum_a(N)\cdot d(\theta,\mathbf{r},t)}, \qquad (3.4.1)$$

where $\sum_a(=N\sigma_a)$ = macroscopic absorption cross section, $\mathbf{r}$ = incident point and d = path length of the neutron.

The self-shielding factor for all neutrons of incident angle θ is obtained by averaging over all incident points:

$$G(N,t,\theta) = \langle G(N,t,\theta,\mathbf{r})\rangle_{\mathbf{r}} . \qquad (3.4.2)$$

Since it is cumbersome to obtain $G(N,t,\theta)$ analytically, the values of $G(N,t,\theta)$ were obtained by a Monte Carlo method for several angles. Assuming isotropic incidence of neutrons, the self-shielding factor is obtained by averaging over the incident angles :

$$G(N,t) = \langle G(N,t,\theta)\rangle_{\theta} . \qquad (3.4.3)$$

The calculated results of are shown in Table 3.2.2 and Fig. 3.2.2. They appear to agree fairly well with the measured R/R_0's, supporting the result of the MS treatment, i.e., self-shielding dominates the flux perturbation. Since the results of the measurement agree well with the Monte Carlo calculation, it seems reasonable to extend the Monte Carlo calculation to other neutron energies, to the extend to which the assumptions of isotropic incidence of neutrons and dominance of absorption over scattering are valid. The self-shielding factors for ^{6}Li-glasses of 0.1, 0.3, 0.6 and 1.0 mm thickness and 1.0, 3.1 and 6.3 weight percent of ^{6}Li were thus calculated for neutron energy from thermal to 16 MeV. ^{6}Li(n, α) ^{3}T cross section from the JENDL-3T[12] library were used. The calculated results are shown in Fig. 3.4.1. This figure shows that the energy range witin which the self-shielding effect is significant extends to less than 1 keV. Since, within that range, the scattering cross section is indeed

negligibly small compared with the absorption cross section, the latter assumption is valid. Moreover, a transport calculation indicated that except at the assembly surface, neutrons below 1 keV were almost isotropic even for anisotropic neutrons. Therefore, the former assumption is also valid. This suggests that the extension of this Monte Carlo calculation over all the neutron energies does not introduce serious errors. In so far as neutrons below 1 keV are dominant for tritium production, the self-shielding factor amounts to a fairly large values. Figure 3.4.1 also shows that the self-shielding effect at 250 keV should be taken into account in thick and high ^{6}Li content glass. Neglect of this effect for such a scintillator in the Li_2O region causes underestimation of the tritium production rate.

3.5 Conclusion

The thermal flux perturbation of ^{6}Li glass scintillators was measured in a graphite pile over a range of for thicknesses and for different ^{6}Li contents. The measurements revealed a decrease of the reaction rate per ^{6}Li atom ranging from 66 % for 1 mm thick, 6.3 wt % glass (τ=1.37), down to 3 % for 0.1 mm thick, 1.0 wt % glass (τ=0.0264). Close agreement between measured and results calculated by the modified Skyrme theory was obtained leading to the conclusion that the flux perturbation of ^{6}Li-glass scintillators of arbitrary thickness and ^{6}Li content can be predicted with reasonable accuracy by this treatment. It was also shown that the overall flux perturbation is mainly caused by self-shielding and that the contribution of the local flux depression tends to be small compared with self-shielding. The energy dependence of the self-shielding effect was examined by a Monte Carlo calculations, which revealed that the effect is negligibly small above 1 keV while it is large below 1 keV.

Using the modified Skyrme theory or the Monte Carlo calculations, the flux perturbation can be corrected to obtain unperturbed TPR values. However, comparison between measured and calculated values in Table 3.2.2 indicates that up to 10 % error in the TPR could be introduced if scintillators with large τ values are used in a soft spectrum, (66 % correction factor). On the other hand, the correction is only 3 % for 0.1 mm thik, 1 % ^{6}Li content glass in this neutron field.

It is therefore recomended to use small τ and large τ scintillators in a suitable combination. The former should be applied to measure the TPR in the soft spectrum near beryllium or graphite layers, while the latter can be used in the harder spectrum of the bulk of the Li_2O breeder region where it would take much time for the small τ scintillator to accumulate adequate statistics.

References

1) Yamaguchi S. : Nucl. Instr. Meth. A274, 568 (1989).
2) Yamaguchi S. and Nakamura T. : "Tritium Production Measurements by the Lithium-Glass Scintillator Method," Proc. 7th Topical Meeting on the Technol. Fusion Energy ; Fusion Technol. 10, 573 (1986).
3) Skyrme T. H. R. : AERE reports MS-91 and MS-91A (1944), 2nd ed. (1961).
4) Ritchie R. H. and Eldridge H. B. : Nucl. Sci. Eng. 8, 300 (1960).
5) Dalton G. R. and Osborn R. K. : Nucl. Sci. Eng. 9, 198 (1961).
6) Beyster J. R., et al. Nucl. Sci. Eng. 9, 168 (1961).
7) Hanna G. C. : Nucl. Sci. Eng. 15, 325 (1963).
8) Niimura N., et al : Kakuriken Kenkyu Hokoku 13, 102 (1980) [in Japanese].
9) Tamura S. and Tamura K. : private communication (1985).
10) Yamaguchi S. : Nucl. Instr. Meth. A274, 573 (1989).
11) Meister H. : Z. Naturforsch. 10a, 669 (1955).
12) JENDL Compilation Group (Nuclear Data Center, JAERI) : JENDL-3T, private communication (1988).

Table 3.2.1 Chemical composition of NS15, NS3 and NS1 lithium-glass scintillators

commercial code	weight percent in melt					
	SiO_2	MgO	Al_2O_3	CeO_2	Li_2O	^6Li
NS15	58	4.0	18.5	4.0	15.4	6.3
NS3	56.6	21.5	10.9	4.0	7.0	3.14
NS1	59.6	22.6	11.5	4.0	2.3	1.03

Table 3.2.2 Measured and calculated values of R/R_0

commercial code	^6Li [w/o]	N [atom/cm^3]	t [mm] nominal	t [mm] measured	τ	R/R_0 expt.	R/R_0 MC*	R/R_0 MS**
NS15	6.30	1.60×10^{22}	0.1	0.096	0.128	0.831±0.026	0.829	0.798
			0.3	0.308	0.411	0.587±0.018	0.611	0.591
			0.6	0.616	0.821	0.434±0.013	0.451	0.431
			1.0	1.026	1.37	0.339±0.011	0.340	0.306
NS3	3.14	7.80×10^{21}	0.1	0.082	0.0533	0.882±0.018	0.919	0.894
			0.3	0.287	0.187	0.754±0.015	0.764	0.750
			0.6	0.595	0.387	0.631±0.013	0.622	0.618
			1.0	1.04	0.676	0.540±0.011	0.499	0.497
NS1	1.03	2.56×10^{21}	0.1	0.124	0.0264	0.967±0.024	0.956	0.943
			0.3	0.323	0.0689	0.877±0.022	0.889	0.886
			0.6	0.616	0.131	0.820±0.021	0.808	0.824
			1.0	1.07	0.228	0.787±0.020	0.712	0.755

* Monte Carlo

** Modified Skyrme theory

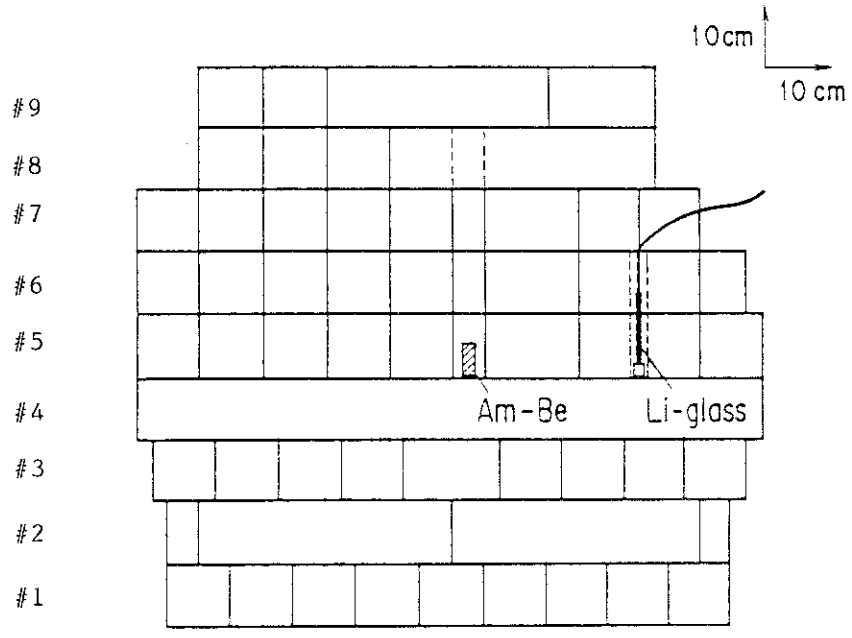

(a)

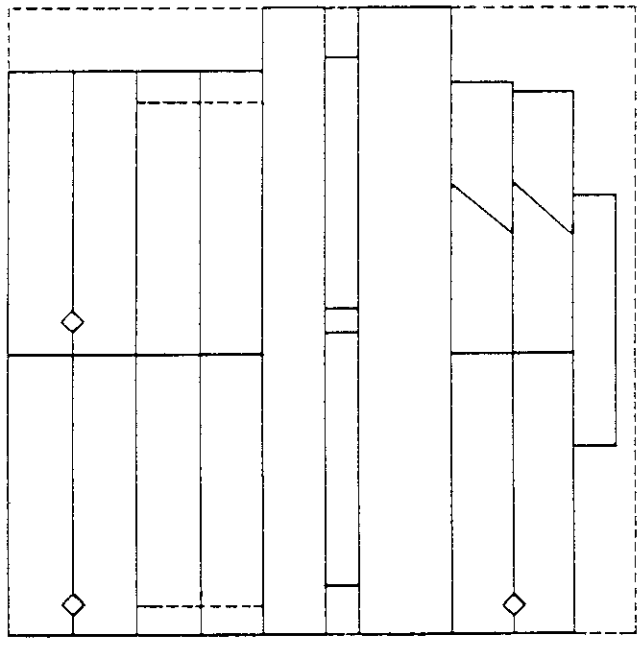

(b)

Fig. 3.2.1 Graphite pile, (a) crosssectional view, (b) plane view at #7 layer

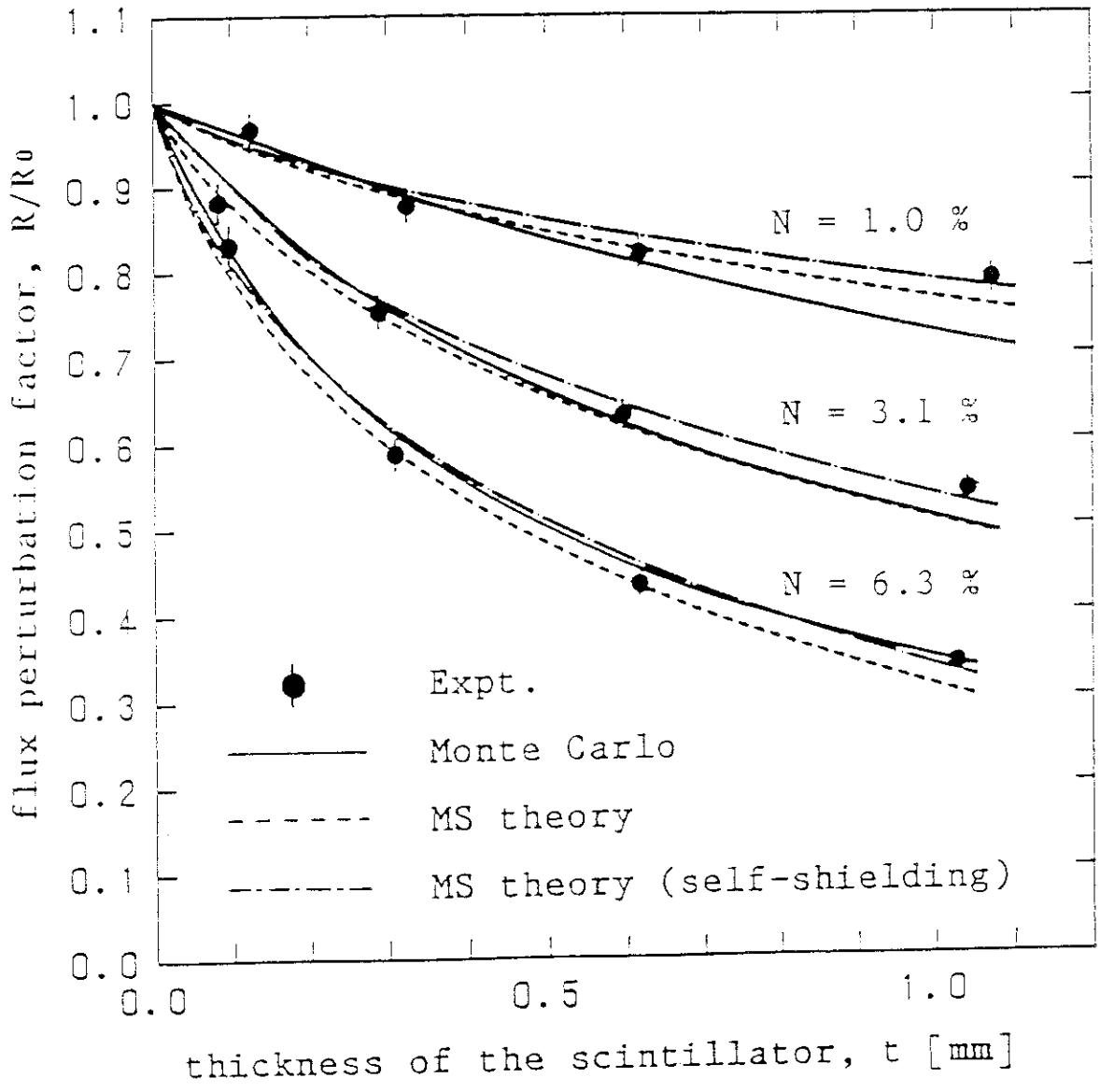

Fig. 3.2.2 Measured and calculated flux perturbation factor for thermal neutrons as a function of the thickness, t (graphite pile measurements, N = ^{6}Li content in wt %)

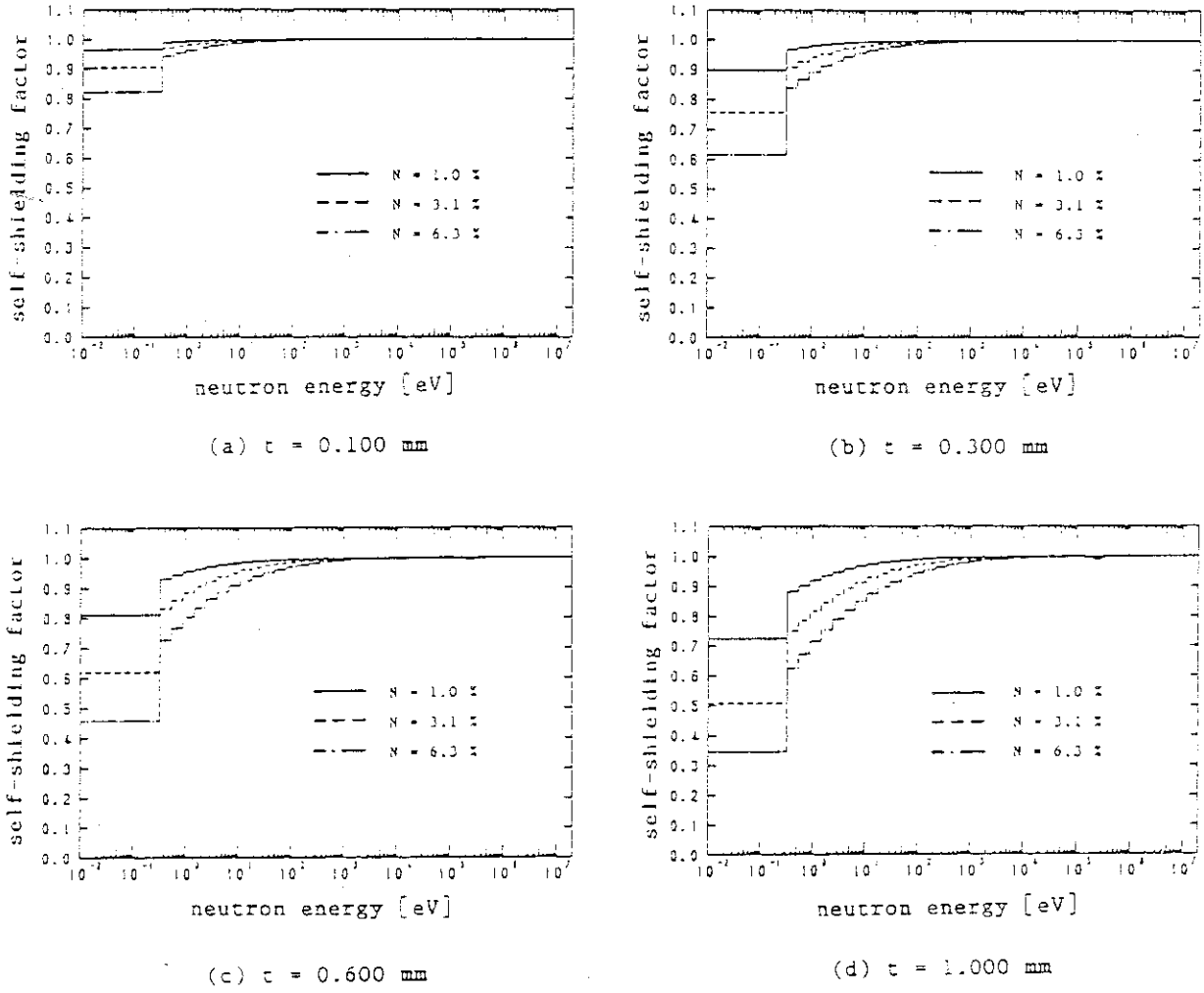

(a) t = 0.100 mm

(b) t = 0.300 mm

(c) t = 0.600 mm

(d) t = 1.000 mm

Fig. 3.4.1 Self-shielding factors calculated by a Monte Carlo Method

4. Edge-Effect of Thin Lithium-Glass Scintillator[1)]

4.1 Introduction

In the present method, very thin (0.3 mm) scintillators are being used to minimize the self-shielding, which was shown to be large for thick (3 mm) scintillators (see Chap. 3).[2)] However, because the thickness of the scintillator is not thick enough compared with the range of the alpha-particle (∿7μm) and the triton (∿50μm), the effect described as follows —— the edge effect ——cannot be neglected. In case that the $^{6}Li(n,\alpha)^{3}T$ reaction takes place near the surface of the scintillator, a part of the kinetic energy of the alpha and/or the triton is not given to the scintillator and a significant distortion of the pulse height spectrum, that is, a "tail" appears at the lower energy part of the thermal peak.

In a soft neutron spectrum, the edge effect is especially large because the fraction of reactions near the surface increases through self-shielding. Typical pulse height distributions of ^{6}Li- and ^{7}Li-glass, exposed in simulated fusion blanket assemblies of hard and soft neutron spectra, are shown in Fig. 4.1.1 (a) and (b), respectively.[3)] The tail is not to be seen in Fig. 4.1.1(a), but is observed in Fig. 4.1.1(b).

A similar effect, caused by the finite size of the detector, is observed in other radiation detectors, for instance, proton recoil proportional counters[4∿6)]. In these counters, the edge effect is fairly large because of the long range of the produced charged particles, and is usually taken into account in the calculation of response matrices. For the Li-glass scintillators, however, the edge effect has been disregarded. While the edge effect may will be negligibly small for thick scintillators, it must be dealt with when one wants to measure the tritium production rate with high accuracy by using thin scintillators.

In the present work, I measured the response of Li-glass scintillators of several thicknesses (from twice to forty times the triton range) in a graphite pile to determine the magnitude of the tail for thermal neutrons. also calculated the scintillator response by a Monte Carlo method based on the scintillation mechanism. Neutron energy dependence of the edge effect was also explored through

this Monte Carlo calculation code.

4.2 Measurement

Measurements were made of the thermal neutron response of ^{6}Li- and ^{7}Li-glass scintillators of five thicknesses. ^{7}Li-glass was provided for gamma-ray background subtraction as described in chapter 2. The scintillators used were of type NS15[7] for ^{6}Li-glass and BS15 for ^{7}Li-glass, manufactured by the Nikon Corp. (equivalent to NE905 and NE906, respectively). The nominal thickness of the scintillators was 0.1, 0.3, 0.6, 1.0 and 2.0 mm. Measured values are shown in Table 4.2.1. Diameter and density of the scintillators were 10 mm and 2.48 g/cm^3, respectively. Each scintillator was coupled to a 13 mm diameter photomultiplier tube (Hamamatsu Photonics corp. R647-01) using a quartz light guide of 10 mm diameter by 4 mm thickness with silicon grease. The electronic circuit was the same as that in Chap. 2.

The thermal neutron field was produced by an Am-Be neutron source set at the center of a graphite pile of 1 m x 1 m x 0.9 m. The scintillators were inserted at a depth of 5 cm from the pile surface.

Fig. 4.2.1 shows the measured and the subtracted pulse height spectra for 0.3 mm thick ^{6}Li and ^{7}Li-glass scintillators. The γ-ray subtracted responses for all thicknesses are shown in Fig. 4.2.2. The count rate at the peak is normalized to unity. It is clearly observed that the proportion of the tail increases with surface-to-volume ratio.

4.3 Calculation by a Monte Carlo Method

4.3.1 Calculational model

The mechanism of the scintillation is explained qualitatively as follows[8] (see Fig. 4.3.1),

(1) when a neutron incident on a scintillator reacts with a ^{6}Li atom, it emits an alpha-triton pair in opposite directions
(2) these charged particles produce ion pairs along their tracks
(3) secondary electrons exite Ce^{3+} to stimulate luminescence.

In the present calculation, we assume that

(1) neutrons are incident isotropically on a cylindrical scintillator,
(2) neutron flux, Φ, is exponentially attenuates in the scintillator :

$$\Phi(x) = \Phi_0 \exp(-\Sigma_a x), \tag{4.3.1}$$

where,

Φ_0 : incident neutron flux,

Σ_a : ($=N\sigma_a$) macroscopic absorption cross section of the $^6Li(n,\alpha)^3T$ reaction (N = atom density of ^6Li in the ^6Li-glass determined by the chemical analysis as 1.600×10^{22} atoms/cm^3 [9], σ_a = average microscopic cross section of ^6Li for thermal neutrons of Maxwell distribution, 833 b),

(3) the alpha and the triton travel in a straight line over their entire range, losing their kinetic energy following the Bragg curve,
(4) scintillation intensity is proportional to the sum of the kinetic energies of the alpha and the triton.

4.3.2 Ratio of luminescence contributions of the alpha and the triton

The pulse height of the alpha and the triton, W_α and W_t, can be represented by the following equations :

$$W_\alpha = k\rho_{ion}^{\alpha}\rho_{Ce}v_{ion}^{\alpha},$$
$$W_t = k\rho_{ion}^{t}\rho_{Ce}v_{ion}^{t}, \tag{4.3.2}$$

where, $\rho_{ion}^{\alpha,t}$: density of ion pairs liberated by the alpha or the triton,
ρ_{Ce} : density of Ce^{3+},
$v_{ion}^{\alpha,t}$: ionization volume for the alpha or the triton,
k : constant.

The ionization volume is the volume of the cylinder that contains the secondary electrons liberated by the alpha or the triton[8] (see Fig. 4.3.1). According to ref. 8), ion pair densities for the alpha and the triton are 9.66×10^{18} cm^{-3} and 2.06×10^{17} cm^{-3}, and the

ionization volumes are 8.45×10^{-15} cm^3 and 5.28×10^{-13} cm^3, respectively. From this, the ratio $R_{t/\alpha}$ of the contributions to luminescence of the triton and the alpha comes to 1.33. However, the ion pair density of the alpha is so high (fifty times the triton ion pair densities), that the contribution of the alpha track to the scintillation is reduced by recombination of ion pairs. Consequently, the value of $R_{t/\alpha}$ will be larger than 1.33. Figure 4.2.2 indicates that the pulse height is zero at energy less than 20 % of the thermal peak. This suggests a value of $R_{t/\alpha}$ of 80/20 = 4.0 because pulse height takes the minimum value when only the alpha particle contributes to the scintillation.

4.3.3 Rate of energy deposition of the alpha and the triton

The rate of energy deposition along the tracks of the alpha or the triton is not uniform, but obeys the Bragg curve. The fact that the relative counts in the tail region increase with declivity pulse height, as can be seen in Fig. 4.2.2, reflects on the Bragg curve of the triton. The stopping power of the α particle and the triton in the Li-glass scintillator were calculated by using a semiempirical formula, which was presented by Sugiyama[10] on the basis of Bethe's formula and by applying the Bragg's additivity rule.

The Sugiyama's formula is expressed as follows:

$$-\frac{dE}{dx} = W \frac{4\pi e^4 Z_1^{*2}}{mv^2} \cdot N Z_2^{*} \log \frac{2mv^2}{I_2^{*}}, \qquad (4.3.3)$$

where

e = electron charge,

m = electron mass,

v = velocity of incident particle,

Z_1 = charge of incident particle,

Z_2 = charge of target material,

I_2 = mean excitation energy of target material,

N = atomic density of target material,

$I_2^{*} = I_2\{1-\exp(-0.71E^{*}/I_2)\}$,

$E^{*} = mE/M$ (M = mass of incident particle),

$Z_2^{*} = Z_2\{1-\exp(-0.64v_r^2/Z_2^n)\}$,

$$v_r = v/v_0,$$

$$v_0 = 2\pi e^2/h \quad (h = \text{Plank constant}),$$

$$n = \frac{2}{3} + \frac{1}{3}\{1-\exp(-145\beta^2)\}$$

$$\beta = v/c \quad (c = \text{light velocity}),$$

$$Z_1^* = Z_1\{1-\exp(-1.35v_r^2/Z_1^k)\},$$

$$k = 0.81 - 0.04\{1-\exp(-0.2v_r)\},$$

$$W^{-1} = 1 - \exp(-3.14v_r/Z_1^{0.19})\}.$$

According to Bragg's additivity rule, the effective parameters of a compound are determined by

$$NZ = \sum_i N_i Z_i, \tag{4.3.4}$$

$$NZ\log I = \sum_i N_i Z_i \log I_i, \tag{4.3.5}$$

where i represents kind of nucleus.

Th parameters, N_i, Z_i and I_i[11] are shown in Table 4.3.1. The calculated results of the stopping power and effective charge Z_1^* for α (2.05 MeV) and triton (2.73 MeV) in the NS15 ^{6}Li-glass scintillator are shown in Fig. 4.3.2. In the case of the triton, the Bragg peak is clearly shown and the rate of energy deposition is in proportion to the inverse of the energy. On the other hand, the Bragg peak of the α is not so sharp as the triton, because of the decrease of the effective charge due to the electron capturing effect. Since the tail shape reflects the triton's Bragg curve as mentioned above, therefore, we can assume that the stopping power is in proportion to the inverse of energy. Accordingly, in the present work, the stopping power is assumed to be represented by the following equation (see Fig. 4.3.3) :

$$-\frac{dE}{dX} = \begin{cases} K/\sqrt{X_R - X} & : \quad 0 \leq X < f_1 X_R \\ k & : \quad f_1 X_R \leq X < f_2 X_R \\ a - bX & : \quad f_2 X_R \leq X \leq X_R \end{cases}, \tag{4.3.6}$$

where,

K,k,a,b : constants, determined by the adjustable parameters f_1 and f_2,

X_R : ranges of the alpha and the triton.

The parameters, f_1 and f_2 were determined by comparing the measured and calculated results.

4.3.4 Alpha Particle and Triton Ranges

Charged-particle ranges in Li-glass were estimad by (1) those data in air and silicon by applying the Bragg-Kleeman rule and by (2) integration of the inverse stopping power.

(1) Bragg-Kleeman rule

Bragg-Kleeman rule is expressed by the next relation :

$$\frac{R_1}{R_2} = \frac{\rho_2}{\rho_1}\left(\frac{A_1}{A_2}\right)^{1/2}, \tag{4.3.7}$$

where,

R_i : range in material i,

ρ_i : density of material i,

A_i : effective atomic weight of material i.

The value of A_i is calculated by the following equation :

$$\sqrt{A_i} = \left(\sum_{j=1}^{L_i} \frac{w_{ij}}{\sqrt{A_{ij}}}\right)^{-1}, \tag{4.3.8}$$

where,

A_{ij} : atomic weight of element j,

w_{ij} : weight ratio of element j,

L_i : number of elements in material A_i.

The range of 2.04 MeV alpha particle is 10.3 mm in air (15°C and 769 mmHg)[12] and 1.91×10^{-3} g/cm^2 in silicon[13]. The range of the 2.72 MeV triton is 60 mm, 57 mm in air (15°C, 760 mmHg)[14,15] and 1.03×10^{-2} g/cm^2 in silicon[13]. Applying the Bragg-kleeman rule to these values, the ranges in ^{6}Li-glass of density 2.48 g/cm^3 come to 5.9 μm and 6.3 μm for the alpha and 33, 35 and 34 μm for the triton, respectively.

(2) Integration of inverse stopping power

The range data is obtained by numerical in tegration of the inverse stopping power :

$$R = \int_0^E (dE/dx)^{-1} dE. \qquad (4.3.9)$$

The ranges of 2.04 MeV α and 2.72 MeV triton calculated by Eq. (4.3.3) are 6μm and 33 μm. These data are consistent with those by the results of the Bragg-Kleeman rule.

The effect of particle ranges on the calculated pulse height spectra turns out to be very small for the alpha particle but large for the tritons. The tail increases with triton range. Results calculated with a triton range of 50 μm agreed well with the measured pulse height spectra. The value of 6 and 50 μm for the alpha and the triton range respectively were adopted through this calculation.

4.3.5 Smearing

The statistical line broadening of the scintillator output was assumed to be subject to a Gaussian energy resolution function $(\Delta E/E)^2 = a + b/E$[16]. The parameters a and b are determined from the measured data. However, the calculated results did not agree with the measured ones in the lower energy part of the thermal peak as shown in Fig. 4.3.4. This discrepancy was resolved by broadening with an asymmetric function, that is, the convolution of a Gaussian and an exponential function :

$$f(x) = \begin{cases} q/p \exp(x/p) & : \ x < 0 \\ q/p \exp(x/p) + (1-q) & : \ x = 0 \\ 0 & : \ x > 0 \end{cases} . \qquad (4.3.10)$$

This asymmetry is considered to be caused by the noise, incompleteness of light collection, etc. Similar low energy distortions are observed in other radiation detectors such as proton recoil counters[5,17] and Ge(Li) detectors[18]. The adjustable parameters p and q were determined by comparing measured and calculated results.

4.3.6 Calculated results

For each thickness, one million neutron histories were processed. The results of the calculations are shown in Fig. 4.3.5. Calculated results agree well with the measured results shown in Fig. 4.2.2, for all thicknesses, both with regard to the shape and the height of the tail. The pulse height spectrum before smearing is shown in Fig. 4.3.6 for 0.3 mm thickness. The "α-edge" corresponds to $^{6}Li(n,\alpha)^{3}T$ reactions at the surface of the scintillator with emission of the alpha imigrate inward of and the triton outward. The "t-edge" corresponds to the opposite situation. The "t-edge" cannot be seen when the pulse height spectrum is smeared.

4.4 Discussion

To indicate the edge effect quantitatively, we define the "tail-to-total ratio" ;

$$R_{tail} = \frac{\sum_{I=I1}^{I2} C(I)}{\sum_{I=I1}^{I3} C(I)}, \qquad (4.4.1)$$

where, C(I) = number of counts in pulse height channel I. Channels I1,I2 and I3 correspond to pulseheights of 20, 65 and 130 ch in Fig. 4.3.4 where the peak has been normalised to unit height at channel 100. In Fig. 4.2.1, experimental values are plotted in a different scale : peak at channel 266, I1 here comes to 20 % of the peak channel and I2 to 65 %, I3 = 350. The values of the "tail-to-total ratio" are shown in Table 4.2.1 and Fig. 4.4.1. Close agreement between observed and calculated values was obtained except for 0.1 mm thickness. For 0.3 mm thickness, the ratio amounts to 4.4 %.

In the D-T fusion blanket, neutron energy spectra extend over a wide range from 14 MeV to thermal. A transport calculation indicated that the energy range which contributed mainly to the tritium production was near 250 keV. The energy dependence on the "tail-to-total ratio" was examined by a Monte Carlo calculation. The calculation was scaled to a cross section of 3.5 b at the 250 keV peak. The tail-to-total ratios for this case are also listed in Table 1 and

plotted in Fig 4.4.1. Evidently, the difference between the tail-to-total ratios for thermal and for 250 keV neutrons increases in proportion to thickness. For 0.3 mm, the difference is very small, hence, a tail-to-total ratio" of 4.4 % can be assumed for all neutron energies at that thickness. It might be thought that this result is caused by the fact that the self-shielding effect increases with scintillator thickness. If the self-shielding effect is small, the tail-to-total ratio should be proportional to the surface to volume ratio $S/V = 2(r+t)/rt$, where t and r are thickness and radius of the scintillator, respectively. In Fig. 4.4.1, a curve proportional to the S/V is drawn. This line passes through the tail-to-total ratio points for σ=3.5 b, showing that self-shielding is small. For thick scintillators, tail-to-total ratio is small, but its neutron energy dependence is large. This results in a large uncertainty of the tail-to-total ratio due to the neutron spectrum if a thick scintillator is used in the D-T neutron field.

4.5 Conclusion

A measurement of the pulse height spectra of Li-glass scintillators of several thicknesses was performed for thermal neutrons to investigate the edge effect of Li-glass scintillator. The tail-to-total ratio was determined as a function of the scintillator thickness. A Monte Carlo simulation of pulse height spectra based on the scintillation mechanism was carriod out. Agreement between measured and calculated values was excellent. Using this Monte Carlo code, the neutron energy dependence on the tail-to-total ratio was examined. It was shown that the dependence of the edge effect on neutron energy is very small for 0.3 mm thick scintillator. A tail-to-total ratio of 4.4 % should be applied to all data obtained with the 0.3 mm thick scintillator currently used in our measurements.

References

1) Yamaguchi S. : Nucl. Instr. Meth. A274, 573 (1989).
2) Yamaguchi S. and Nakamura T. : "Tritium Production Measurements by the Lithium-Glass Scintillator Method," Proc. 7th Topical Meeting on the Technol. Fusion Energy ; Fusion Technol. 10, 573 (1986).
3) Oyama Y., et al. : "Experimental Results for Phase II of JAERI/USDOE Collabolative Program on Fusion Blanket Neutronics," Proc. Int. Symp. on Fusion Nucl. Technol., Tokyo (1988).
4) Snidow N. L. and Warren H. D. : Nucl. Instr. Meth. 51, 109 (1967).
5) Bennett E. F., et al. : "Analysis and Reduction of Proton-Recoil Data," ANL-7394 (1968).
6) Petler J. S. and Scott M. C. : Nucl. Instr. Meth. 228, 425 (1985).
7) Niimura N., et al. : Kakuriken Kenkyu Hokoku 13, 102 (1980) [in Japanese].
8) Spowart A. R. : Nucl. Instr. and Meth. 135, 441 (1976).
9) Tamura S. and Tamura K. : private communication (1986).
10) Sugiyama H. : "Stopping Power and Range Tables for Heavy Ions," Circulars of the Electrotechnical Laboratory, No. 181 (1976).
11) Seltzer S. M. and Berger M. J. : Int. J. Appl. Radiat. Isot. 33 (1982) 1189.
12) Jesse W. P. and Sadauskis J. : Phys. Rev. 78, 1 (1950).
13) Williamson C. F., et al. : "Tables of Range and Stopping Power of Chemical Elements for Charged Particles of Energy 0.05 to 500 MeV," CEA-R 3042 (1966).
14) Wolke R. L. and Bishop W. N. : Phys. Rev. 129, 6 (1963).
15) Boggild J. K. and Minnhagen L. : Phys. Rev. 75, 782 (1949).
16) Bisi A. and Zappa L. : Nucl. Instr. Meth. 3, 17 (1958).
17) Akioka T., et al.: Nucl. Instr. Meth. 227, 311 (1984).
18) Sasamoto N., et al. : Nucl. Instr. Meth. 125, 507 (1975).

Table 4.2.1 Relation between tail-to-total ratio and thickness of scintillators

thickness [mm]		tail-to-total ratio [%]		
nominal	measured	experiment	calculation (σ=833 [b])	calculation (σ=3.5 [b])
0.1	0.096	10.8	12.0	12.6
0.3	0.308	4.36	4.28	4.31
0.6	0.616	2.70	2.33	2.20
1.0	1.026	1.98	1.85	1.51
2.0	2.000	1.50	1.39	0.75

Table 4.3.1 Li-glass parameters used for the stopping power calculation

	atomic density [/cm^3]	atomic number	ionization potential [eV]
^{6}Li	1.59×10^{22}	3	40
^{7}Li	6.45×10^{20}		
O	4.77×10^{22}	8	95
Mg	1.49×10^{21}	12	156
Al	5.46×10^{21}	13	166
Si	1.46×10^{22}	14	173
Ce	3.66×10^{20}	58	523
Li-glass	8.62×10^{22}	8.654	118.4

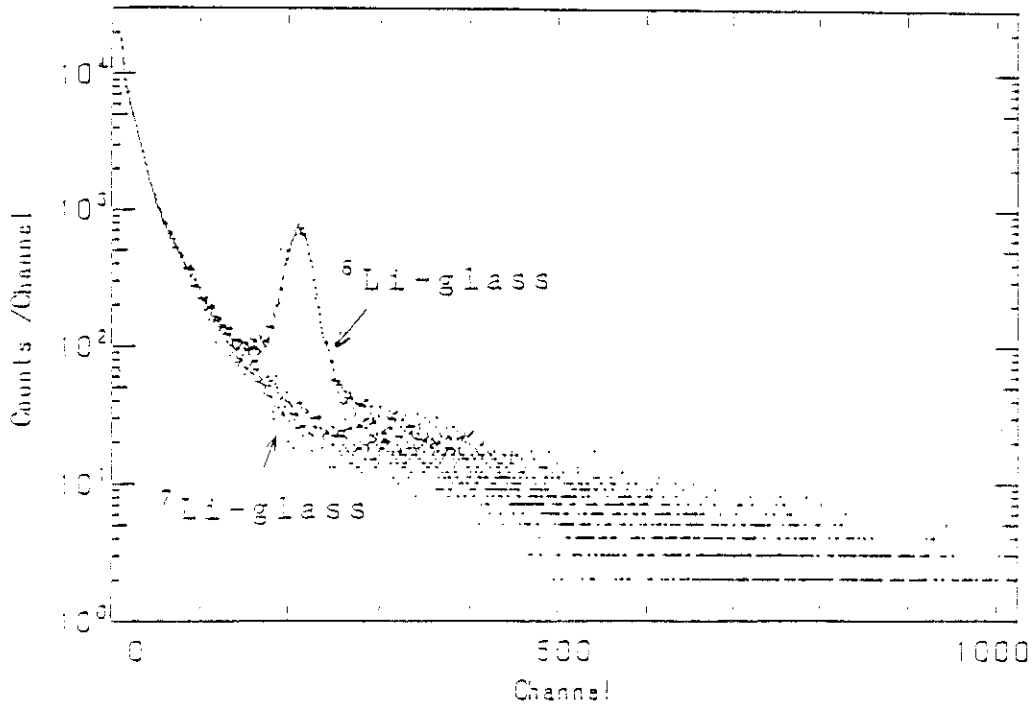

(a)

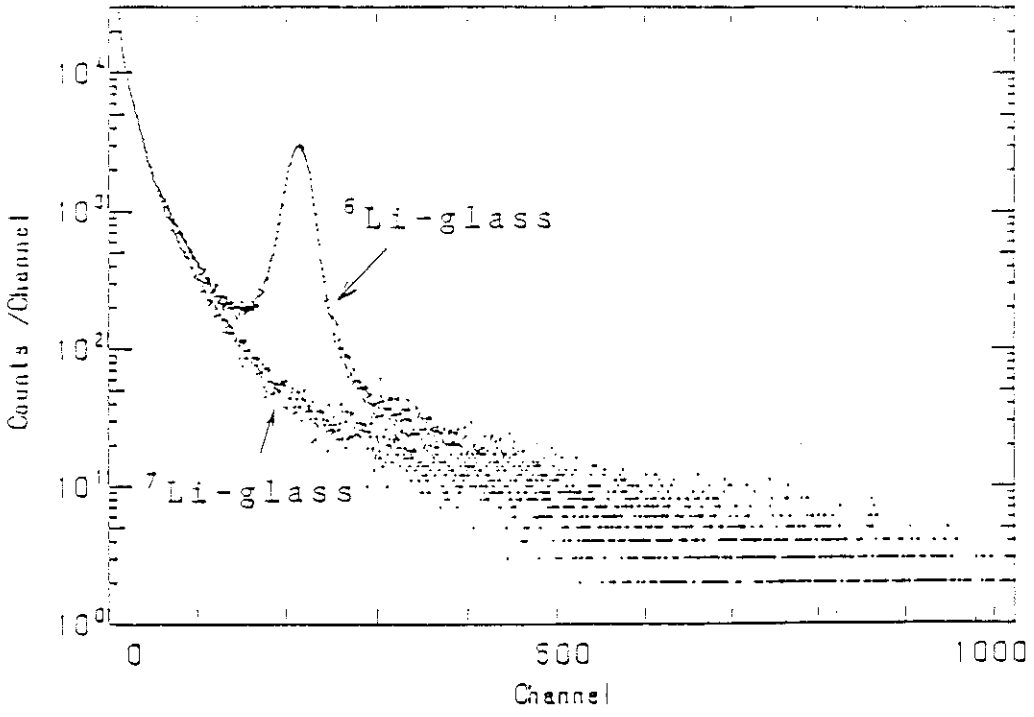

(b)

Fig. 4.1.1 Pulse height spectra of ^{6}Li and ^{7}Li-glass scintillators, (a) hard neutron spectrum, (b) soft neutron spectrum

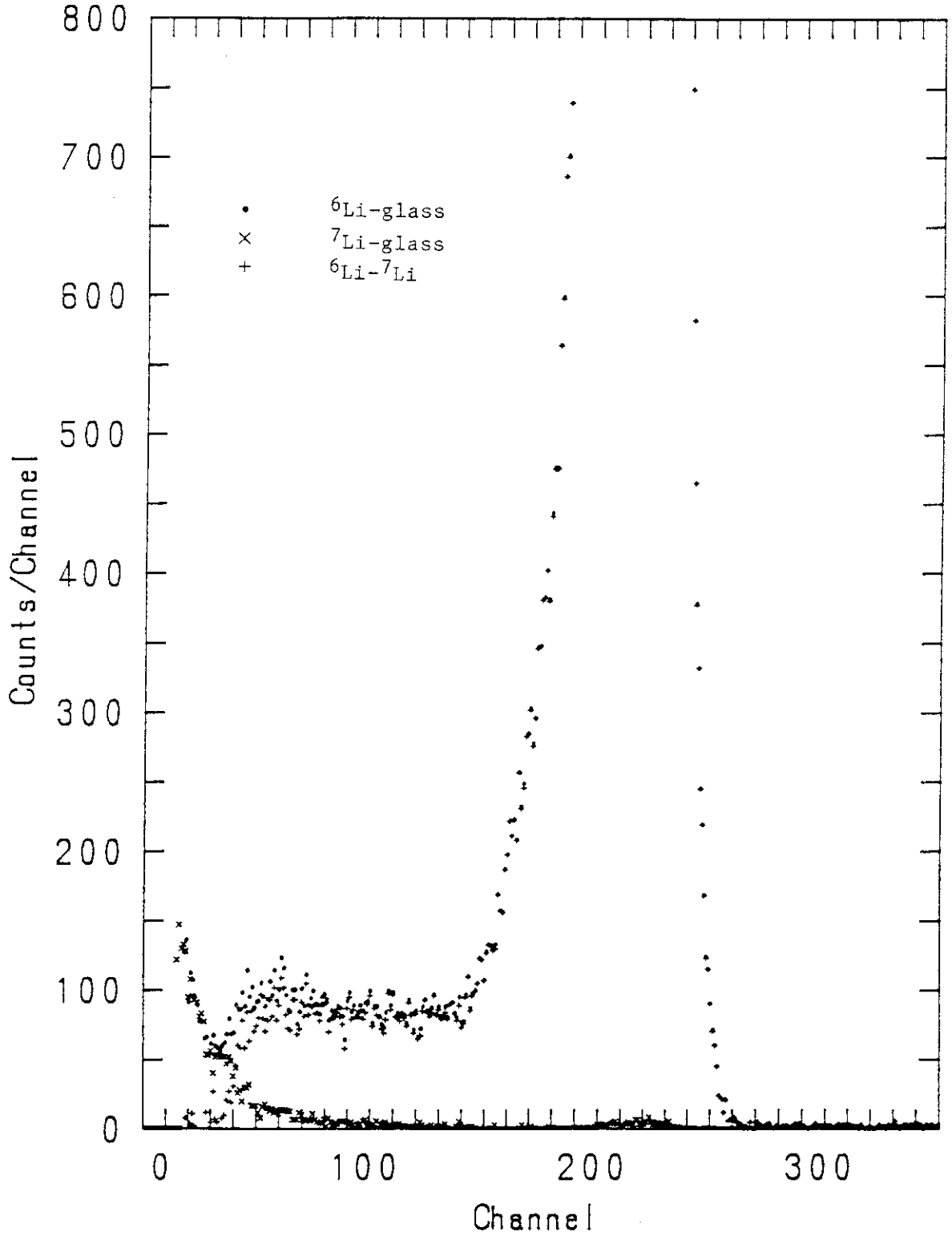

Fig. 4.2.1 Pulse height spectra of ^{6}Li and ^{7}Li-glass scintillators and the subtracted spectrum in a graphite pile

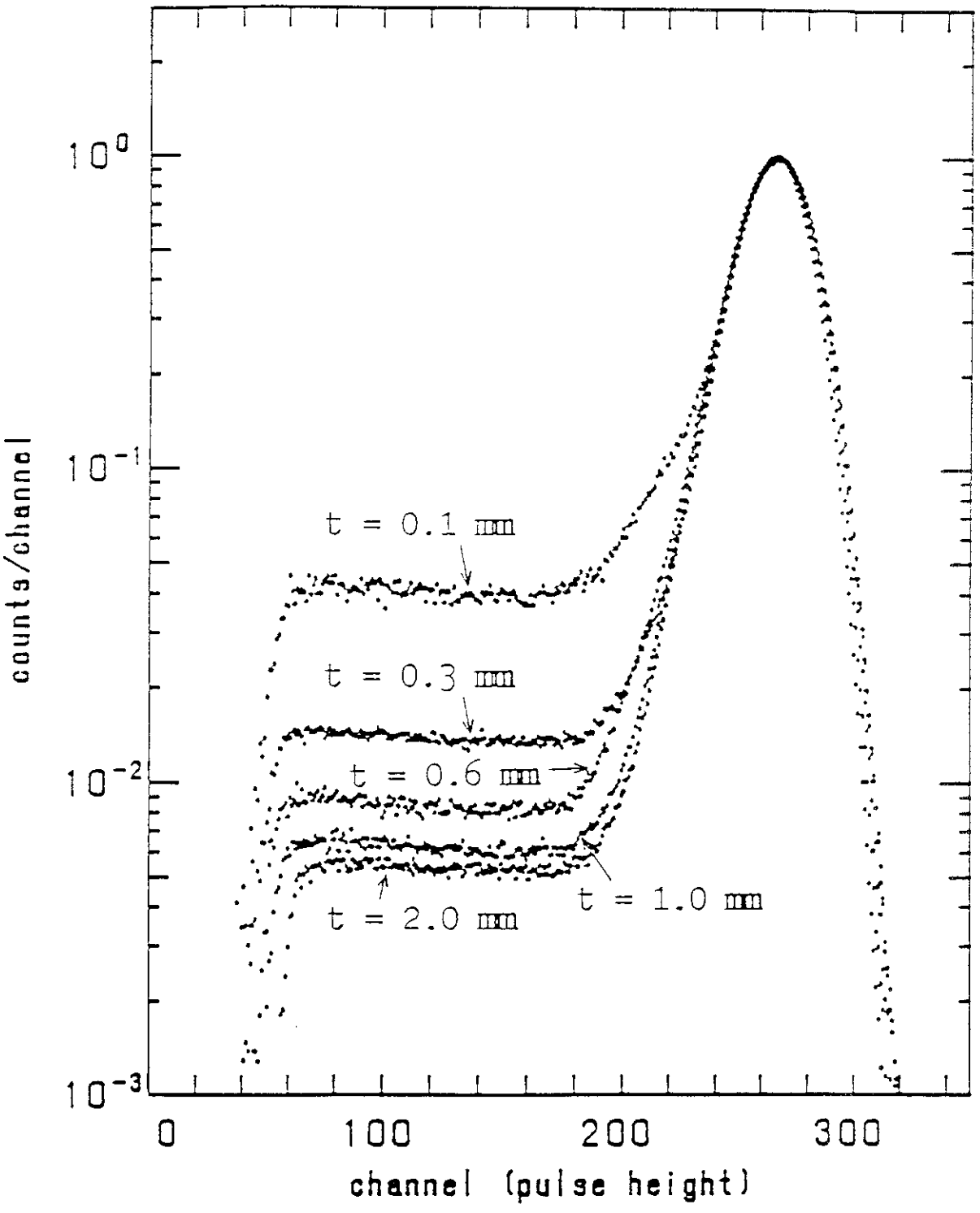

Fig. 4.2.2 Subtracted pulse height spectra of ^{6}Li-glass scintillators in a graphite pile. The horizontal axis is the channel number of the multi-channel analyzer. The vertical axis is the counts normarized to the value of the thermal peak

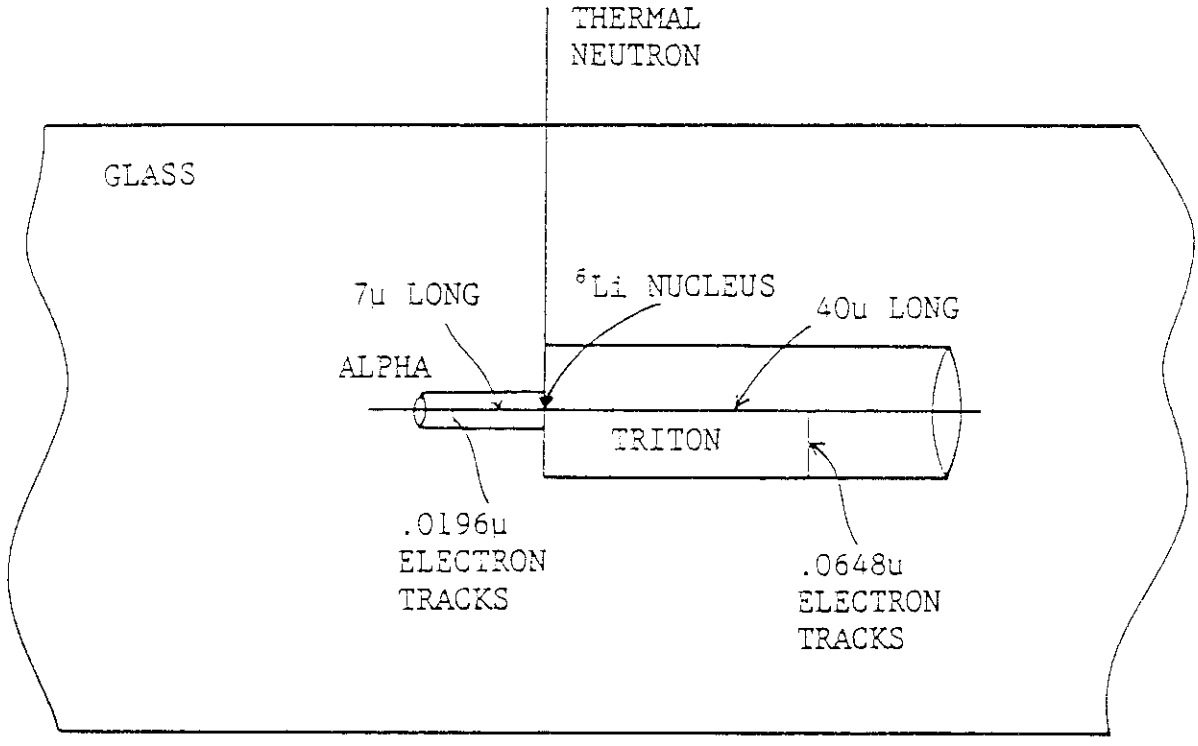

Fig. 4.3.1 Mechanism of the scintillation of lithium-glass scintillator (from Ref.[8])

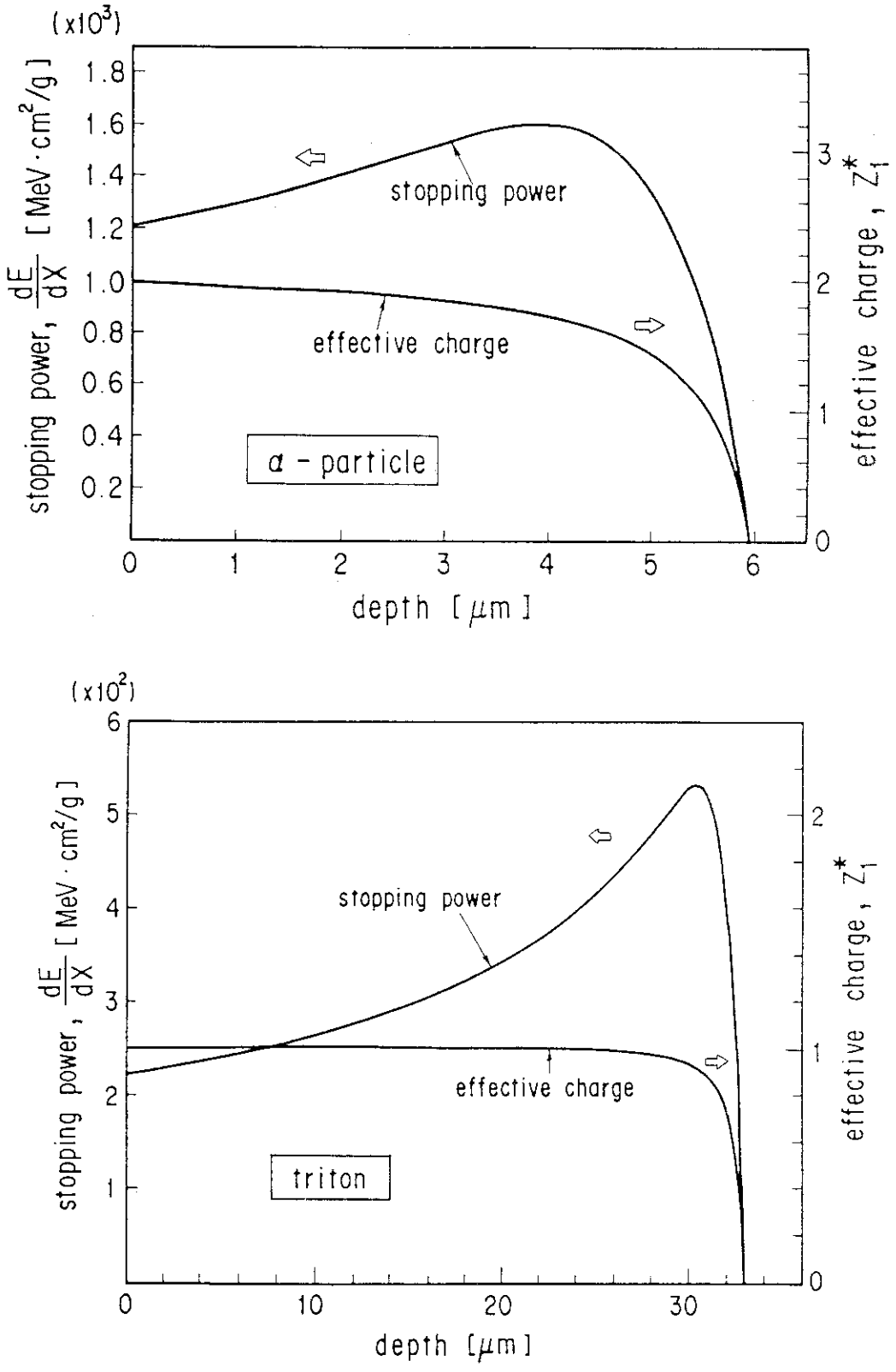

Fig. 4.3.2 Stopping power and effective charge of α and triton in ^{6}Li-glass scintillator

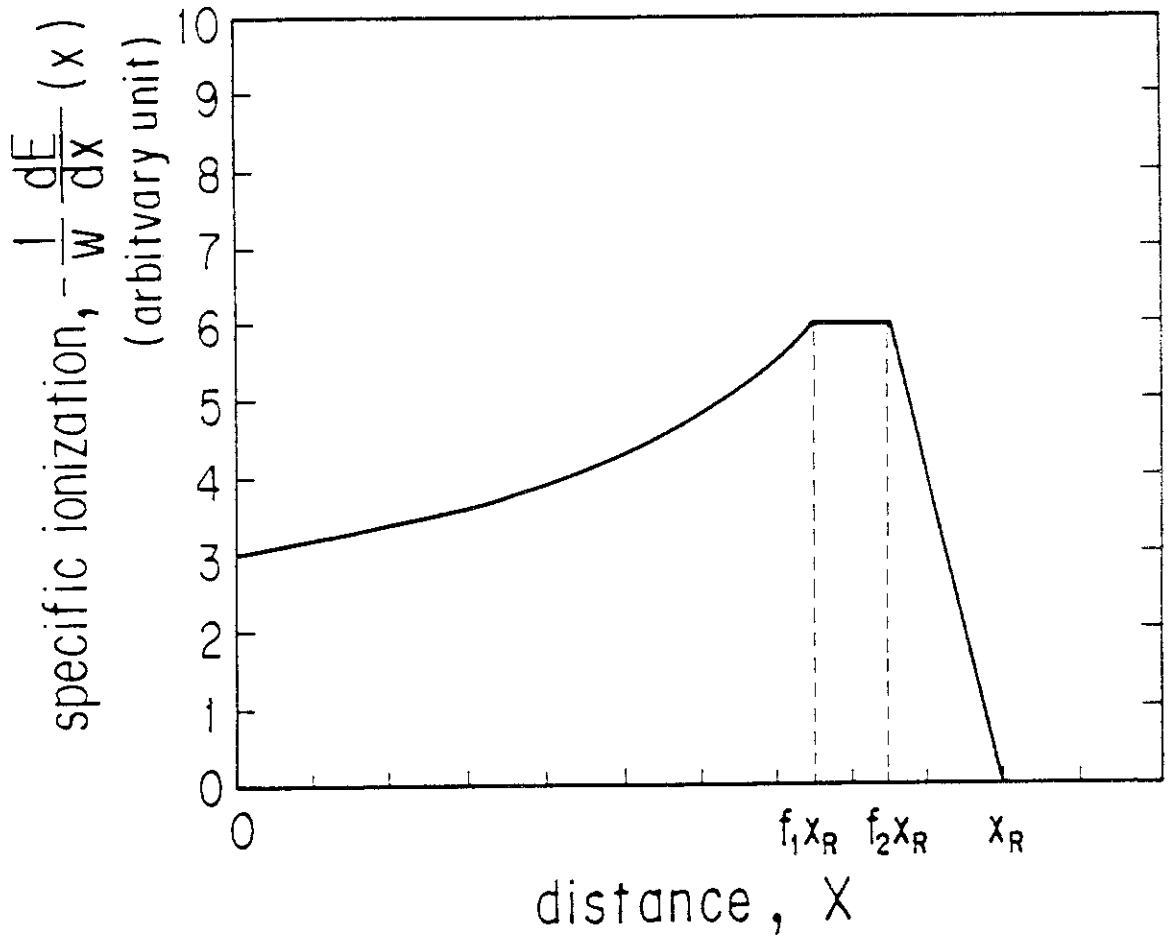

Fig. 4.3.3 A model for Bragg curve

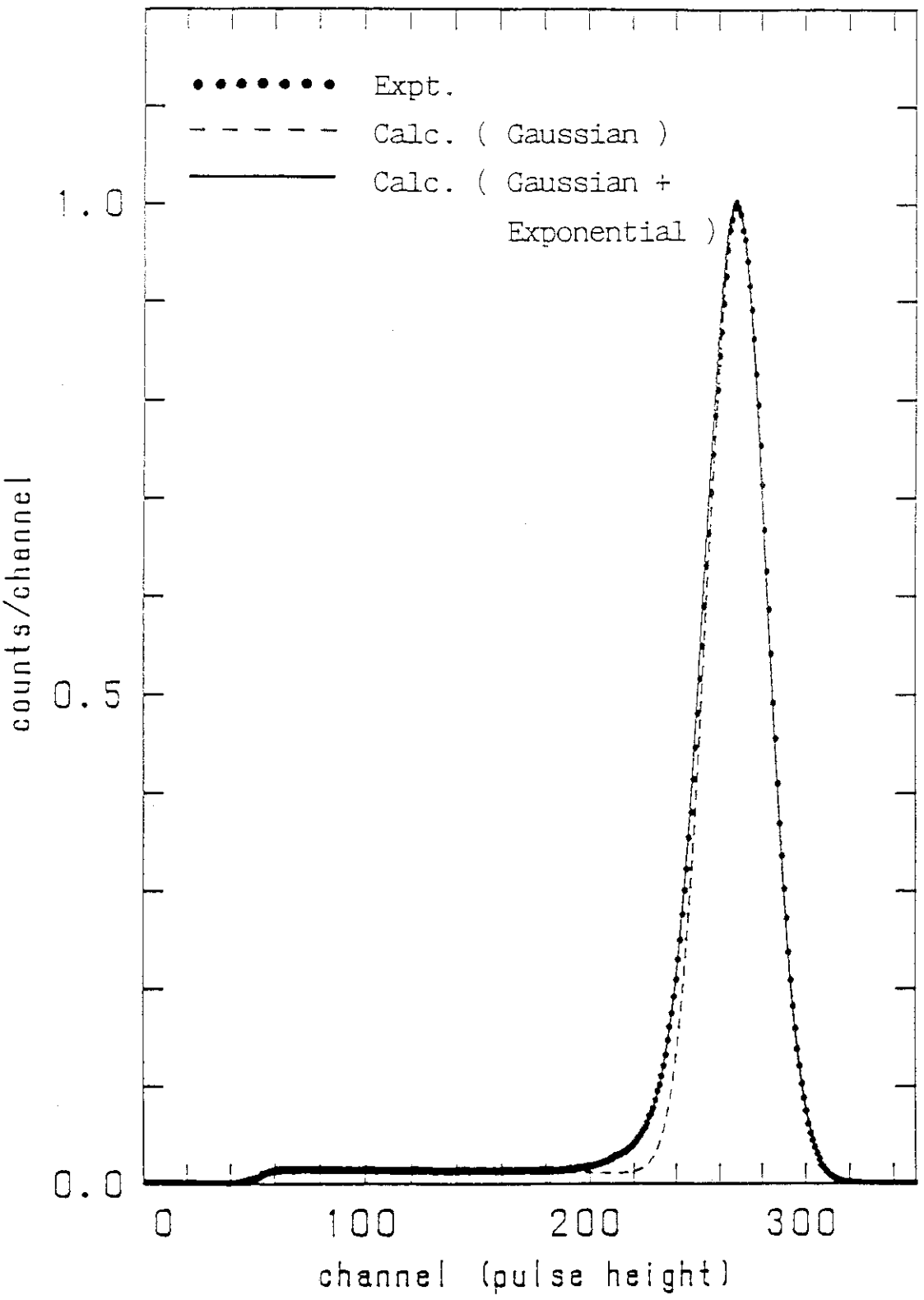

Fig. 4.3.4 Calculated pulse height spectrum of ^{6}Li-glass scintillator smeared by Gaussian function and Gaussian + exponential functions

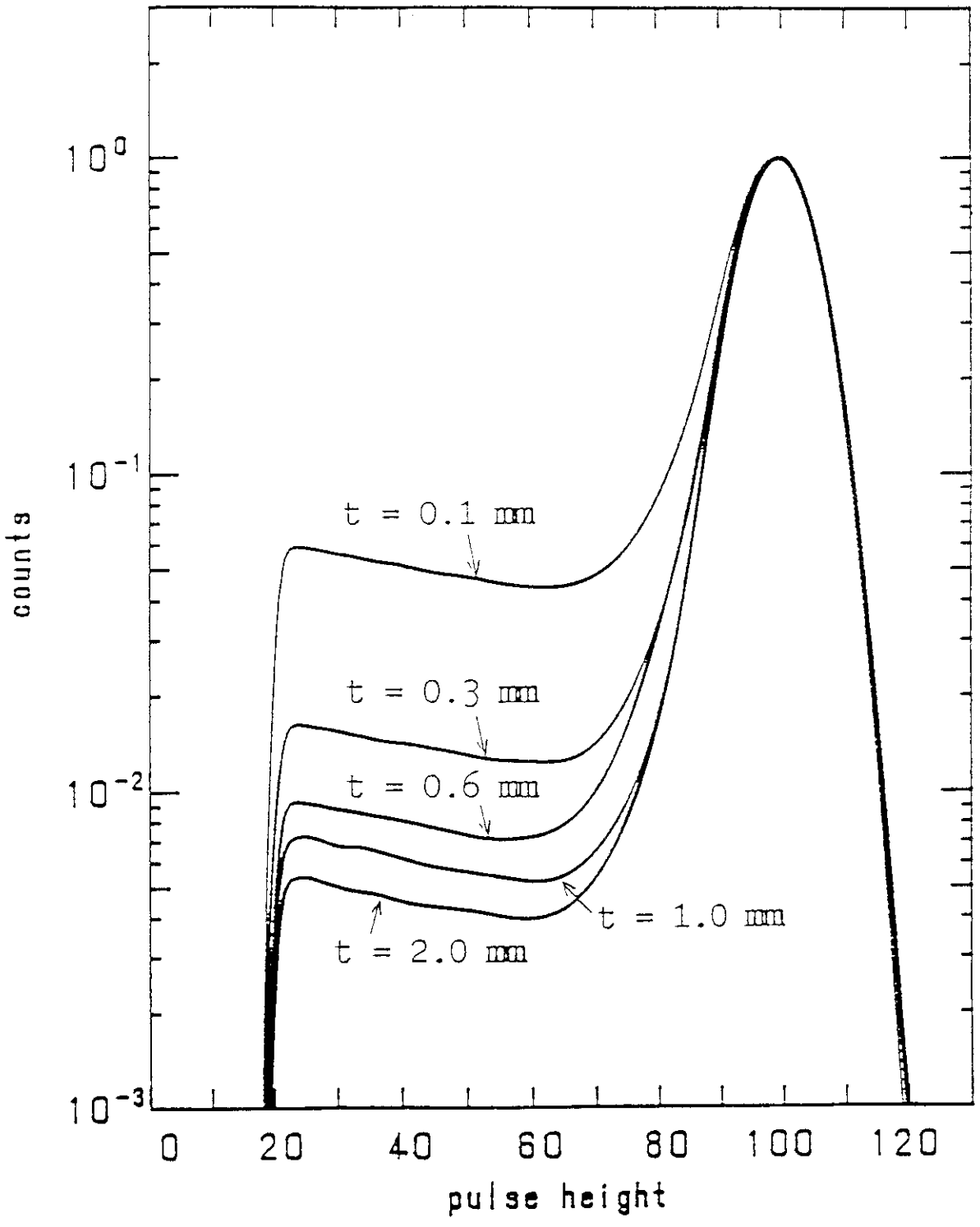

Fig. 4.3.5 Calculated pulse height spectra of ^{6}Li-glass scintillator of various thickness for thermal neutrons (smeared)

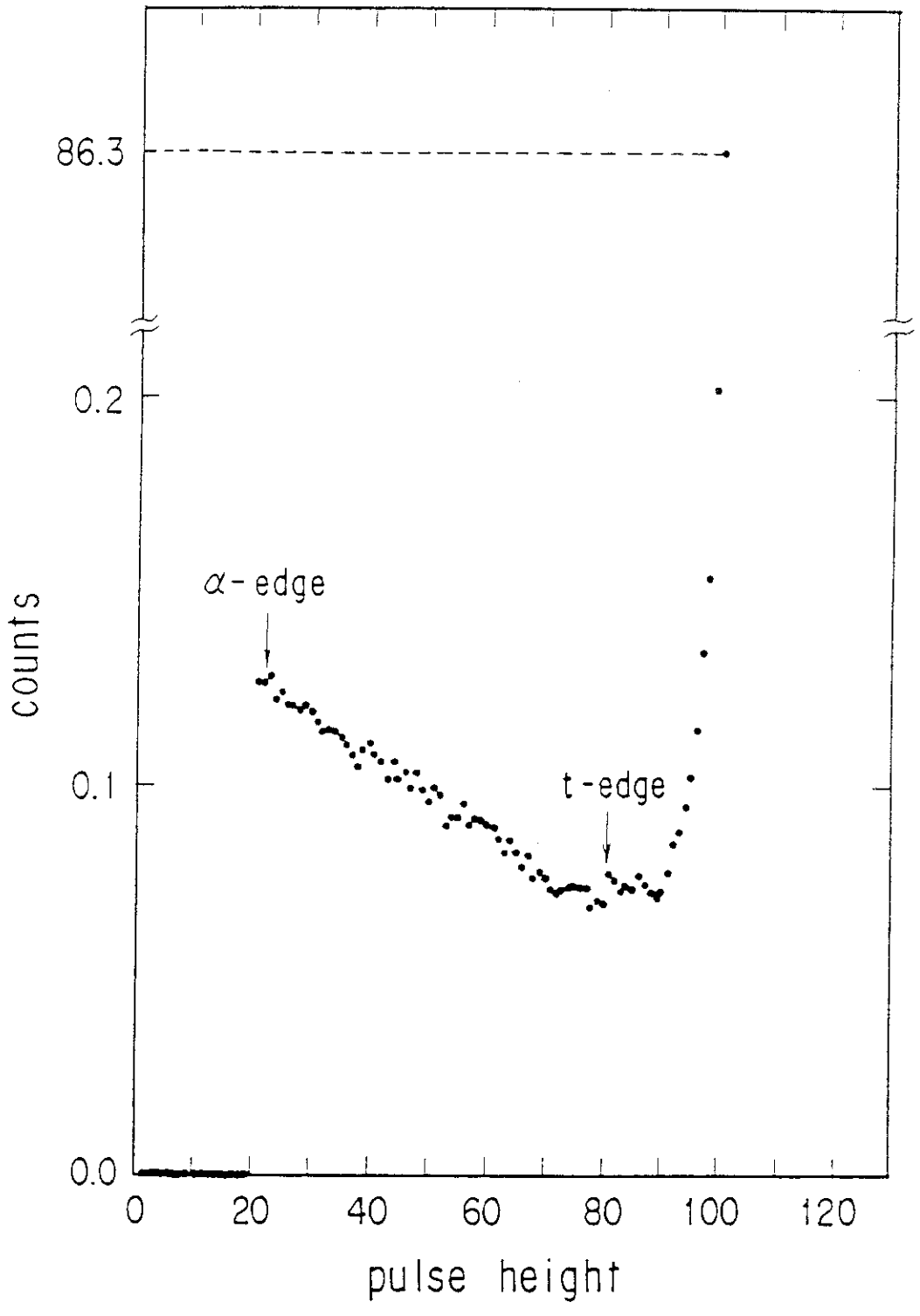

Fig. 4.3.6 Calculated pulse height spectrum of ^{6}Li-glass scintillator (0.3 mm thick) for thermal neutrons (not smeared)

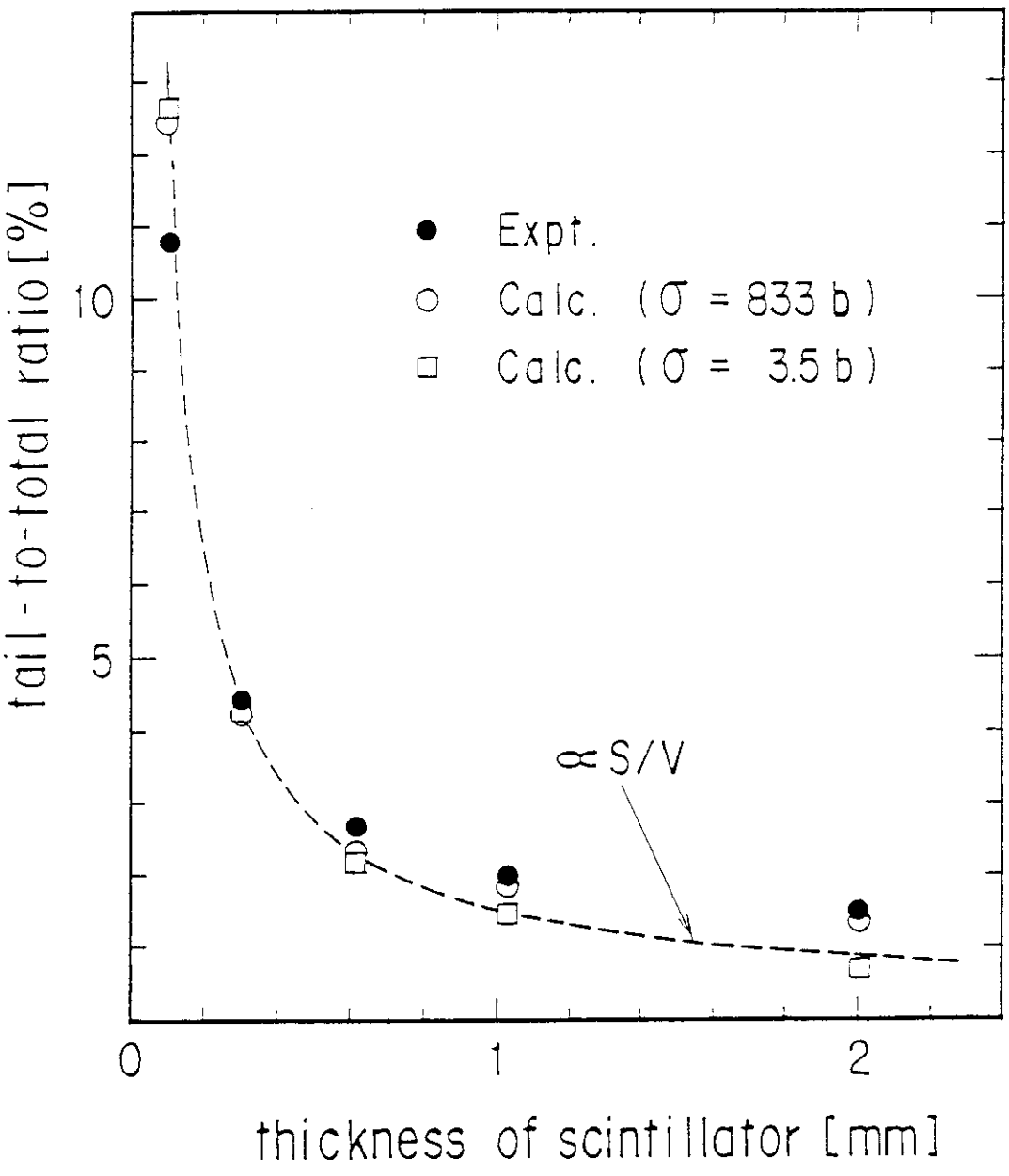

Fig. 4.4.1 Relation between the tail-to-total ratio and the thickness of the scintillators

5. Measurement of Tritium Production Rate Distributions in Simulated Fusion Blanket Assemblies by the Li-Glass Method

5.1 Introduction

In this chapter, measurements of TPR distributions by the Li-glass method, performed as a part of the JAERI/USDOE(United States Department of Energy) Collaborative Experiments, are described. The Collaborative Experiments are conducted to check the validity of computational methods and nuclear data bases as well as provide experimental data in support of blanket design. So far, three series of experiments have been run : Phase I,[1~3] Phase IIA[4] and Phase IIB.[5] In these series of experiments, neutronic parameters such as TPR's, reaction rates, neutron spectra and gamma heating rates were measured at many locations within large blocks of blanket materials. Three kinds of techniques measurements made use of:

(1) Li-glass and NE213 detector traverse,

(2) Li-metal emplacement (Li-metal method),

(3) Li_2O block emplacement (zonal method).

In this chapter, Phase IIA TPR measurements by the Li-glass method are described and compared with other measuring techniques.

5.2 Assemblies

The experimental system for Phase IIA provide a lithium-oxide blanket test region (870 mm x 870 mm x 610 mm) within a lithium-carbonate enclosure (200 mm thick) and polyethylene buffer (50 mm thick) that surrounded the neutron source. A cross sectional view and plane view of the Phase IIA experimental system are shown in Figs. 5.2.1 and 5.2.2, respectively. The assembly is supported by tables that can be displaced laterally on tracks, so as to provide access to the test region and neutron source. The distance between the source center point and the test region surface was 780 mm. For some runs, the test region included Be layer in addition to Li_2O. The following three systems were constructed :

(1) Reference system ------- 610 mm Li_2O

(2) Be front system -------- 50 mm Be + 560 mm Li_2O

(3) Be sandwich system --- 50 mm Li_2O + 50 mm Be + 510 mm Li_2O

The Li_2O blocks were cold-pressed to a standard size of 49 mm x 49 mm x 50 mm and inserted in stainless steel container of 50.6 x 50.6 mm base, 50.6, 203 and 406 mm height(See, Fig. 5.2.3). The cans were sealed by electron beam welding to protect the Li_2O from moisture.

Four experimental channels were incorporated in the test region to itraverse the Li-glass detctor and NE213 detector or emplace samples (see Fig. 5.2.4). In addition to a central axial channel, these included an off-central axial channel, a front radial channel whose axis was 125 mm from the front surface and a rear radial channel whose axis was 425 mm from the front surface.

5.3 Neutron Source and Neutron Yield Monitor

The 14 MeV DT neutrons were generated by the reaction :

$$^2D + {}^3T \rightarrow n + {}^4He + 17.6\ MeV. \qquad (5.3.1)$$

Deuteron beams were accelerated to 310 keV by the Cockroft-Walton type electrostatic accelerator of the Fusion Neutronics Source facility (FNS) at JAERI.[7] A plane view of the FNS accelerator system is shown in Fig. 5.3.1. The beam current for counter traverse was 5 - 200 μA depending on the detector location and on the experimental systems and 20 mA for sample irradiation. The target was a rotating type tritium-metal target (see Fig. 5.3.2), loaded with 900 Ci (3.3×10^4 GBq) of tritium within a 40 g/m^2-thick titanium layer evapolated on a 1 mm-thick copper backing that was cooled by water circulation.

The neutron yield at the target was monitored by detecting the associated alpha particles. The absolute total neutron yield at the target Y_n is given by :

$$Y_n = \frac{4\pi}{\Delta\Omega} \cdot C_\alpha \cdot R_\alpha(E_d, \theta_\alpha), \qquad (5.3.2)$$

where,

$\Delta\Omega$: solid angle of the target subtended by the detector aperture,

C_α : α-particles counts,

R_α : anisotropy correction factor,

E_d : incident deuteron energy,

θ_α : angle of α-particle emission.

Figure 5.3.3 shows the alpha detector arrangement. A silicon surface-barrier detector (SSD) was used for alpha particle detection. An aluminum foil of 4.1 g/m^2 thickness was inserted to stop other particles, such as protons from the ^{3}He(d,p)^{4}He reaction and from the D(d,p)^{3}T reaction (^{3}He is formed by β-decay of ^{3}T in the target, and deuterium is gradually accumulated through irradiation) as shown in Fig. 5.3.4. The anisotropy correction factor was calculated from kinematics considering the slowing-down process of deuterons in the titanium-tritium layer.[7)]

5.4 Measurement

TPR distributions were measured along the central axis and the two radial axes for all three systems described in section 5.2. Behind the detector, blocks with a central channel (20 mm x 20 mm for Li_2O block, 20 mm$^\phi$ for Li_2CO_3, Be and polyethylene blocks) were used for insertion of the detector assembly (sse Fig. 5.4.1). A typical loading pattern of the blocks in the central drawer is shown in Fig. 5.4.2, for the case of detector position 15 cm. Because only one detector assembly can be inserted, the measurements of ^{6}Li- and ^{7}Li-glass could not be made simultaneously in the same drawer. For the axial direction, the measurements were thus carried out by traversing the ^{6}Li- glass along the central axial drawer and the ^{7}Li-glass along the off-central axial drawer. The TPR measured in this manner and that measured separately along the central axial drawer agreed within 1 %. For the radial direction, measurements were made by traversing the ^{6}Li and ^{7}Li-glass detectors in turns.

The neutron flux ranged from 10^3 to 10^5 neutrons/s/cm^2, depending on the detector locations. The measuring time was 1000 s.

To minimize the gain drift, the anode current of the photomultiplier was kept by adjusting the beam current of the neutron generator to keep the pulse height spectrum integral constant :

$$\sum_I I \times C(I) = \text{const.} \qquad (5.4.1)$$

Readjustment of the beam current was carried out for each run, thus keeping the gain drift within a few percent during the traverse. Imperfect adjustment of the beam current coild lead to 20 ∿ 30 % gain drift.

Measured results for the axial direction are shown in Figs. 5.4.3 - 5 together with results obtained by other measuring techniques. The results for the radial traverses are shown in Fig. 5.4.6.

5.5 Experimental Errors

5.5.1 Systematic Errors

Neutron yield

The systematic error of the absolute neutron yield, Y_n included uncertainty of the anisotropy correction factor R_α and that of solid angle $\Delta\Omega$ subtended by the SSD aperture. The anisotropy correction factor has the uncertainty of about 1.5 %, mainly due to nonuniformity of the tritium distribution caused by depletion of tritium by deuteron beam bombardment.[8] The uncertainty of $\Delta\Omega$ is estimated as 0.85 %. The overall error in the neutron yield thus comes to

$$\frac{\delta Y_n}{Y_n} = \sqrt{1.5^2 + 0.85^2} = 1.72\ [\%]. \qquad (5.5.1)$$

^{6}Li atom number

The ^{6}Li atom number in the ^{6}Li-glass scintillator (NS15) was determined by isotope dillution analysis (see Sect. 2.7) within an uncertainty of ±0.5 %.

5.5.2 Random Errors

Neutron counts

The neutron count error, originating in count statistics, was less than 0.5 %.

Couunts of ^{6}Li(n,α)^{3}T reaction

The random error of ^{6}Li(n,α)^{3}T reaction counts is subject to

count statistics. If, I and B are the integrated pulse height spectra in the $^6Li(n,\alpha)^3T$ peak region for ^6Li-glass and ^7Li-glass, respectively (see Fig. 5.5.1), the error of subtracted integrated pulse height spectra, C(=I-B) is,

$$\frac{\delta C}{C} = \frac{\delta(I-B)}{I-B} = \frac{\sqrt{(\Delta I)^2 + (\Delta B)^2}}{I-B} = \frac{\sqrt{I+B}}{I-B} = \frac{\sqrt{C+2B}}{C} . \qquad (5.5.2)$$

If,

$$K \equiv \frac{I}{I-C} = \frac{C+B}{B} ,$$

then,

$$\frac{\delta C}{C} = \sqrt{\frac{K+1}{K-1}} \cdot \frac{1}{\sqrt{C}} . \qquad (5.5.3)$$

In the Phase IIA measurements, C and K are 10000 - 100000 and 1.7 - 20.5, respectively. Consequently, $\Delta C/C$ = 0.3 - 1.1 %.

Fitting Error

Errors of the fitting method described in section 2.4 are estimated as follows :

(1) Calculate the statistical error $error_s$ of $S_0 = S(a_{min}, b_{min})$. Put, $S_1 = S_0 \times (1+error_s)$.

(2) Obtain the set of (a', b'), that satisfies $S(a', b') \leq S_1$ (see Fig. 5.5.2).

(3) The fitting error comes to $(S_{max}/S_0-1)\times 100$ [%], where S_{max} is maximum value of $S(a', b')$.

The overall errors for the Lithium-glass method are summarized in Table 5.5.1. As is shown, the main errors are the systematical error of the anisotropy correction factor R_α and the random error of the fitting method.

5.6 Comparison with the Other Measuring Techniques

The results of the Li-glass method were compared with those of the Li-metal method[9] and the zonal method.[10] Since the measuring

positions for these three methods were different, these comparisons were made by interpolating the Lithium-glass data to the positions of Li-metal and zonal data. Zonal data were compared with Li-glass data averaged over the zones. The interpolation was done by a linear-log scheme.

The comparisons for the Reference and the Be-sandwiched systems are shown in Figs. 5.6.1 and 5.6.2, respectively. Only the Li-glass method was applied for the Be-front system. The "experimental error of Li-glass" in the figures comprises all errors (systematic + random) of the Li-glass measurements. Li-glass results agree well with the Li-metal and zonal method within the experimental errors for both systems, except for locations adjacent to the beryllium layer in Be-sandwich system. It is believed that the discrepancies are caused by two factors :

(1) Interpolated values near the Be layer depend sensitively on the interpolation method because of the steep profile of the TPR distribution;
(2) Corrections for self-shielding are needed but not provided, for both the Li-glass and Li-metal results

5.7 Conclusion

The Lithium-glass method was applied to the measurement of tritium production rate distributions in simulated fusion blanket assemblies. An estimation of the experimental error was provided. The total systematic error was ±1.93 %; total random error came to ±0.60 - 3.90 %. Measured results were compared with β-counting methods (Li-metal method and zonal method); agreement was within the experimental errors except for the region adjacent the beryllium.

References

(1) Nakamura T. and Abdou M. A. : "Summary of Recent Results from the JAERI/US Fusion Neutronics Phase I Experiments," Proc. 7th Topical Meeting on the Technol. of Fusion Energy, San Francisco, (1986); Fusion Technol., 10, 541 (1986).

(2) Maekawa H., et al. : "Measured Neutron Parameters for Phase I Experiments at the FNS Facility," Proc. 7th Topical Meeting on the Trchnol. Fusion Energy, (1988); Fusion Technol. 10, 564 (1988).

(3) Yamaguchi S. and Nakamura T. : "Tritium Production Measurements by the Lithium-Glass Scintillator Method," Proc. 7th Topical Meeting on the Technol. Fusion Energy (1986); Fusion Technol.,10, 573 (1986).

(4) Oyama Y., Tsuda K., Yamaguchi S., et al. : "Experimental Results for Phase II of JAERI/USDOE Collaborative Program on Fusion Blanket Neutronics," Proc. Int. Symp. on Fusion Nucl. Technol., Tokyo, April 10-15 (1988); to be published in J. Fusion Eng. Design.

(5) Oyama Y., Yamaguchi S., et al. : "Phase-IIB Experiment of JAERI/ USDOE Collaborative Program on Fusion Blanket Neutronics," submitted to 8th Topical Meeting on the Technol. Fusion Energy (1988).

(6) Nakamura T., et al. : "A DT Neutron Source for Fusion Neutronics Experiments at the JAERI," Proc. Int. Ion Eng. Congress — ISIAT '83 & IAPT '83, Kyoto, Japan, vol.1, 567 (1983).

(7) Logan C. M. and Heikikinen D. W. : Nucl. Instr. Meth. 200, 105 (1982).

(8) Yamaguchi S., et al. : "Calculation of Anisotropy Correction Factor for Determination of D-T Neutron Yield by Associated α-particle Method," JAERI-M 84-109 (1984).

(9) Porges K., private communication.

(10) Tsuda K., et al. : "Development of a Measuring Technique of Zonal Tritium Production Rate and Its Application," JAERI-M 87-126, p.104 (1987).

Table 5.5.1 Error estimation of the TPR measurement by the Lithium-glass method

source of error	systematic error [%]	random error [%]
statistic	———	± 0.18 ∿ 0.94
fitting	———	± 0.30 ∿ 2.20
neutron yield	± 1.86	± 0.05 ∿ 0.53
^{6}Li atom number	± 0.50	———
total	± 1.93	± 0.60 ∿ 3.90
overall	± 2.56 ∿ 5.86	

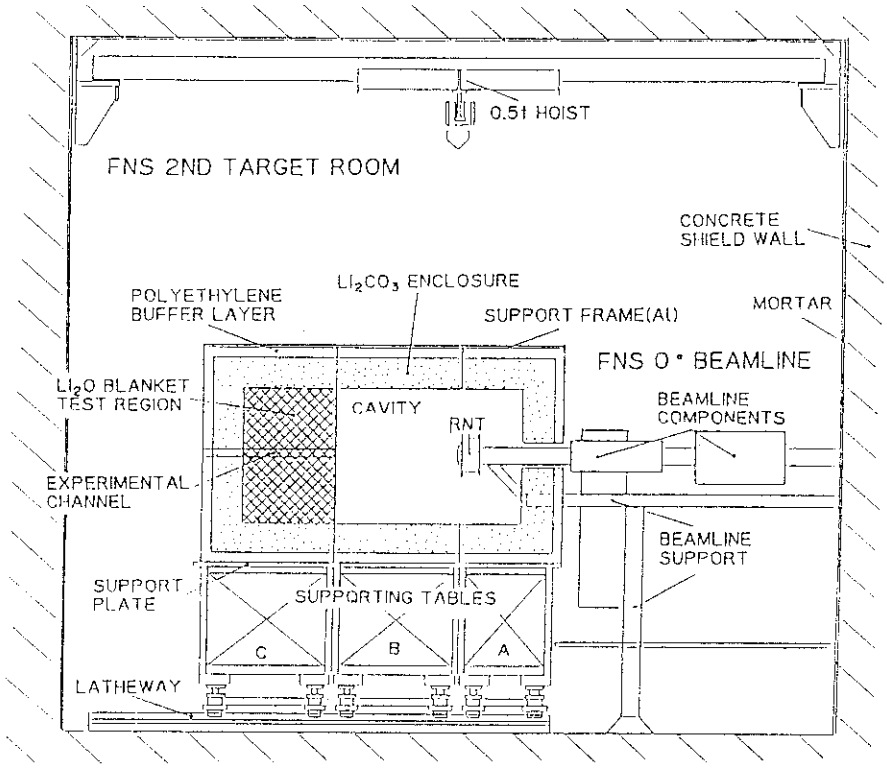

Fig. 5.2.1 Cross sectional view of the Phase II experimental arrangement

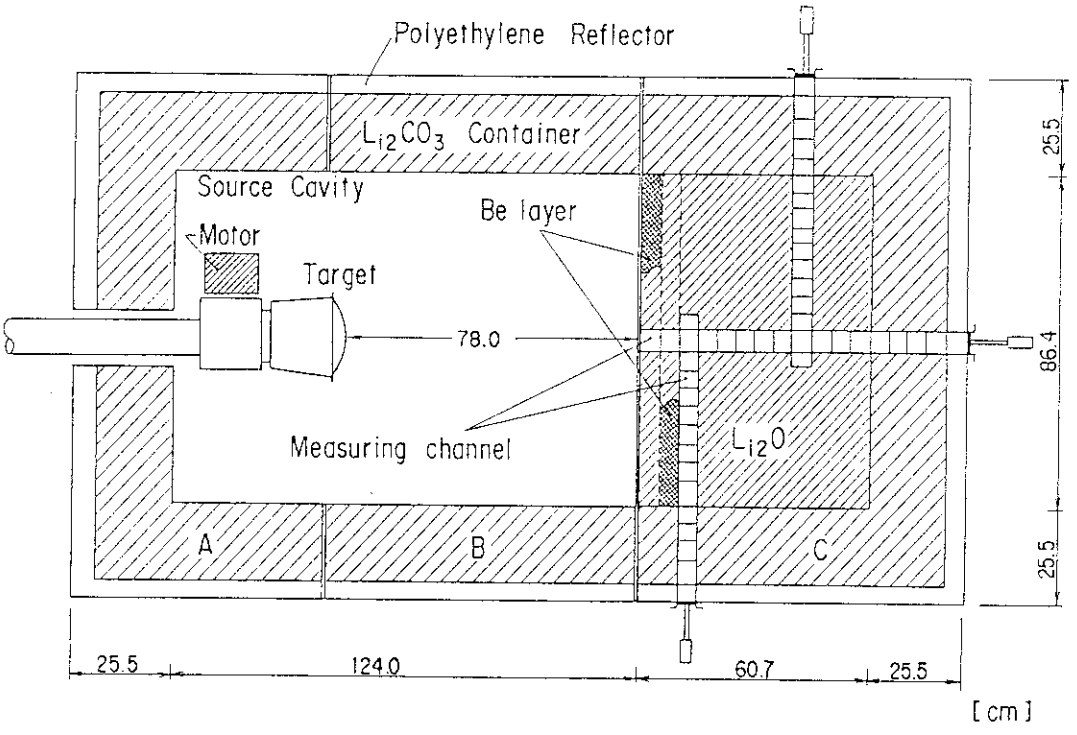

Fig. 5.2.2 Top view of thge Phase II experimental arrangement

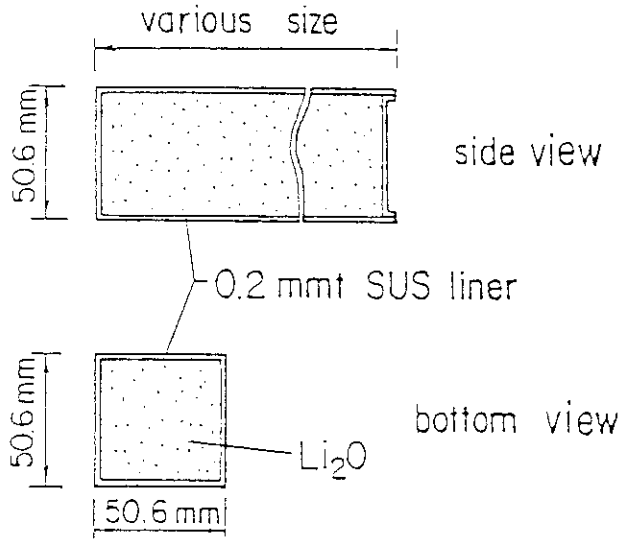

Fig. 5.2.3 Li_2O blocks

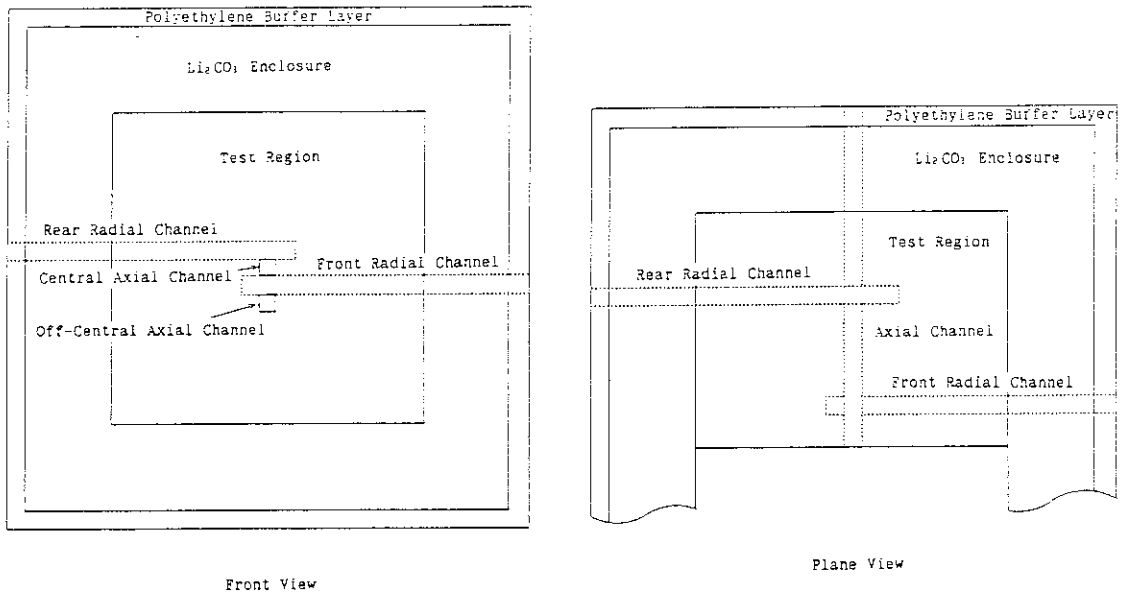

Fig. 5.2.4 Locations of the experimental channels in the test zone

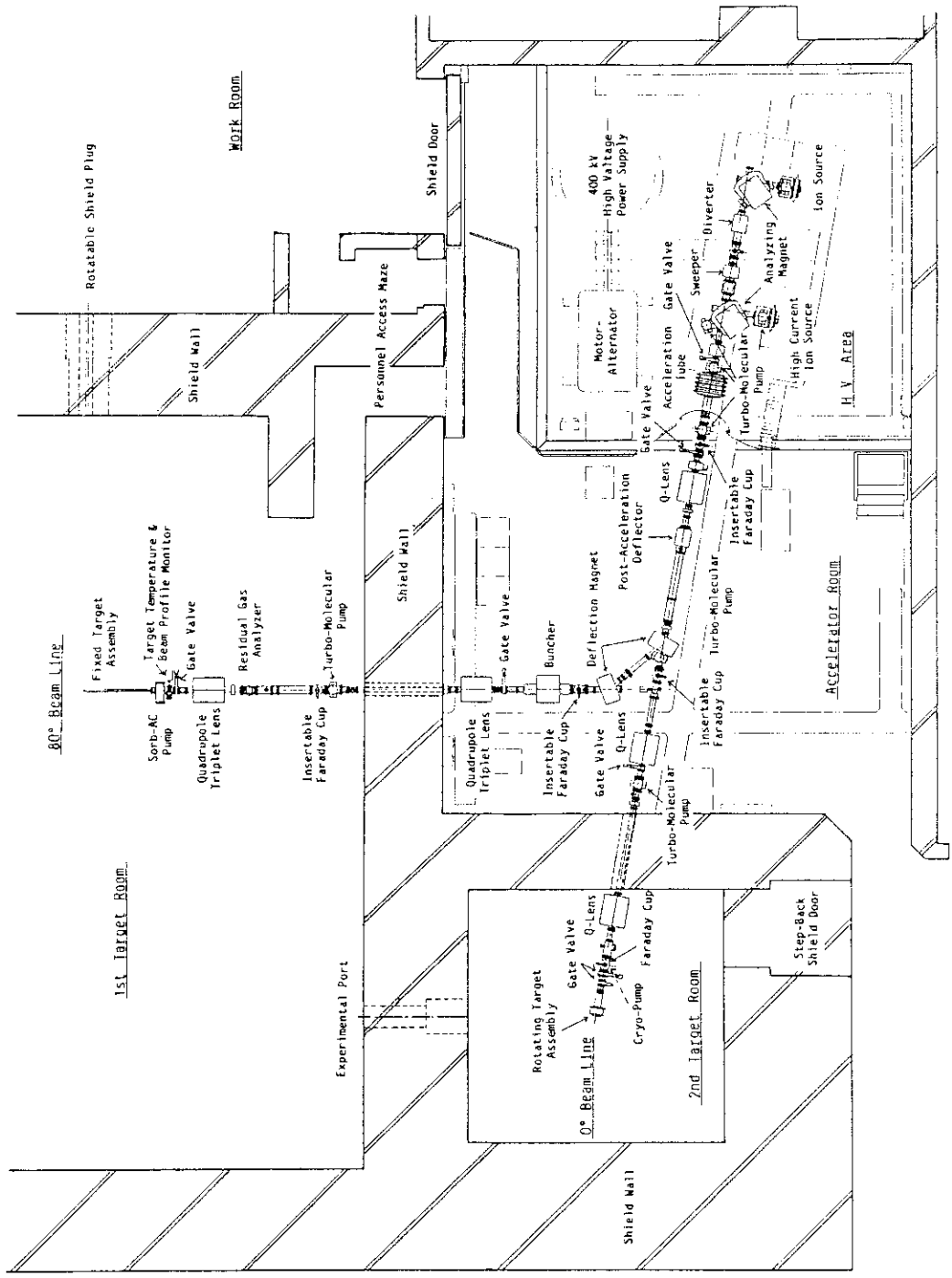

Fig. 5.3.1 FNS accelerator system

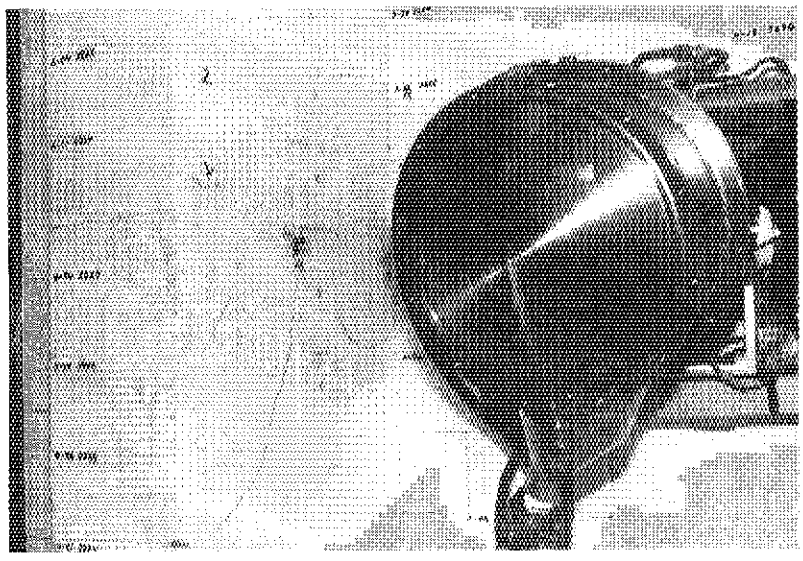

Fig. 5.3.2 Rotating target assembly

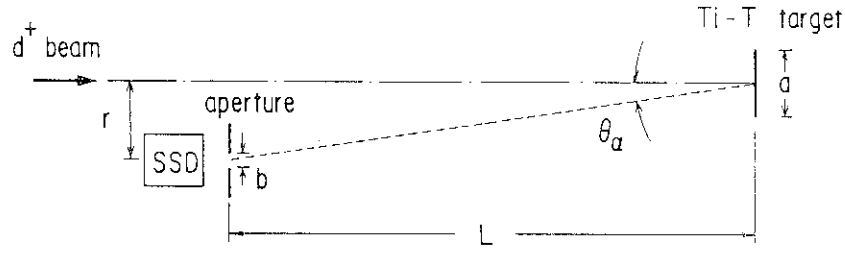

Fig. 5.3.3 Geometrical configuration of the α-monitor in the beamline (a ∿ 10 mm, b = 0.9489±0.0035 mm, L = 967.3±2 mm, r = 26.65±1 mm, θ_α = 1.6°)

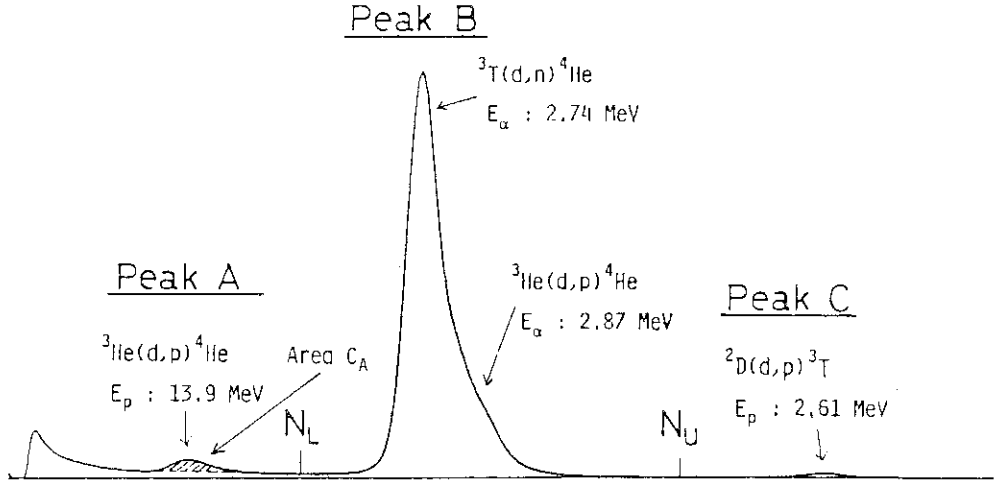

Fig. 5.3.4 Typical pulse height spectrum of the α-monitor

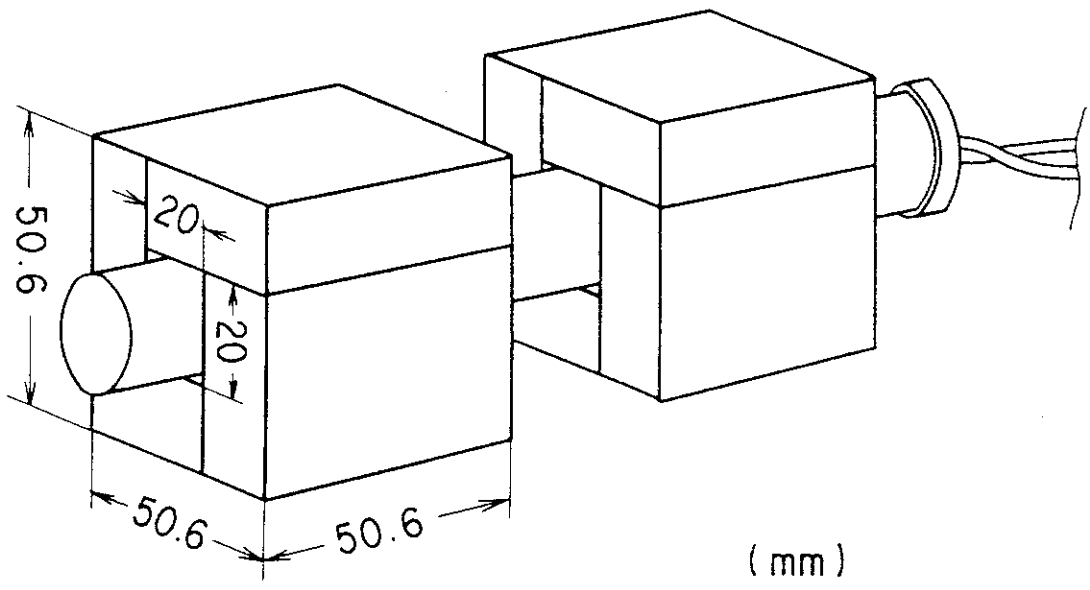

Fig. 5.4.1 The Lithium-glass detector assembly in Li_2O block with experimental hole

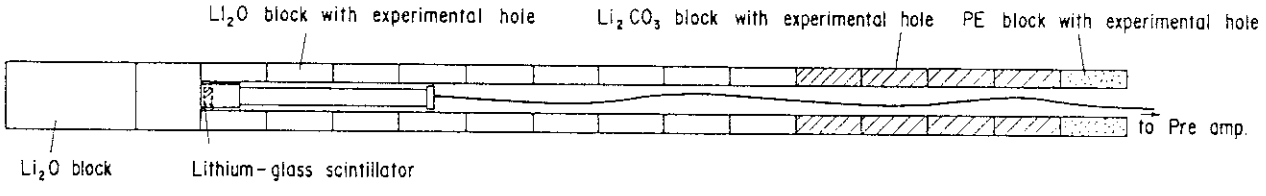

Fig. 5.4.2 A loading pattern of Li_2O blocks in an experimental channel

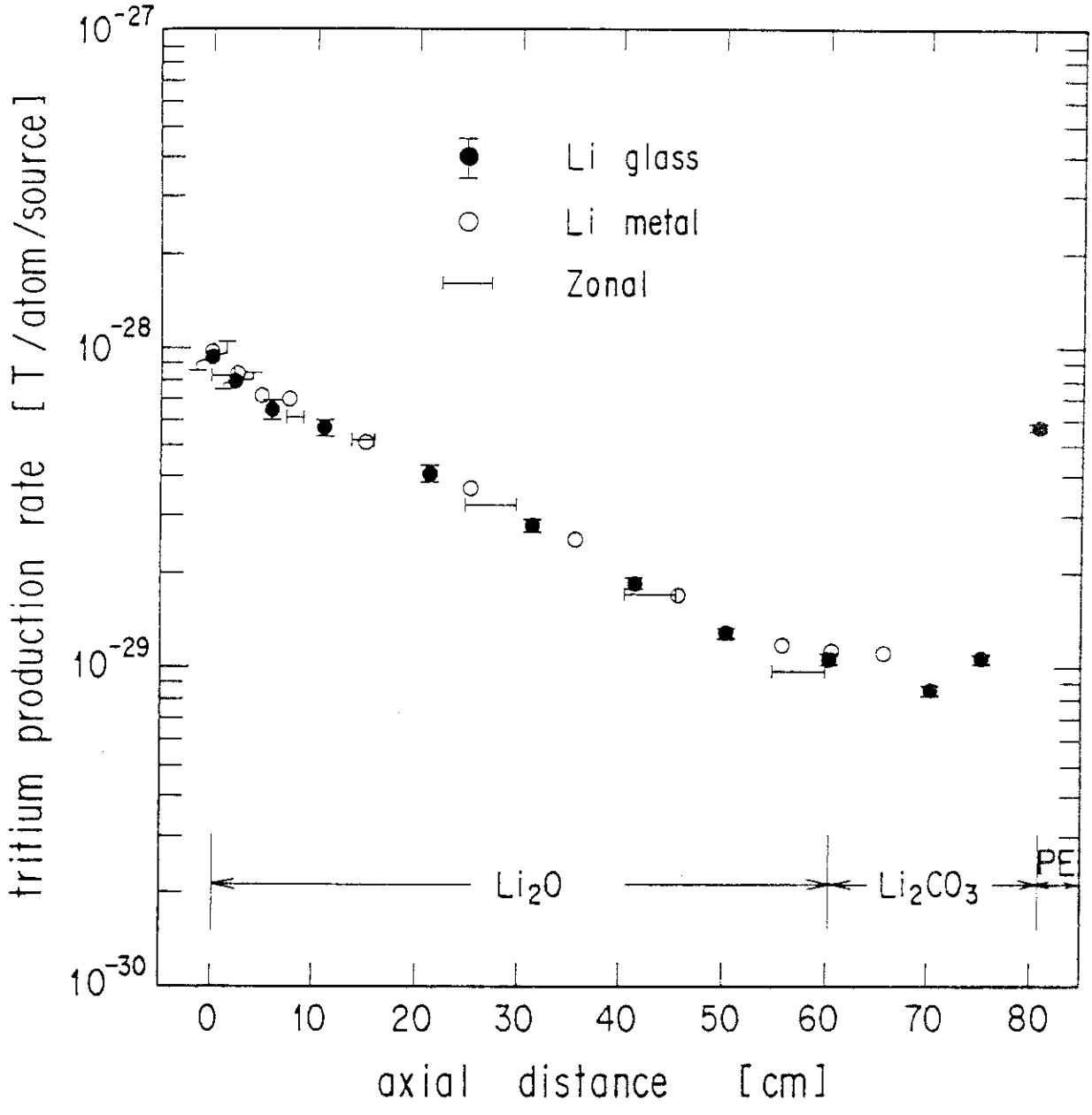

Fig. 5.4.3 Measured tritium production rate distribution in the Reference system with Lithium-glass, Li-metal and Zonal methods

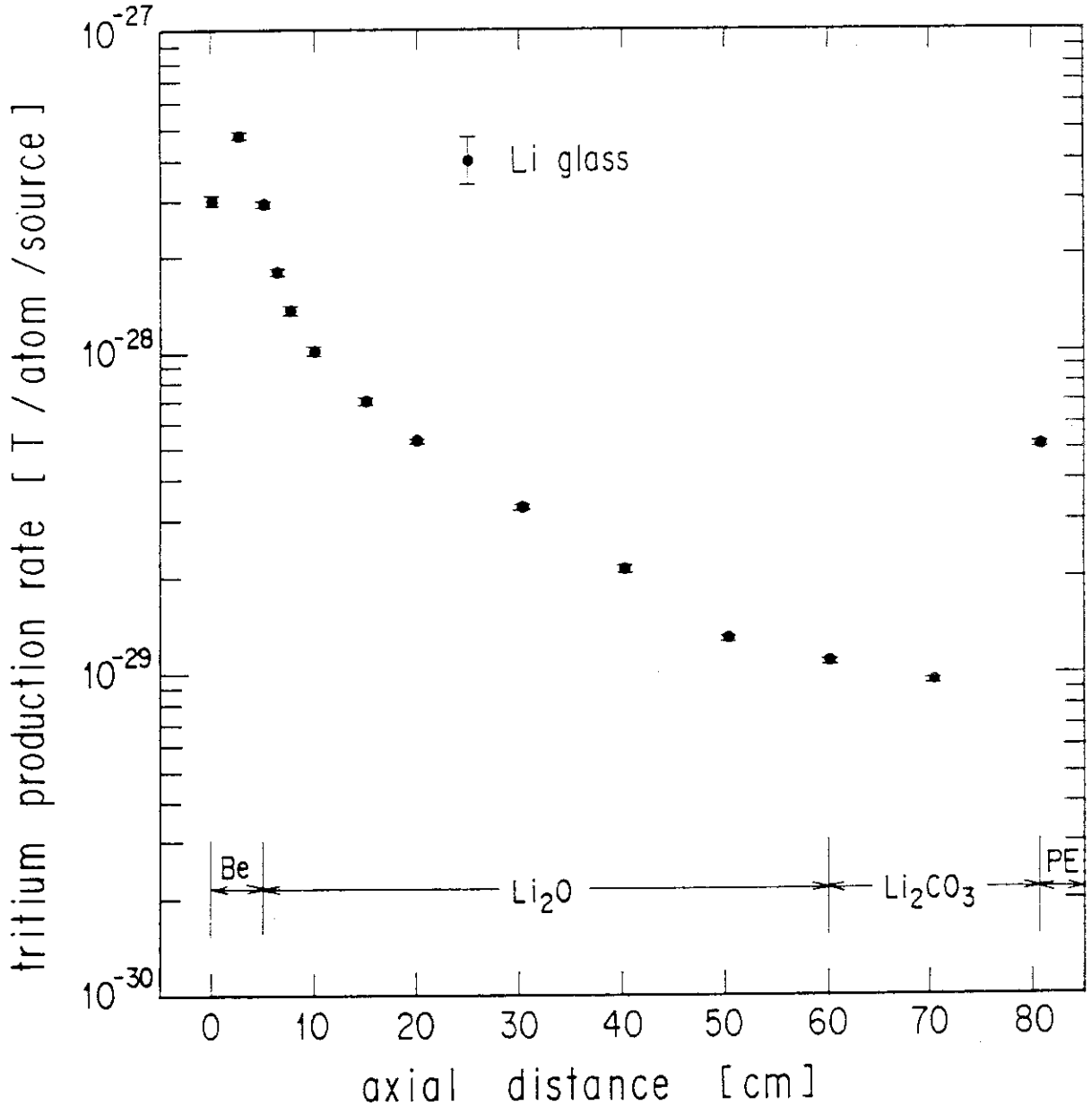

Fig. 5.4.4 Measured tritium production rate distribution in the Be front system with Lithium-glass method

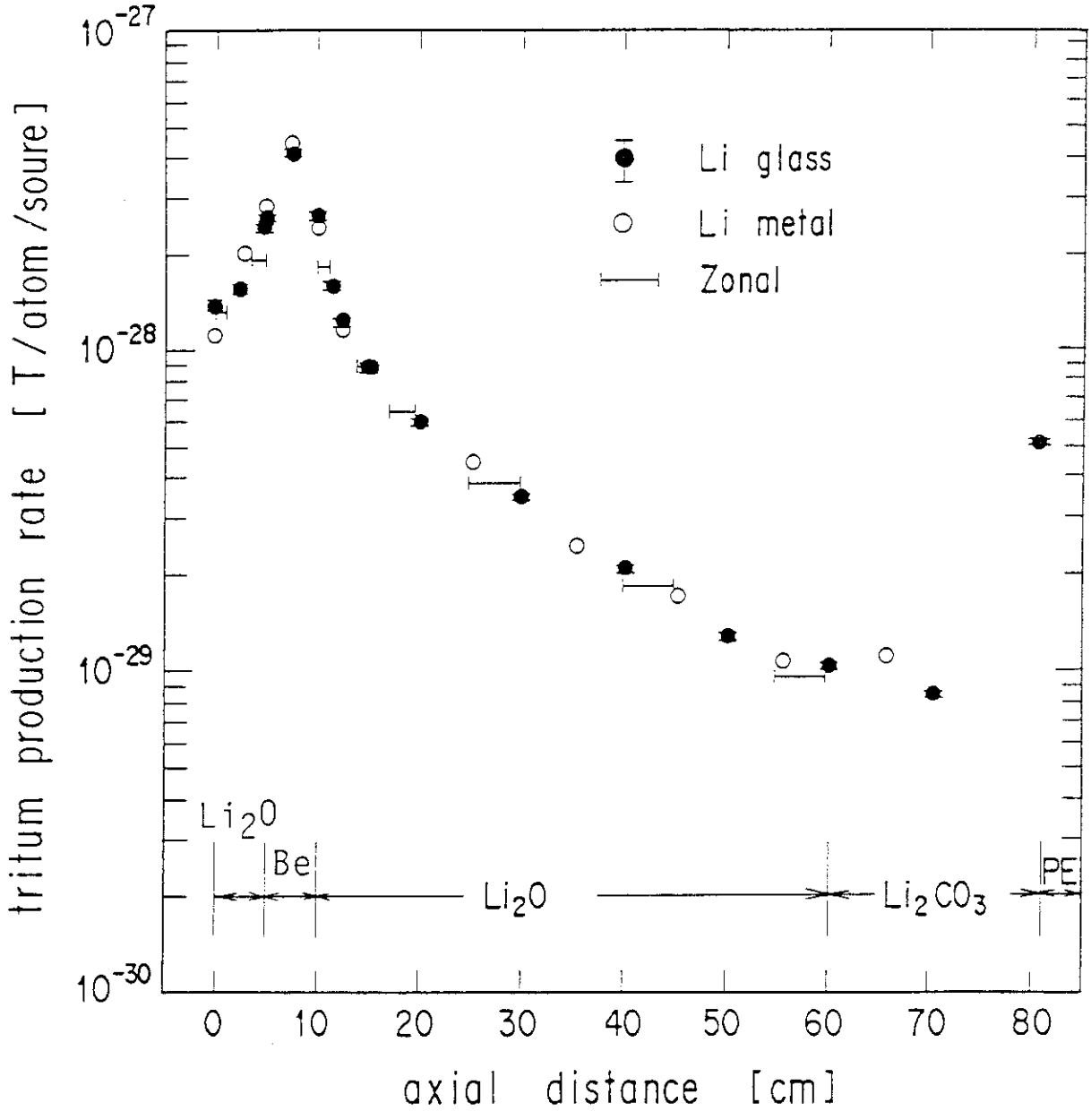

Fig. 5.4.5 Measured tritium production rate distribution in the Be sandwiched systrem with Lithium-glass, Li-metal and Zonal methods

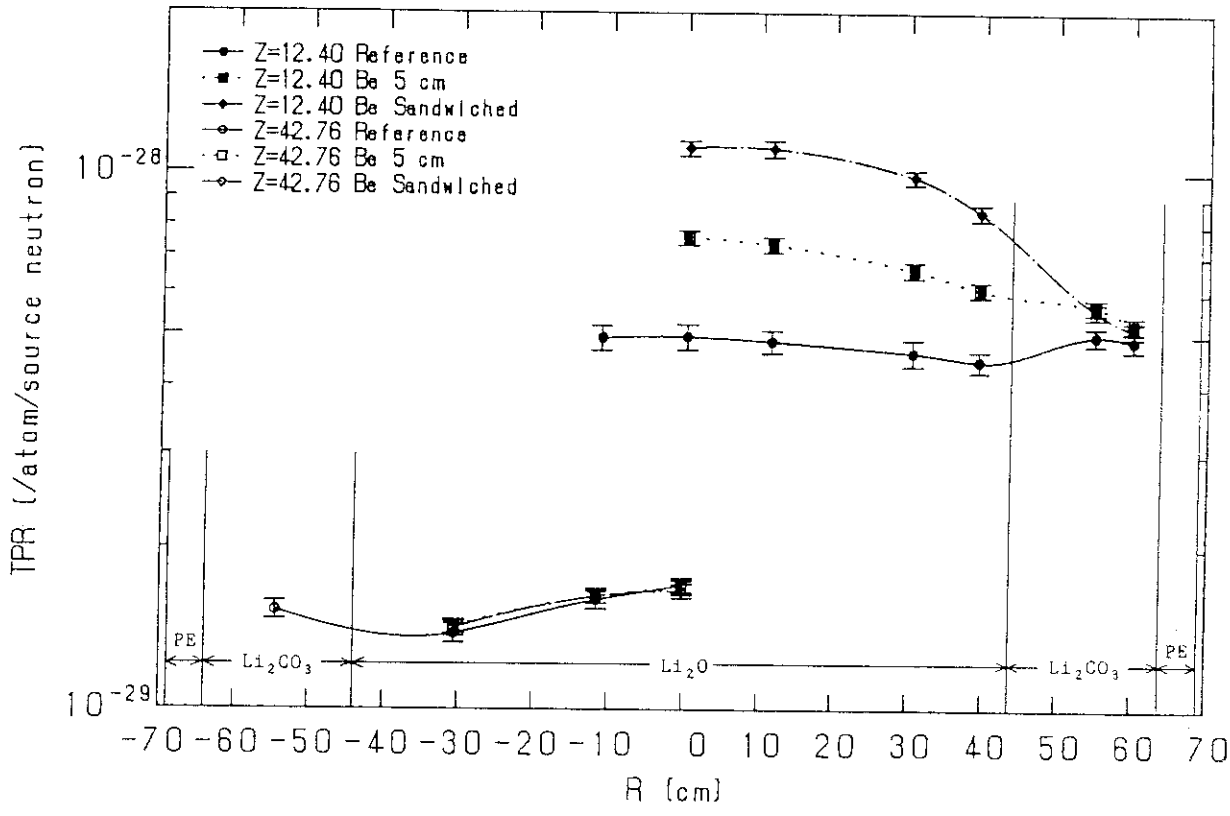

Fig. 5.4.6 Measured tritium production rate distributions in the radial directions with Lithium-glass method

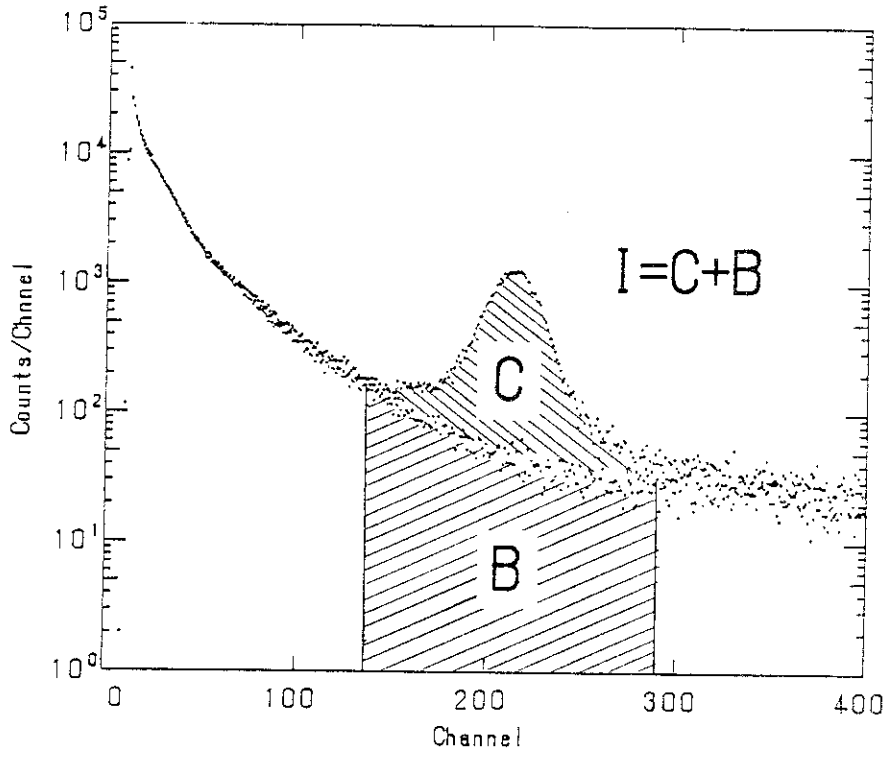

Fig. 5.5.1 Pulse height spectra of ^{6}Li and ^{7}Li-glass scintillators. I and B are total count of ^{6}Li and ^{7}Li-glass in the $^{6}Li(n,\alpha)^{3}T$ peak, respectively. C=I-B.

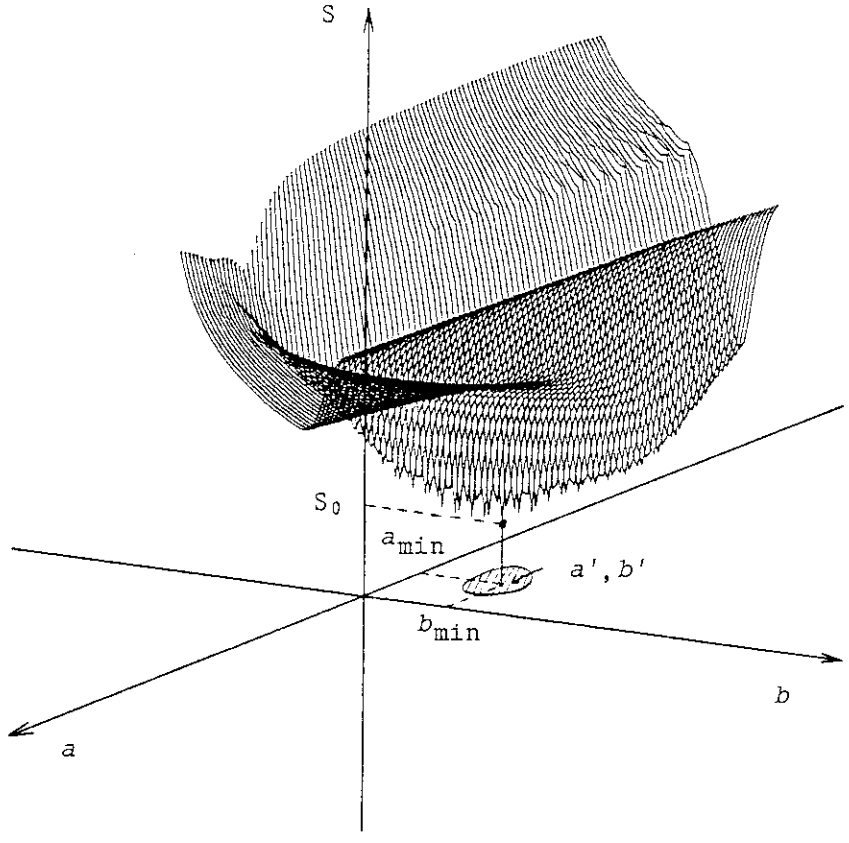

Fig. 5.5.2 Estimation of the fitting error

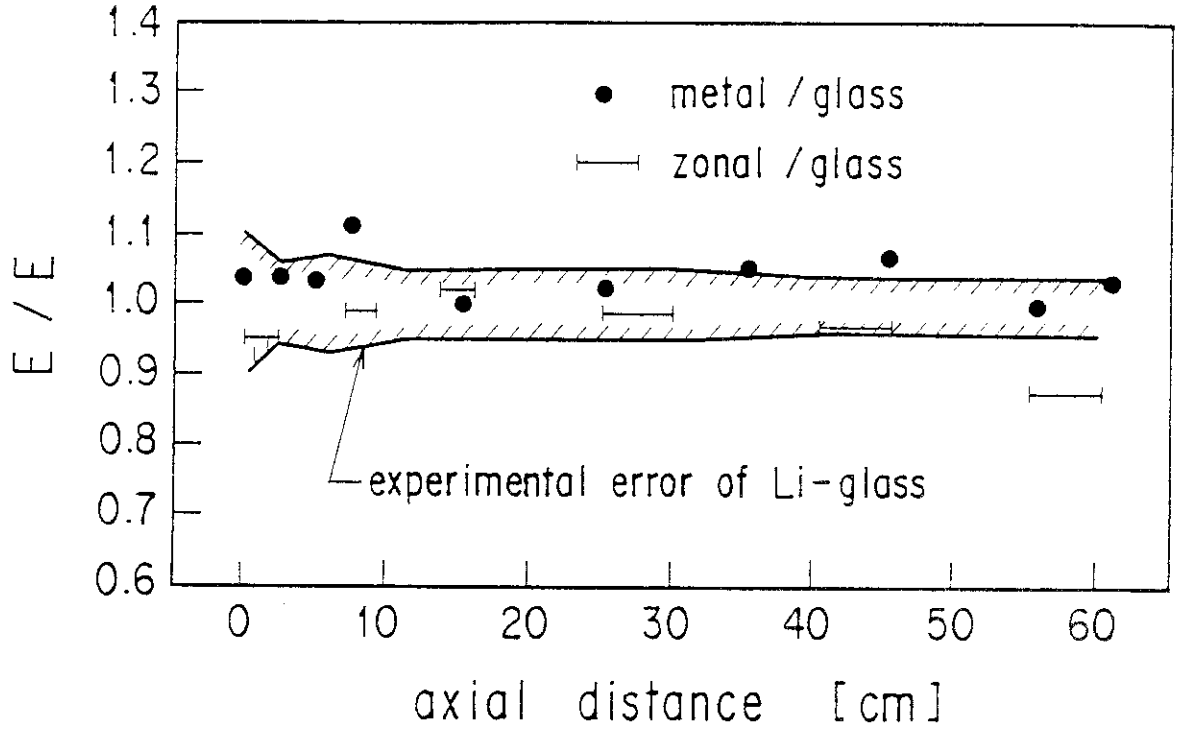

Fig. 5.6.1 The ratio of the measured TPR's of Li-glass method to those of the other measuring techniques for the Reference system

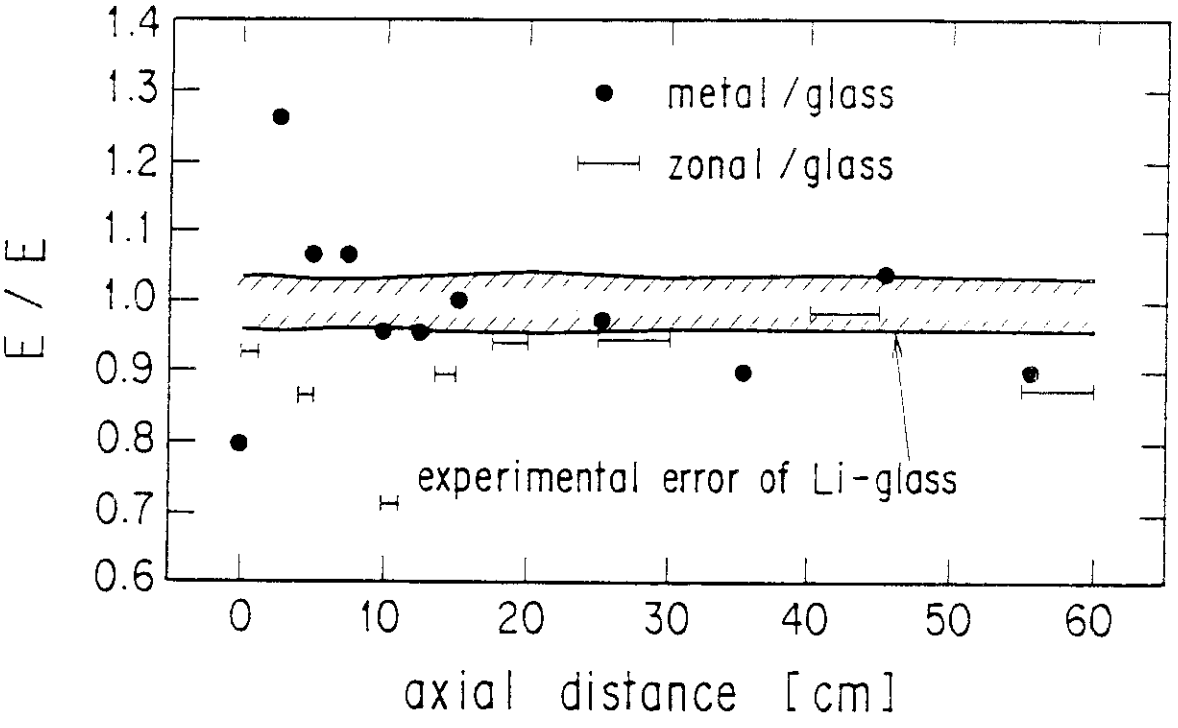

Fig. 5.6.2 The ratio of the measured TPR's of Li-glass method to those of the other measuring techniques for the Be sandwiched system

6. Application of Optical Fiber Light Guides to the Li-Glass Method[1)]

6.1 Introduction

A system connecting miniature ^{6}Li and ^{7}Li-glass scintillators (1.6 mm x 4.0 mm x 0.3 mm) with photomultiplier tubes (PMT's) using optical fiber was developed with a view of exploiting the following possibilities :

1) Simultaneous measurement of the pulse height spectra of ^{6}Li and ^{7}Li-glasses at the same position,
2) Reduction of the flux perturbation due to the insertion of the detector assembly, especially when the neutron current from PMT side is large,
3) Reduction of gain drift due to local release effect on the PMT and potential application in high temperature blankets,
4) Measurement in a strong electromagnetic field.

The thermal neutron response of this fiber system was measured, it was then applied to a TPR measurement in a simulated fusion blanket assembly irradiated by 14-MeV neutrons. The extraction of scintillation signals using optical fiber light guide in a Tokamak installation has been proposed by Seiler and Hendel[2)], Miley and Kislev,[3)] and Elevant.[4)] The TFTR group[5)] reported a measurment of tritons generated by the D-D reaction using ZnS scintillator and a 15 m-long light guide. The measurement described in this chapter is the first application of fiber-coupled scintillators in a DT neutron field.

6.2 Structure of the Optical Fiber System

The system included ^{6}Li and ^{7}Li-glass scintillators, an optical fiber light guide and a PMT/voltage divider unit. A photograph of the whole system is shown in Fig. 6.2.1. The electronic circuit was the same as that in Chap. 2.

Scintillators

The ^{6}Li and ^{7}Li-glass scintillators (NS15 and BS15, respectively) were manufactured from the same batch as described in Chap. 2, in rectangular pieces of 1.6 mm x 4.0 mm x 0.3 mm size. One side of the

scintillators was smoothed by optical polishing and the other sides were roughened. Silicon grease was used to couple the scintillators to the optical fiber via quartz light guide of 1.6 mm x 4.0 mm x 2.0 mm size. NE560 reflector was applied to the surfaces of the scintillators and light guides.

Optical fiber

The optical fiber was ultraviolet-ray(UV) transmitting type, manufactured by the Mitsubishi Cable Industries Ltd. The Transmission characteristics of this optical fiber are shown in Fig. 6.2.2. The wave length of the NS15 lithium-glass scintillator which gives maximum intensity is 0.39 μm as shown in Fig. 2.2.1. The transmittance at this wave length is about 0.88. Diameters of the core and clad are 230 μm and 250 μm, respectively (see Fig. 6.2.3). Refractive indices of the core and clad are 1.49405(n_1) and 1.4585(n_2) for 0.38 μm wave length, respectively. The numerical aperture ($NA=\sqrt{n_1^2-n_2^2}$) is 0.324. Accordingly, the maximum incident angle ($\theta = \sin^{-1}(NA)$) and the maximum incident solid angle ($\Delta\Omega = 2\pi(1-\cos\theta)$) comes to 18.8° and 0.339, respectively.

Each of the bundle coupling ^{6}Li and ^{7}Li-glass pieces is composed of 121 fibers, and measures 1 m in length. Cross sectional views of the fiber are shown in Figs. 6.2.4 (a) (scintillator side) and 6.2.4 (c) (PMT side). The diameter of the bundle at the PMT side is 3.0 mm. A teflon plate was inserted between the two bundles (see Fig. 6.2.4 (a)) at the scintillator end in order to avoid the interference of light from both scintillators. The aluminum cap (see Fig. 6.2.4 (b)) was manufactured by discharge processing.

PMT/voltage divider unit

Plane and crosssectional views of the PMT/voltage divider unit are shown in Fig. 6.2.4. The PMT's were R647-01 (Hamamatsu Photonics Corp.) The optical fibers were coupled to the faces of the PMT's by pressure, using a spring in the PMT case and that in connectors.

6.3 Characteristics of the Optical Fiber System

The response of the optical fiber system to thermal neutrons was inferred from measurements with and without optical fiber. The thermal

neutron field was produced by an Am-Be neutron source moderated in a graphite pile (see Chap 3). Measured responses are shown in Fig. 6.3.1. Different amplifier gains were used. The optical fiber reduced output pulse height by a factor of 28. Energy resolution was 68.1 % and 12.6 %, respectively with and without the optical fiber system.

Decrease of the light output by the use of optical fiber light guide can be estimated as follows (see Table 6.3.1). Total transmission efficiencies for with and without optical fiber light guide, η_1, η_2 are given by:

$$\eta_1 = g \times \varepsilon_4, \tag{6.3.1}$$

$$\eta_2 = g \times a \times s \times \varepsilon_1 \times \varepsilon_2 \times \varepsilon_3, \tag{6.3.2}$$

where

g : geometrical factor, that is, the ratio of scintillator cross section (scintillator is connecting to light guide on this surface) to its surface area,

a : light incidence efficiency, $\Delta\Omega/2\pi$,

s : effective cross section ratio, that is, the ratio of total cross section of cores to the scintillator cross section,

ε_1 : transmission efficiency of optical fiber light guide,

ε_2 : transmission efficiency between scintillator and optical fiber light guide,

ε_3 : transmission efficiency between optical fiber light guide and PMT,

ε_4 : transmission efficiency between scintillator and PMT.

The values of ε_2, ε_3 and ε_4 are calculated by Fresnel's law. The values of η_1 and η_2 come to 0.396 and 0.0147, respectively. Decrease of light output, therefore, comes to 0.0147/0.396 = 0.0372 = 1/27. This value approximately agrees with the observed value of 1/28. It is shown that the dominant factor for the decrease of light intensity is the light incidence efficiency, a. In order to alleviate the light intensity decrease, it is necessary to develop an UV-transmitting optical fiber with large maximum solid angle, or in other words, with large numerical aperture.

6.4 Application of the Optical Fiber System

The optical fiber system was applied to the measurement of the TPR distribution in a simulated fusion blanket assembly located in a DT neutron field. The assembly was the "Phase IIA Be sandwiched system" described in Chap. 5. Li_2O blocks with an experimental hole of 7 mm by 7 mm were used (see Fig. 6.4.1). Typical pulse height spectra and the subtracted spectrum are shown in Fig. 6.4.2. As is shown in this figure, the $^6Li(n,\alpha)^3T$ peak still featured a large signal-to-noise (S/N) ratio even in a DT neutron field. However, the S/N ratio was somewhat worse at the lower energy side of the peak, and the subtraction error thus became fairly large. In the present study, the TPR's were calculated by multiplying a factor k by the integral over the subtracted spectrum above the peak. The factor k, obtained from the spectrum including the edge-effect described in Chap. 4, came to 2.49. TPR distribution measured with and without the optical fiber system are shown in Fig. 6.4.3. The data at deeper locations were not obtained because of poor S/N ratios, in the front, however, good agreement was obtained. The discrepancy of TPR's between with and without optical fiber system may be caused by fitting error due to low S/N ratio for optical fiber system. This discrepancy should be improved if large S/N ratio is obtained by development of optical fiber with large numerical aperture and alleviation of light intensity decrease.

6.5 Conclusion

A TPR measuring system using optical fiber light transmission was designed and fablicated. Measurement of the thermal neutron response, indicated that the output pulse height is reduced by a factor of 27 while the energy resolution increases from 12.6 % to 68.1 % by using the optical fiber system. This system was applied to a fusion blanket assembly TPR measurement in a DT neutron field. The measured distribution agreed well with conventional methods. Important advantages that can be claimed for an optical fiber system include : 1) capability of simultaneous measurement of ^6Li and ^7Li-glasses, 2) small perturbation of the neutron flux, 3) high temperature insensitivity and 4) magnetic field compatibility. Disadvantages of the system are low pulse height and large energy resolution. Thus an optical fiber system would be useful for a survey experiment,

conducted in a high temperature, high electromagnetic field environment when high accuracy is not required. To apply this optical fiber system to actual fusion environment, however, radiation effects on scintillator response, transmittance of optical fiber light guide and background noise should be investigated.

References

1) Yamaguchi S., et al. : to be submitted to Nucl. Instr. Meth.
2) Seiler S. and Hendel H. : Bull. Am. Phys. Soc. 23, 701 (1978).
3) Kislev H. and Miley G. : Bill. Am. Phys. Soc. 29, 1309 (1984).
4) Elevant T. ; Royal Institute of Technology Report No, TRITA-RFU-84-4, (1984).
4) Zweben S. J. : Rev. Sci. Instrum. 57[8], 1774 (1986).

Table 6.3.1 Transmission efficiency of the optical fiber system

	without fiber	with fiber
geometrical factor, g	0.396	0.396
light incidence efficiency, a	———	0.0539
effective cross section ratio, s	———	0.785
ε_1(fiber)	———	0.88*
ε_2(scinti. - fiber)	———	0.999*
ε_3(fiber - PMT)	———	1.000*
ε_4(scinti. - PMT)	1.000*	———
total efficiency	0.396 = η_1	0.0147 = η_2

ε_1 : transmission efficiency of optical fiber

ε_2 : transmission efficiency between scintillator and optical fiber

ε_3 : transmission efficiency between optical fiber and PMT

ε_4 : transmission efficiency between scintillator and PMT

* : for wave length of 380 nm

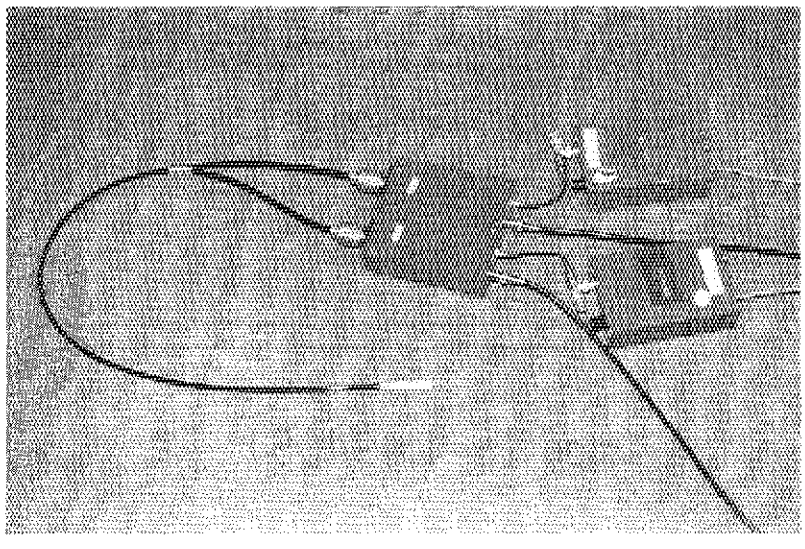

Fig. 6.2.1 Photograph of the optical fiber system

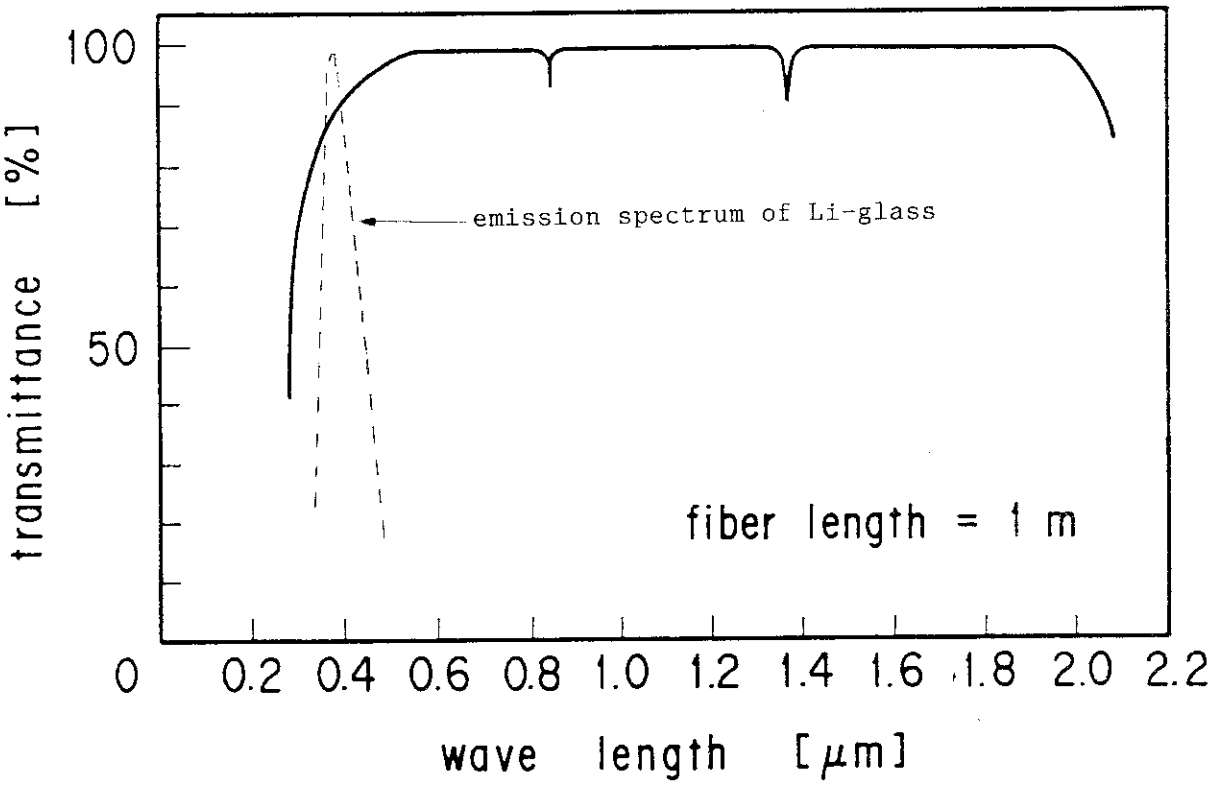

Fig. 6.2.2 Transmittance of the optical fiber

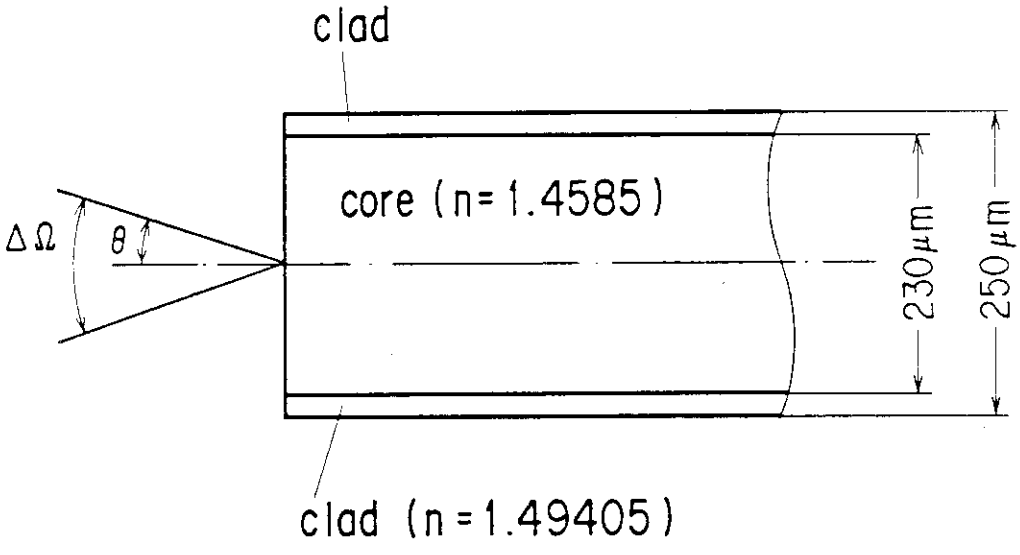

Fig. 6.2.3 Cross sectional view of optical fiber,
n = refractive index, θ = maximum incident angle,
ΔΩ = maximum incident solid angle

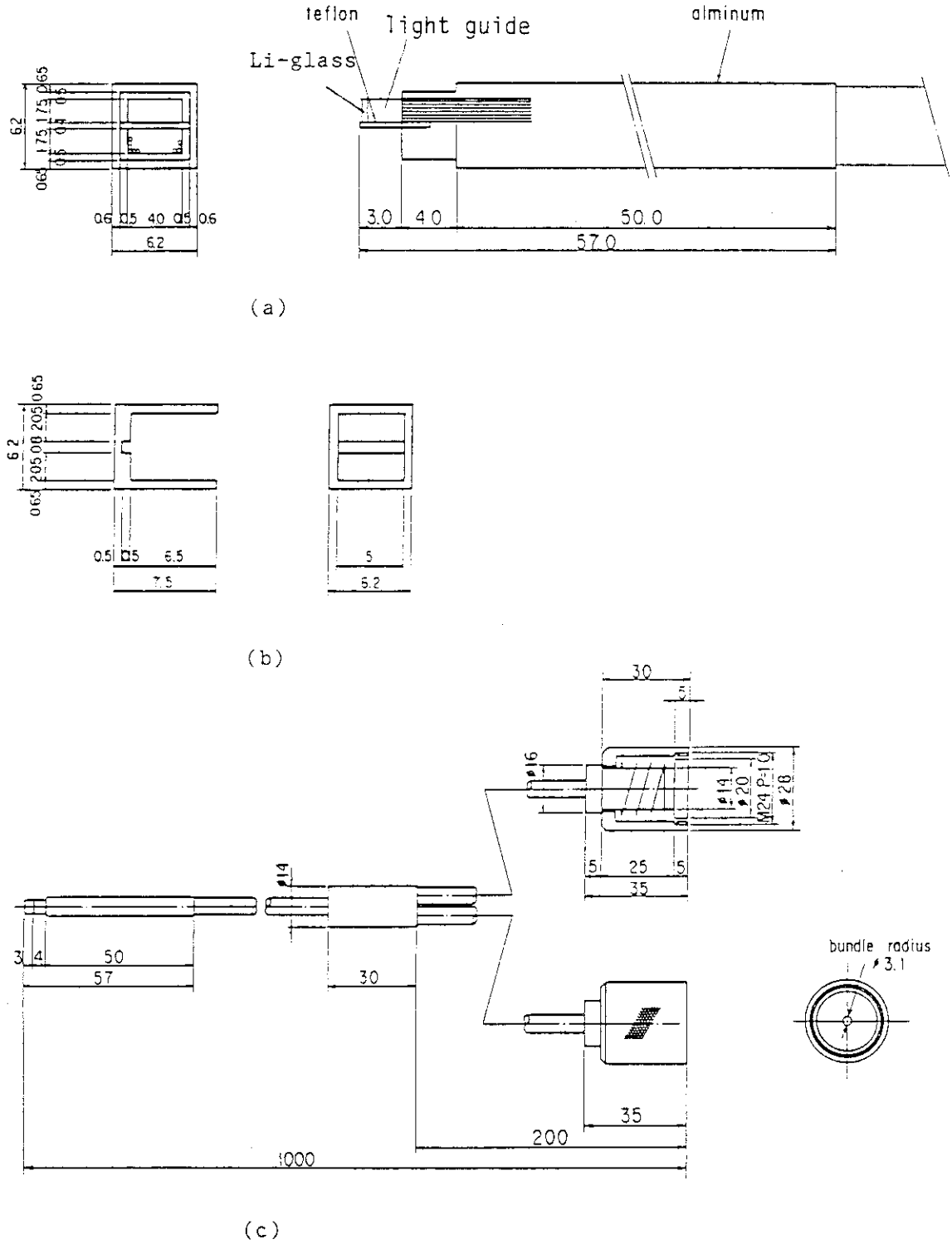

Fig. 6.2.4 Structure of the optical fiber system, (a) head of fiber, (b) alminum cap, (c) conector to the photo-multiplier tube

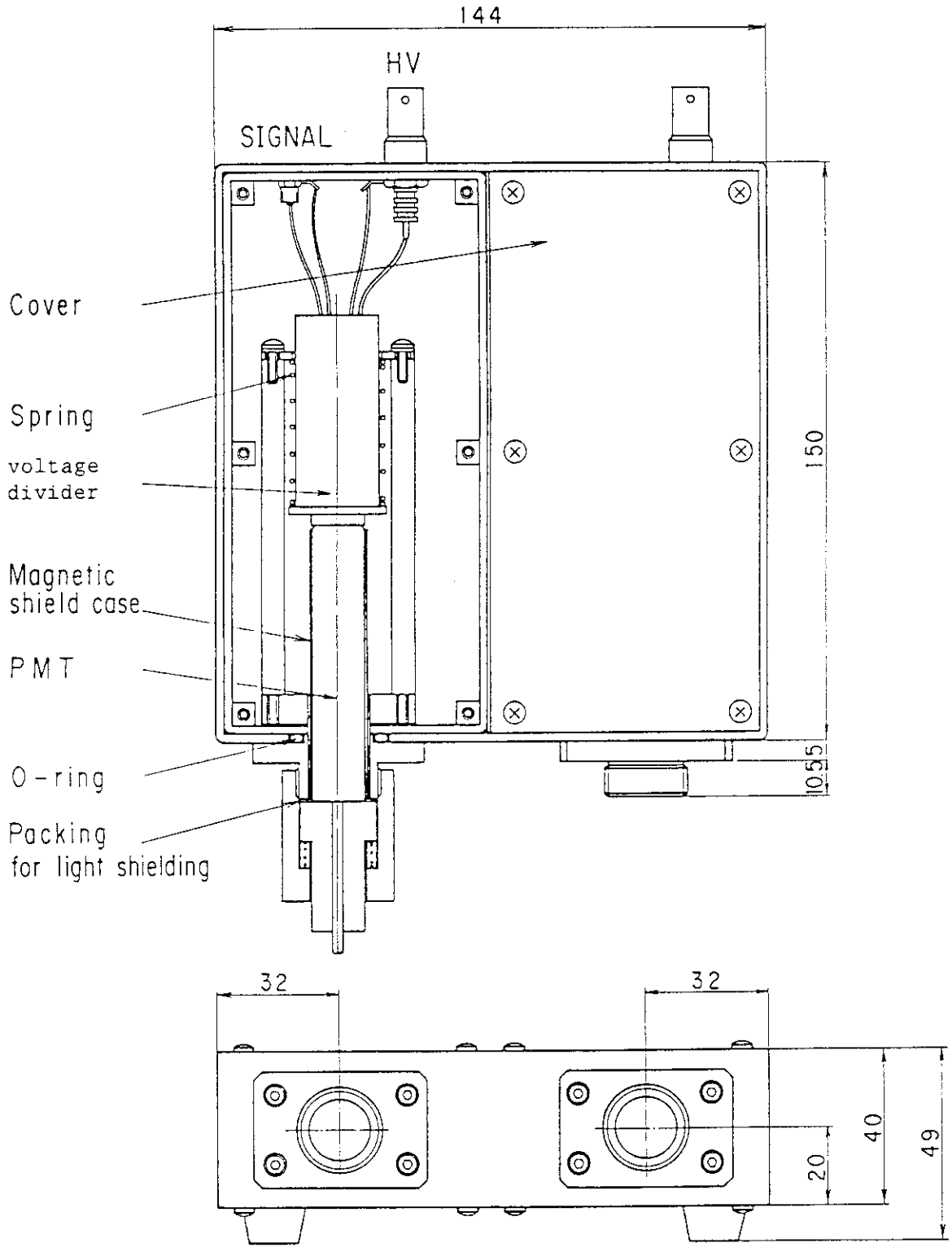

Fig. 6.2.5 Structure of the PMT/voltage divider unit

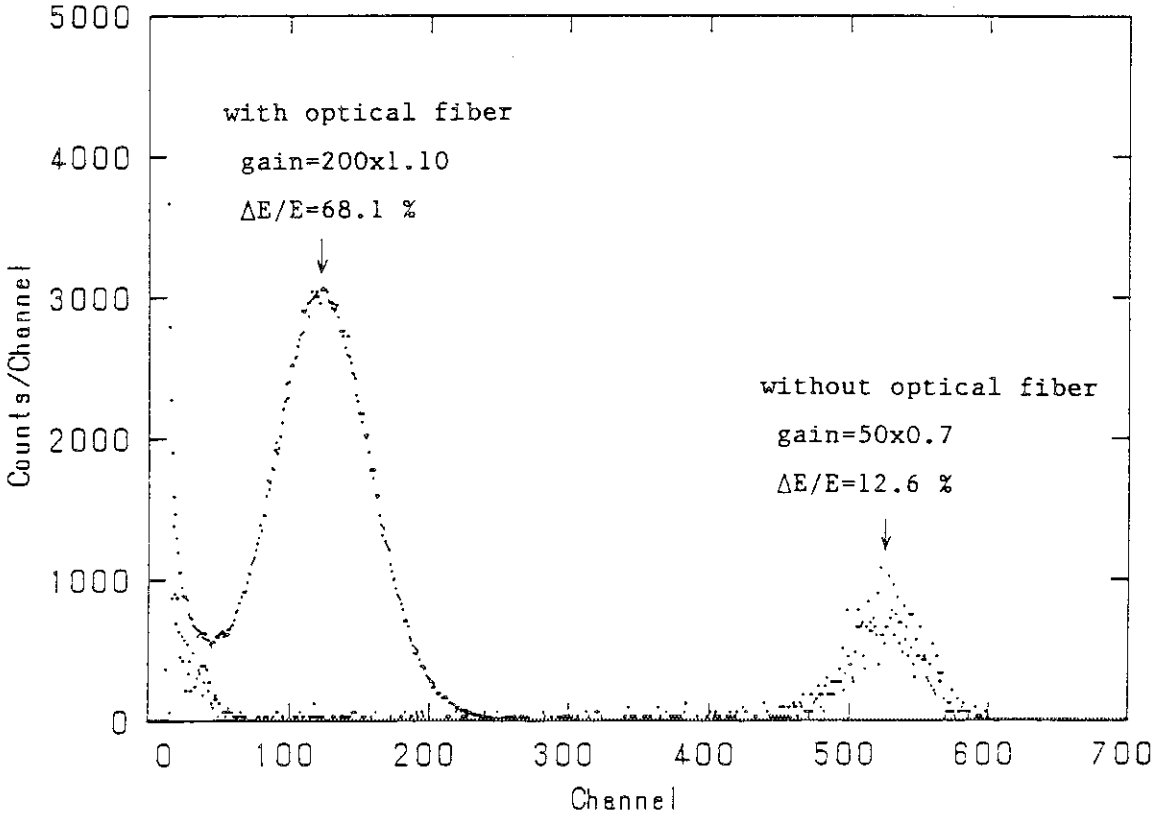

Fig. 6.3.1 Pulse height spectrum of the ^{6}Li-glass scintillator with and without optical fiber system for thermal neutrons

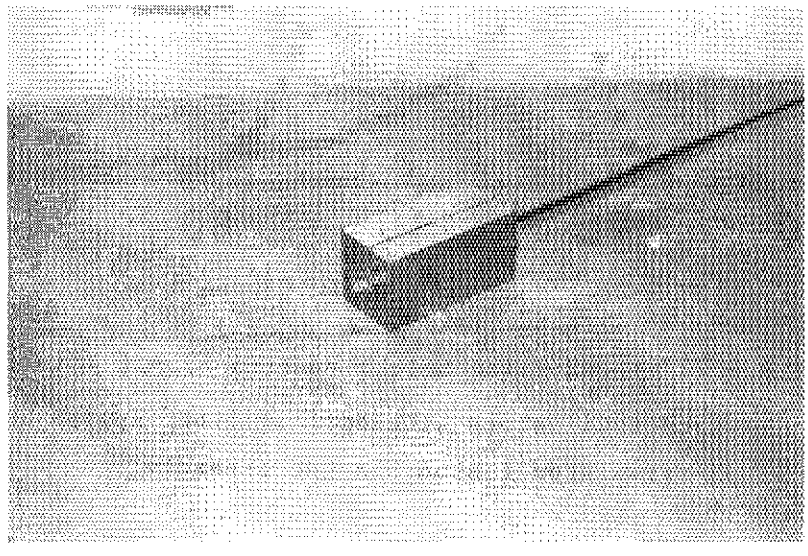

Fig. 6.4.1 Optical fiber system in the Li_2O blocks with experimental hole (7 mm x 7 mm)

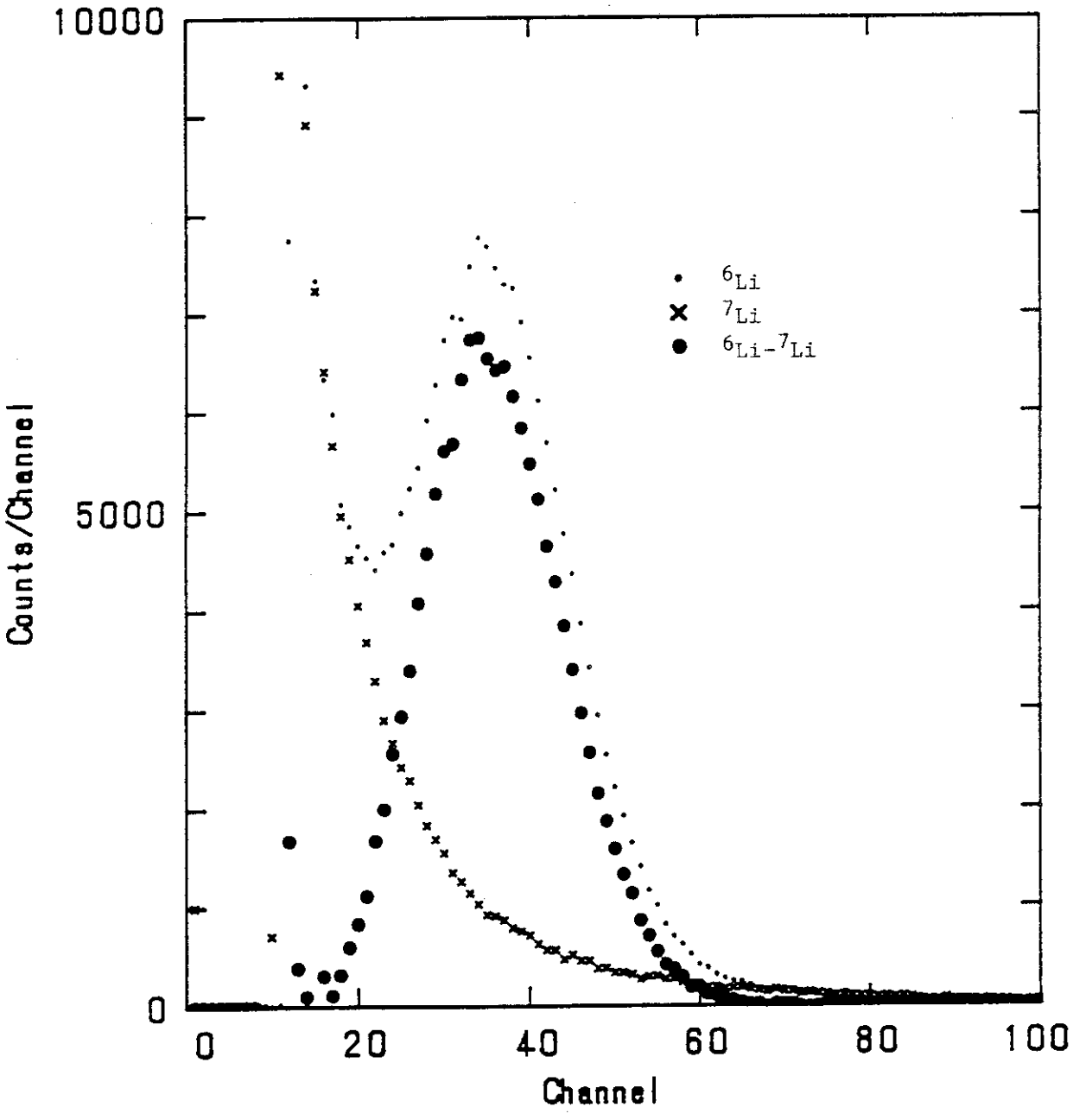

Fig. 6.4.2 Typical pulse height spectra of ^{6}Li and ^{7}Li-glass scintillators with optical fiber system in a simulated fusion blanket assembly

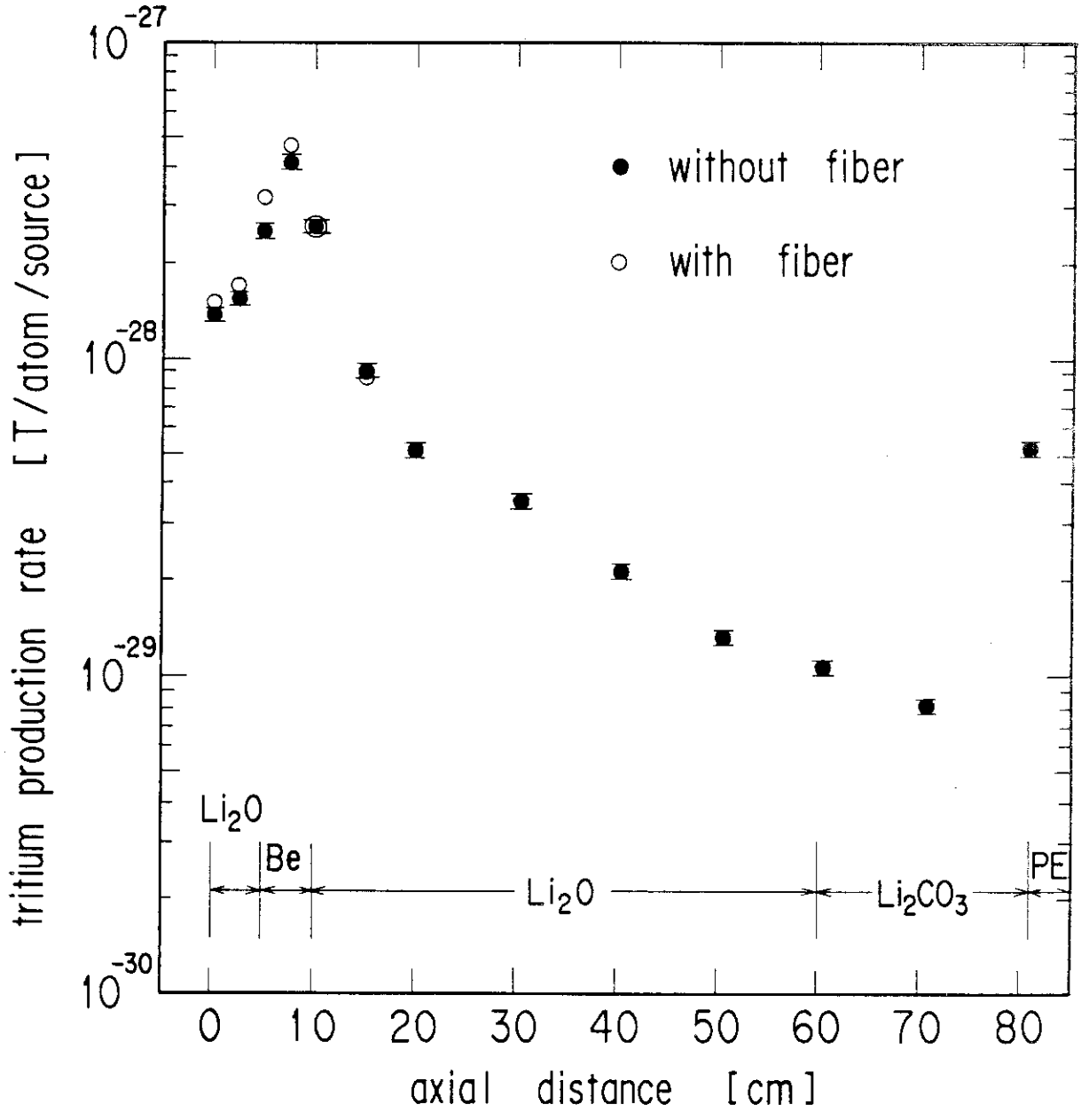

Fig. 6.4.3 Measured TPR distribution with and without optical fiber

7. Conclusions

A high-sensitive on-line method for measuring the tritium production rate of ^{6}Li with a pair of small-sized ^{6}Li- and ^{7}Li-glass scintillators (10mm-diameter by 0.3 mm-thickness each) is presented. In this method, the TPR of ^{6}Li is measured by using the difference between the response of ^{6}Li-glass and that of ^{7}Li-glass scintillator in a mixed neutron-gamma radiation field. Differences in the gamma-ray detection efficiency and in the gain between the two detector channels are taken into acount. Contributions of competing reactions were evaluated by an analytical method. The atom number of ^{6}Li in the ^{6}Li-glass scintillator was determined by isotope dilution analysis.

The thermal flux perturbation of ^{6}Li enriched lithium-glass scintillators was investigated by experiment and calculation. (n,α) reaction rates were measured for glass scintillators having four different thicknesses and three different ^{6}Li contents. It was shown that the decrease of the reaction rate due to the flux perturbation comes to 66 % for 1 mm thick ^{6}Li-glass of 6.3 % ^{6}Li content, and to 3 % for 0.1 mm thick ^{6}Li-glass of 1.0 % ^{6}Li content. A calculation of the flux perturbation was performed by the modified Skyrme theory and close agreement with measurement was obtained. The self-shielding effect and its dependence on energy was also calculated by a Monte Carlo method.

The edge effect of thin lithium-glass scintillators —— the distortion of pulse height spectrum at low energy side of the thermal peak due to the partial energy deposition of the alpha particle and/or the triton —— was examined. The pulse height spectra of the scintillators of various thickness were measured for thermal neutrons. It was shown that the "tail-to-total ratio" is 1.5 % for 2.0 mm thick scintillator and 10 % for 0.1 mm thick one. A Monte Carlo simulation of the pulse height spectra was also made. The results of the simulation explained well the specific features of measured spectra. The neutron energy dependence on the value of "tail-to-total ratio" was examined by this Monte Carlo code and it was shown that the dependence is very small for 0.3 mm thick scintillator.

The Lithium-glass method was applied to the measurement of the TPR distribution in assemblies simulating a fusion blanket. The results were compared with those of the β-counting methods with good

agreement. The data obtained by the Li-glass method were used as a benchmark to validate neutronics calculations.[1~3)]

A TPR measuring system using optical fiber was developed and applied to the measurement of the TPR distribution in a DT neutron field. The possibility of simulataneous measurement of ^{6}Li and ^{7}Li-glasses was demonstrated. The optical fiber system can be used in high temperature and strong electromagnetic field environments.

References

1) Youssef M. Z., et al. : "Analysis and Intercomparison for Phase I Fusion Integral Experiments at the FNS Facility," Proc. 7th Topical Meeting on the Technol. Fusion Energy; Fusion Technol., 10, 549 (1986).

2) Youssef M. Z., et al. : "Analysis of Neutronics Parameters Measured in Phase II Experiments of the JAERI/USDOE Collaborative Program on Fusion Blanket Neutrons Part II: Tritium Production and In-System Spectrum," Proc. Int. Sympo. on Fusion Nucl. Technol., Tokyo, April 10-15, (1988); to be published in J. Fusion Eng. Design.

3) Nakagawa M., et al. : "U.S./JAERI Collabolative Program on Fusion Neutronics Phase I Fusion Integral Experiments Vol II : Analysis," JAERI-M 88-177 (1988) ; UCLA-ENG-88-15 (1988).

Acknowledgments

The author wishes to express his gratitude to Professor Keishiro Niu of Tokyo Institute of Technology for his guidance and support during the preparation of this work.

Thanks are due to Mr. Tomoo Nakamura, Head of Fusion Reactor Physics Laboratory, JAERI, whose continuous encouragement, support and advice have been invaluable, to Drs. Hiroshi Maekawa and Yukio Oyama for their valuable advices, and to the seniors of the Department of Reactor Engineering, JAERI, who have supproted the present work.

The author is also deeply indebted to Mr. Shuzo Tamura and Mrs. Kimiko Tamura for their chemical analysis of the ^{6}Li content.

The author also would like to express his appreciation to Professors Kazutaka Kawamura, Susumu Shiota, Makoto Okamoto and Hiroshi Sekimoto for their benefitical suggestions on the work. The author would like to express his thanks to Professor Masaharu Nakazawa of University of Tokyo and Dr. Kensuke Kitao of National Institute of Radiological Science for their suggestions on this work.

The author greatly appreciates for reliable operations of the machines at the FNS facility by Messers. Joichi Kusano, Chuzo Kutsukake, Shigeru Tanaka and Yuji Abe.

In addition, the author is grateful to Dr. Karl G. Porges of Argonne National Laboratory for critical reading of the manuscript.